Department of Structures for Engineering and
Architecture, University of Naples "Federico II", Italy

In plane seismic performance assessment of Lightweight Steel Walls used for Structural and Non-structural applications

Doctoral thesis

Sarmad Shakeel

Naples, 2020

Supervisor: Professor Raffaele Landolfo
Co-supervisor: Dr. Luigi Fiorino

بِسْمِ اللهِ الرَّحْمٰنِ الرَّحِيْمِ

In the name of ALLAH, The most Gracious, The most Merciful

Contents

Acknowledgements

First and foremost, I am thankful to ALLAH Almighty, who has bestowed me with so much that I did not deserve. I am also thankful to ALLAH, that I have great parents: Shakeel Amjad and Ambreen Shakeel; and siblings: Asad, Saad, Izza and Munazza, whose support and prayers were always by my side. May ALLAH bless them with good health and cheerful life. Amen!

I would like to present my gratitude to my supervisor Professor Raffaele Landolfo, who not only supported me financially during my PhD, but also guided me on several occasions to make the right decisions. He was always kind towards me and welcomed me with open arms.

I also present my gratitude to my co supervisor Dr Luigi Fiorino, who guided me to become a more mature researcher and professional. I also thank him for being patient towards me.

I also thank the CFS team at UNINA, especially Alessia Campiche, who was not only my colleague but also a friend. I would also like to express my gratitude towards Vincenzo Macillo, Bianca Bucciero, Tatiana Pali and others, which were part of the CFS team and help me during various stages of my PhD.

I would also like to thank Professor Colin Rogers and Professor Daniel-Viorel Ungureanu for providing me with their feedback on my thesis and helping me to improve its quality.

Lastly, thanks to my friends in Naples, who made these few years in Naples cheerful and fun for me.

Sarmad Shakeel

Naples, Italy

Abstract

The European earthquake design standard: Eurocode 8 does not address the seismic design of lightweight steel (LWS) buildings. This has limited the use of LWS buildings in the earthquake prone regions of the European continent, where Eurocodes are enforced by law as the mandatory design reference documents. Moreover, architectural non-structural building components made with the LWS framing are also finding it hard to penetrate in the building markets of such regions due to the absence of the documented data on their seismic performance. In this context, the main objective of the research presented in this thesis is to develop a scientific database to assist engineers in achieving a rational performance based seismic design (PBSD) of LWS buildings. The scientific database includes the numerical and statistical tools for estimating the in plane seismic performance of LWS walls and a set of seismic design guidelines that can be proposed for the inclusion in the next edition of Eurocodes. Different objectives have been pursued for the structural components, which include the lateral force resisting systems (LFRS) for providing the earthquake resistance in the LWS buildings i.e. strap braced and shear walls and for the non-structural architectural LWS components i.e. partition walls and façades. The approach for the structural components involves the checking of collapse fragility of strap-braced and shear walls using the iterative procedures of FEMA P695, while the approach for non-structural architectural components focuses on developing the numerical models for the most widely used architectural components: partition walls and façades assisted with an extensive experimental campaign.

Behaviour factor for the two most commonly used LWS LFRS systems: CFS strap braced walls and CFS shear walls with gypsum or wood sheathing is evaluated through FEMA P695 methodology. For each type of system, a set of archetypes, which represent a range of design parameters and building configurations is designed following the capacity design approach and their response is idealized by nonlinear models in OpenSees software. The performance of archetype models is evaluated systematically through the static pushover and the incremental dynamic analysis under a suite of forty-four normalized and scaled earthquake records, representing the probable seismic hazard to the buildings. Finally, by calculating the collapse probability while also considering the uncertainties from various sources, the suitability of trial value of behaviour factor used in the design phase of archetypes is evaluated. Based on the results, it is concluded that a behaviour factor of 2.5, 2.0 and 2.5 for CFS strap-braced walls, CFS gypsum sheathed shear walls and CFS wood sheathed shear walls is appropriate.

Seismic performance of infilled façades made of LWS drywall systems is investigated via in plane quasi-static cyclic tests on eight different configurations of façades. Eight specimens are built following the common European construction practices and are infilled in a steel pendulum structure. The specimens differ from each other in terms of construction details: dual or single metal framed façades; types of boards used on different faces of the façades; presence of the cladding; fixed or sliding connections to the surrounding structural elements; profile dimensions of the frame elements. The effect of these construction details is examined through the comparison of strength and secant stiffness of the

tested specimens. The main types of damages observed during the tests are examined and associated to three damage limit states. Subsequently, fragility curves are developed for the assessment of seismic fragility of the tested façades and compliance is checked with the inter storey drift limits for architectural non-structural elements required by Eurocode 8.

Finally, a set of simplified numerical models are proposed for LWS indoor partition walls, to simulate their in-plane seismic response, that can be easily integrated with the building models and possess the ability to better estimate damages in them, when linked to their fragility information. The models are developed in OpenSees software by using a single discretized spring to simulate the lumped behavior of the walls for the twelve individual different configurations of the tested partitions. The accuracy of model is demonstrated by comparing the experimental and the numerical results in terms of the hysteretic response curves and the cumulative energy dissipated**.**

1. Introduction

1.1. Overview

Increased vulnerability of the world population to the rising global seismic hazard [1] and the growing number of structurally obsolete constructions is fuelling the research for more innovative structural systems that combine the benefits of lower cost with higher strength and make use of more sustainable technologies. Lightweight steel (LWS) buildings made with cold formed steel (CFS) profiles are one such type of innovative structural systems, whose application has been steadily increasing over the years due to their greater economic feasibility and ecological performance [2]. LWS building allows to solve a range of "built-in" issues associated to common constructional systems, providing, at the same time, earthquake safety relevant properties and without making any compromise on the performance requirements of the building. Nevertheless, the ultimate objective of research on these innovative systems, whether inventing a system or improving the functioning of existing system is its proper representation in building codes through availability of robust guidelines, hence making the research findings more accessible to the practicing engineers.

Earthquake codes follow a different approach for the design of structural and non-structural elements. For the design of structural elements, they provide rules for main lateral force resisting elements along with the rules governing the overstrength in rest of the structural elements. These rules ensure the development of dissipative mechanism only in the lateral force resisting elements, while keeping rest of the elements

essentially in an elastic state. The so-called approach is called capacity design approach. On the other hand, rules for non-structural element are mainly preventive in nature, hence focused only on limiting the damages in them through proposing proper anchorage details. These rules are fundamentally based on assumption that non-structural components can be considered dynamically uncoupled from the structural system to which they are connected [3].

Eurocodes provide the regulatory framework for new and existing constructions for buildings in Europe. The Eurocode 8 part 1 [4] covers the seismic design guidelines for new constructions. These guidelines include the definition of seismic loads, building acceptable performance goals and the construction typology related design requirements. The current edition of EN 1998-1 does not provide any rules for the common Lateral Force Resisting System (LFRS) used in LWS buildings while there is a need to check the compliance of current damage limitation requirements given for non-structural components on the components fabricated with CFS profiles.

Another important focus among the structural engineering community is to better accommodate the current shift in the seismic design philosophy, which has its emphasis changing from strength to performance-based design to achieve better predictable results in the event of an earthquake. Even if the structural elements of a building are able to achieve an immediate occupancy performance level after an earthquake, the damages in non-structural elements may lower the performance level of whole building [5]. This demands the harmonization of the performance

levels between structural and non-structural, which can be achieved through the availability of robust numerical tools and guidelines.

Given the absence of guidelines for LWS building in Eurocodes and the need to better accommodate the performance based seismic design for LWS buildings, this doctoral thesis attempts to fill these gaps through the numerical and experimental in plane seismic performance evaluation of LWS wall components. The investigated wall typologies include the lateral force resisting walls, which include strap-braced walls and shear walls, indoor partition walls and outdoor façades.

1.2. LWS buildings

A typical LWS building is made by erecting walls on a reinforced concrete foundation and covering them on top with a lightweight floors or roof (Figure 1-1). The walls in LWS building are made of studs, fastened at their ends to tracks. The studs and track of wall frame are the cold-formed steel (CFS) C or Z shaped members spaced usually 300 to 600 mm apart. For studs, the cross sections of the member profile are usually stiffened with the edge stiffeners called lips (Figure 1-2). There are several fastening methods available to join together studs and tracks depending upon the wall function. They could be either joined together with the connections made with screws or by simple mechanical techniques such as clinching or punching the flanges of studs and tracks. Usually, CFS frames of walls are sheathed with wood, gypsum, cement boards or steel panels (Figure 1-3a). The result is a sandwich element, where the internal cavity is ideal for inserting cables, pipes and insulation. An unlimited range of materials can be used as finishing of both the inner and the outer surfaces such as paint, wallpaper, coating, fabric, etc.

Figure 1-1 Typical lightweight steel construction [6]
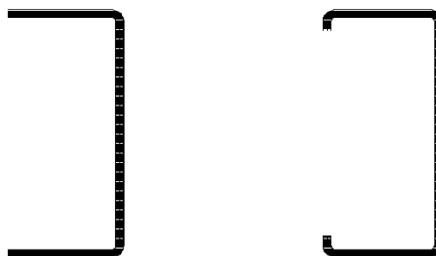
Figure 1-2 C shaped CFS profile (with and without lips) [4]
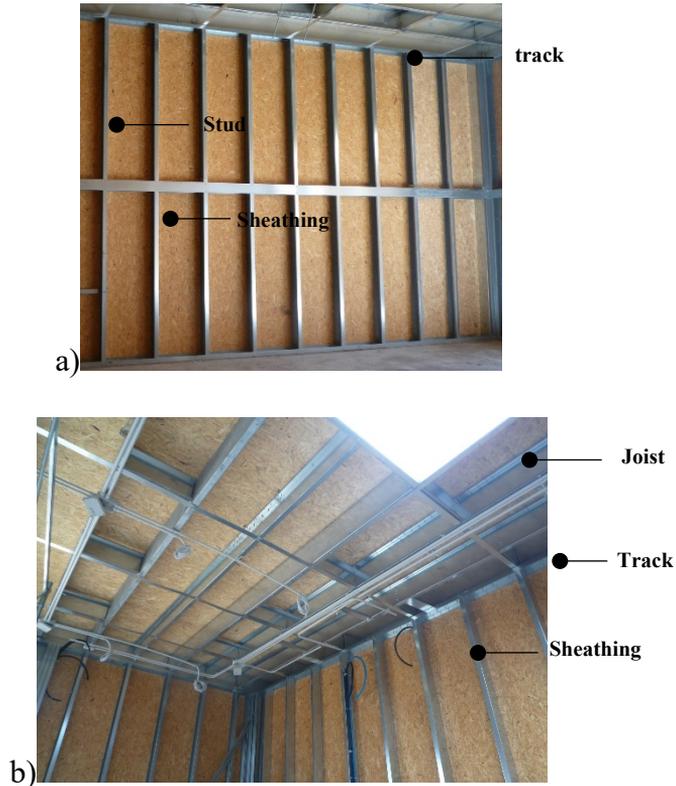
Figure 1-3 a) Wall framing; b) Floor framing.

Walls can serve different functions in any LWS construction. They can be either used to resist actions of different forces (structural applications) or can serve different architectural demands (non-structural applications). In case of structural applications of the walls, they are designed to withstand the gravity loads or lateral loads from wind or earthquake actions. The lateral force resisting walls are different than the gravity load resisting walls in a sense that special hold down devices are placed at the wall ends to transfer the uplift forces to the foundation. The studs, the type of sheathing and the spacing of sheathing connections to studs and tracks could be different depending upon the intensity of seismic or wind actions. Different types of lateral force resisting walls can be used:

CFS strap-braced wall or CFS shear walls. In strap-braced walls, the main resistance is provided by the steel straps placed in an X configuration (Figure 1-4), while in case of shear walls, the resistance is mainly provided through the interaction between the steel frame and the wall sheathing panels (Figure 1-4). The hysteretic response of strap-braced walls is characterized by strength degradation, stiffness degradation and pinching behaviour (Figure 5 a), whereas in the case of shear walls laterally braced with steel sheets or other sheathing boards the response is also affected by a strong nonlinearity even at the lower load levels (Figure 5 b). However, despite the strength and stiffness degradation observed in their pinched hysteretic response, LWS framed system can be a very competitive solution for low to medium rise buildings thanks to their lightness, which allows satisfactory structural performances for applications in seismic zones.

Figure 1-4 A LWS building equipped with CFS strap-braced walls (left)-(The Elan Westside building in Atlanta); CFS steel sheathed shear walls (right)-(Photo courtesy of J. Ellis, Simpson Strong-Tie Co. Inc.)
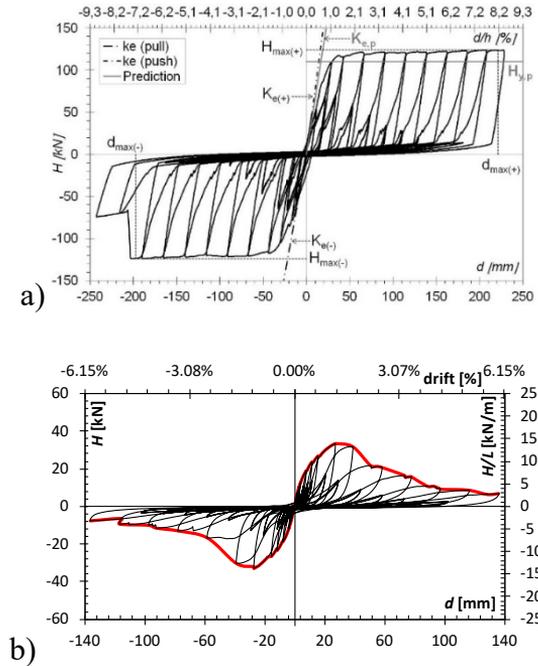
Figure 1-5 Typical hysteretic response curves of seismic resistant LWS walls under in-plane cyclic loads [7]. *a) Solution with strap-bracing; b) Solution with sheathing boards* [8]

The floors are made in a similar manner as gravity load resisting walls except they are oriented in a horizontal direction and are covered with panels or composite steel trapezoidal sheathing-concrete deck. In addition to lateral force resisting walls, floor elements have also proven to provide reasonable amount of seismic resistance [9].

Apart from the structural walls, a typical LWS building also constitutes non-structural walls like partition walls, façades and curtain walls, which are not designed nor anticipated to contribute to the primary load-bearing system of the building [10].

There are two different possibilities to design the structural wall and floor components: all-steel design and sheathing-braced design. In all-steel design of an LWS building, the actions are only assumed to be

resisted by the steel frame members, hence neglecting the presence of sheathing boards. Therefore, the generic profile is assumed as an isolated (free-standing) element, by neglecting the interaction between profiles and sheathing. In case of sheathing-braced design, the load bearing capacity is evaluated by taking into account the presence of the sheathing.

As far as the non-structural walls are concerned, partition walls are mainly frames made of the cold-formed steel (CFS) C or Z shaped members (usually 0.6 mm thick). For studs, the cross sections of the member profile are usually stiffened with the edge stiffeners called lips (Figure 1-2). Stud profiles are generally installed with a spacing equal to a half width of the sheathing board (about 600 mm). Usually the sheathing panels are gypsum boards screwed to the steel frame. Insulation material is inserted into the cavities between the cladding in order to achieve the expected safety and serviceability requirements related to non-structural performances, e.g. the fire and acoustic performances (Figure 1-6 a, b, c). The use of metal stud partitions allows to achieve high performances in terms of wall height (up to 12 m), sound insulation (up to 80 dB), fire protection (up to 120 minutes, fire resistance), and the seismic response can be fulfilled as well with very flexible and light solutions.

Most common solutions of façades can be grouped in two main typologies: "Integrated" and "Curtain" walls (Figure 1-6 d, e, f). "Integrated" façades can be made of single or double CFS frames. They are placed on the load-bearing slab and the surrounding perimeter connections are attached directly to the supporting frame. "Curtain" façades are made of a double LWS frame, in which only the interior frame is connected to the ceiling slab of the main structure. Usually, a specific

thermal insulation material is applied in the wall cavity in order to guarantee the desired energetic performance. The exterior face of façade walls is generally cladded with cement boards and finished with glass fibre tape with an alkaline-resistant coating and cement-based plaster.
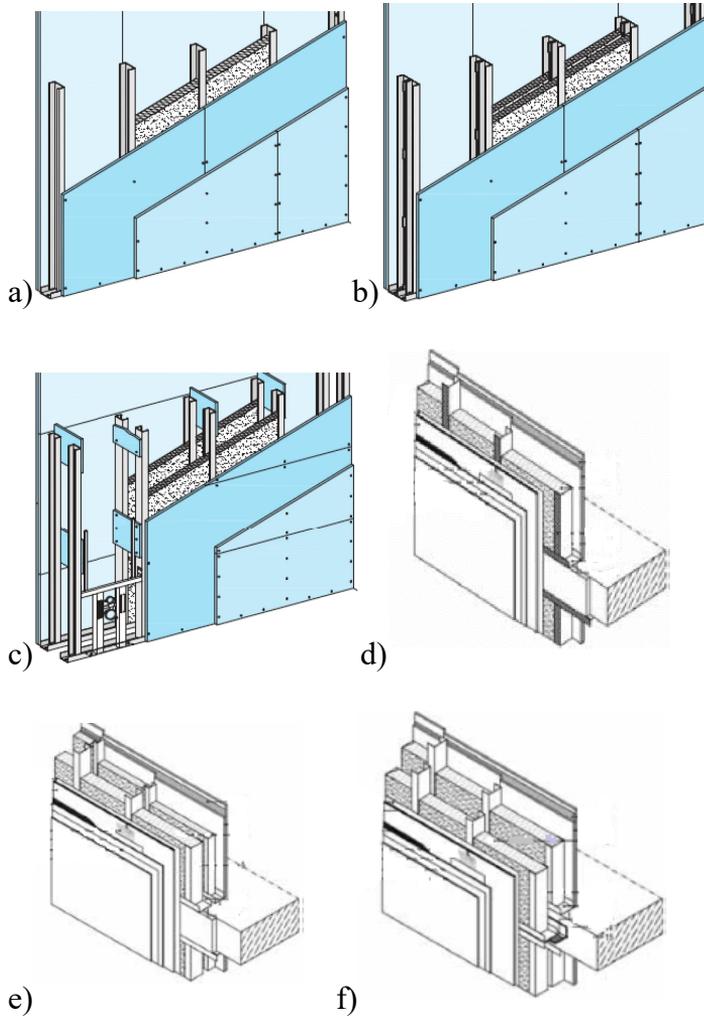
Figure 1-6 Typical application of LWS drywall elements in non-structural architectural systems. a) Single stud partition; b) Double stud partition; c) Double stud partition, braced; d) "Integrated" façade with single frame; e) "Integrated" façade with double frame; f) "Curtain" façade with double frame [11].

1.3. Research objectives

The main goal of the PhD research is to create a scientific database for assisting engineers in achieving a rational performance based seismic design of lightweight steel (LWS) constructions. The scientific database includes the numerical and statistical tools for estimating the in plane seismic performance of LWS walls and a set of seismic design guidelines that can be proposed for the inclusion in next edition of Eurocodes. Different objectives have been pursued for the structural components: strap braced and shear walls and for the non-structural architectural components: partition walls and façades. The approach for the structural components involves the checking of collapse fragility of strap-braced and shear walls using the iterative procedures of FEMA P695 [12], while the approach for non-structural architectural components focuses on developing the numerical models for the most widely used architectural components: partition walls and façades assisted with an extensive experimental campaign. The outline of the research work has been drawn to achieve following particular objectives.

Structural components:

1. To develop and calibrate numerical models for individual units of strap braced and shear walls that are capable of simulating the response until collapse, are representative of the physical characteristics of wall and are simple enough to be used in complete building models.

2. To make the numerical model of LWS buildings using strap braced and shear walls for conducting incremental dynamic analysis following the procedures of FEMA P695, so that the acceptability

of proposed design guidelines can be established by measuring the collapse fragility of wall systems under the set of earthquake records.

Non-Structural components:

3. To test the lateral in plane performance of lightweight steel façades under quasi-static cyclic load for investigating their contribution to global building lateral resistance and develop a fragility database.

4. To develop simplified models for partition walls in plane behaviour using the test results to have a more complete numerical realization of LWS building seismic performance and have a better estimate of damages in them under different intensities of earthquake hazard, hence to have a realistic picture on building performance levels after an earthquake event.

1.4. Scope of the thesis

In order to achieve the aforementioned objectives, the research on the structural wall systems is limited to three very common LFRS used in LWS buildings i.e. CFS strap braced walls, CFS gypsum sheathed shear walls and CFS wood sheathed shear wall. For these three LFRS-s, a series of experimental campaign including the tests at micro, meso and macro levels have already been carried out in past. Using the test results, a numerical model is developed for each LFRS, which are then used in a series of building archetype models. These archetype models are then analysed using Incremental Dynamic Analysis (IDA) procedures following the methodology outlined by ATC-63 "Quantification of Building Seismic Performance Factors" in FEMA P695 [12] to evaluate a behaviour factor and the collapse fragility of each system. Additionally, a

method to predict the design strength of each LFRS is also proposed. Concerning the objectives related to the seismic performance of LWS non-structural components, this thesis reports a series of in plane quasi-static cyclic test results of façades made with CFS profiles. Additionally, in line with the need to have complete set of tools for the performance based seismic design (PBSD) of LWS buildings, numerical models of the partition walls are also developed. The tests on façades are part of a major experimental campaign, which when complete would have results available from tests on twenty different specimens of façades. Until now only eight specimens have been tested and results are reported here. Once the experimental campaign on façades will be finished, numerical models would also be developed for them in future. Nevertheless, this thesis marks an important step towards the PBSD of LWS buildings by making available the numerical and statistical tools for them and would pave the path for further research in this arena. The terms used in this thesis refer to the terminologies used by Eurocode, if not specified at a particular instance.

1.5. Thesis Outline

This thesis is organized to give an overview of the studies available in literature on LWS wall systems including both structural and non-structural categories in Chapter 2, which then is followed by the seismic performance evaluation of LWS structural wall systems in Chapter 3 (CFS strap-braced walls) and Chapter 4 (CFS shear walls). Then, Chapter 5 summarizes the results from the experiments carried out on the façades and Chapter 6 describes the numerical models developed for LWS indoor partition walls, which is then followed by the conclusions in Chapter 7.

Each chapter presenting the portion of research conducted in this thesis has its also accompanying Annex, which shows further detailed results.

2. Literature review

This Chapter covers the present state of the art concerning the design guidelines in building earthquake standards along with the relevant numerical and experimental studies on LWS wall systems. The approach proposed by different standards around the globe for the seismic design of buildings made with LWS wall systems for both structural and non-structural applications is summarized (Section 2.1 and 2.2). Experimental studies reviewed in this chapter includes the cyclic and monotonic tests carried out on the individual wall specimens and the shake-table tests conducted on the building representations of the LWS wall systems (Section 2.3, 2.4 and 2.5). Likewise, the numerical studies examined in this chapter includes the numerical models with different levels of complexity developed for the individual wall units and the building representations (Section 2.3, 2.4 and 2.5). Moreover, an overview of the numerical studies using the statistical approaches like FEMA P695 [12] to evaluate the building seismic performance factors for LWS structural wall system is also provided (Section 2.6).

2.1. Earthquake Codes for LWS wall systems-structural applications

Earthquake resilience in the structures is guaranteed through different structural control techniques. Seismic energy can either be dissipated by allowing the development of the plastic mechanism in certain parts of the structure (LFRS) while keeping the rest of structure in an elastic state, or by using the active control devices to modify the structural response. The former approach is implemented in building codes through the adaption of the Capacity design rules at structure, member and

connection level in the design process. Ductility is the fundamental requirement of dissipative structure. Capacity design rules ensure the ductile behaviour of certain pre-defined ductile members or connections through proper over strength in brittle parts of structure. As a result of the development of this inherent ductility in the structure, a reduced value of seismic action can be considered in the design process. This reduction of seismic action is obtained by dividing the forces obtained from a linear analysis by a factor (greater than 1). This factor accounts for the non-linear response of structure associated with the material and the structural system itself and is expressed as 'Behaviour factor (q)' in European earthquake standard Eurocode 8 Part 1 EN 1998-1 [4] and 'Response modification coefficient (R)' in United States earthquake standard ASCE/SEI 7 [13] .

Extensive research and product development in the past has led to well-advanced national design specifications for LWS structural systems in many countries [14–16]. On the contrary, only the North American Codes [13,17,18] cover properly the design of LWS buildings in seismic areas, whereas in Oceania and Europe specific rules for seismic design of this structural typology are not available. In particular, seismic performance factors (R-response modification coefficient, Ω_o-over strength factor and C_d- deflection amplification factor) are provided for different typologies of LWS LFRS in ASCE 7 [13] for USA and Mexico, and in NBCC [17] for Canada (Table 2-1), whereas capacity design rules are provided in AISI S400 [18] for USA, Canada and Mexico. These capacity design rules are provided in the form of limitations on the geometrical and the mechanical characteristics of the different components of the wall systems. Design with a compliance of these limitations would lead to the development of plastic mechanism in the main energy

dissipating components of the wall. AISI 400 also specifies the main energy dissipating mechanism and provides the design capacities associated to the mechanism for certain predefined wall configurations. Except for the CFS steel sheathed shear walls, for which a procedure [19] for evaluating the design strength is also formulated, AISI S400 permits to use only the certain predefined wall configurations for any type of LFRS, whose design strengths are listed in a tabulated form. Furthermore, the application of any LFRS in a building is also limited by its height and the maximum seismic demand, which are provided in ASCE 7 [13] for USA and Mexico and in NBCC [17] for Canada. It must be noted that the seismic performance factors given in codes [13,17,18] are mostly evaluated experimentally, or on the basis of experiences learned from the past earthquakes. One the other hand, FEMA P695 [12] provides a more coherent methodology to evaluate these factor by using nonlinear analysis techniques and explicitly considering uncertainties in ground motion, modelling, design, and test data to achieve an acceptably low probability of collapse of the seismic-force resisting system. The methodology is used in this thesis to evaluate the behaviour factor for the investigated structural wall systems for their application in Europe. More details on the seismic performance evaluation through the FEMA methodology and studies conducted following this methodology on LFRS common to LWS buildings are provided in Section 2.6.

Table 2-1 Seismic performance factors given by North American Codes for different typologies of lightweight steel seismic resistant systems.

Typology of LFRS	ASCE 7 [13] (USA and Mexico)			NBCC [17] (Canada)	
	R	Ω_o	C_d	R_d	R_o
CFS wood sheathed shear walls	6.5^1 7.0^2	3.0^1 2.5^2	4.0^1 4.5^2	2.5	1.7
CFS steel sheathed shear walls	6.5^1 7.0^2	3.0^1 2.5^2	4.0^1 4.5^2	2.6^3	
CFS strap-braced walls	4.0	2.0	3.5	1.9	1.3
CFS special bolted moment frames	3.5	3.0	3.5	no provisions	
CFS shear walls with wood sheathed on one side and gypsum sheathed on the other side	no provisions			1.5	1.7
CFS gypsum or fibreboard panel sheathed shear walls shear walls	2.0^1 2.5^2	2.5^1 2.5^2	2.0^1 2.5^2	no provisions	
CFS strap-braced walls [4]	no provisions			1.56	

[1]Bearing wall systems
[2]Building wall systems
[3]System not yet adopted in NBCC [17], value is product of R_d and R_0 given in AISI S400[18] for Canada
[4]Conventional constructions

In Oceania, earthquake loading standard AS/NZ 1170.4 [20] does not cover LWS structures. However, the Australian standard for CFS

structures AS/NZS 4600-05 [16] provides a response modification factor no greater than 2, if CFS members are used as primary seismic load-bearing elements. Similarly, currently in practice edition the European seismic code EN 1998-1 [4] also does not provide any behaviour factor or capacity design rules for LWS structures. Though as explained in the proceeding paragraphs, there is a possibility to design LWS structures by considering them as common steel structures made of Class 4 cross-sections [4].

EN 1998-1 [4] defines two fundamental requirements for structures designed to withstand seismic loads, which should be met with appropriate degree of reliability: Damage limitation requirement and No-collapse requirement. In order to fulfil damage limitation requirement, structure must be able to resist seismic action having 10% probability of exceedance in 10 years (return period of 95 years) without occurrence of damage and the associated limitations of use. While, for a structure to meet the no-collapse requirement, it should be able to resist seismic action having 10% probability of exceedance in 50 years (return period of 475 years), while keeping its structural integrity and residual load bearing capacity. In light of these fundamental requirements, EN 1998-1 [4] defines two limit states for which structures must be checked: Damage limit state, related to damage beyond which specified service requirements are no longer met, and Ultimate limit state associated with the collapse or with other forms of structural failure which might compromise the safety of people. Seismic hazard is defined in terms reference peak ground acceleration, $a_{g,R}$, corresponding to no-collapse requirement of EN 1998-1 [4], as stated earlier. Seismic action is defined in terms of design response spectrum, which depends on the design ground acceleration, a_g, ($a_g = a_{g,R} \cdot \gamma_I$,

where γ_I is importance class of building), soil type and the behaviour factor (q). These guidelines are used in conjunction with other relevant parts of Eurocodes, which provide rules for the gravity design of buildings.

For the seismic design of buildings, EN 1998-1 [4] provides guidelines specific to the material and elements used in building. In particular, Section 6 of EN 1998-1 gives rules for the steel buildings. It classifies the structures in two categories based on their ability to dissipate seismic energy: low dissipative or dissipative. Low dissipative structures are classified as low ductile structures with a behaviour factor less than or equal to 1.5. For dissipative structures being classified as medium to high ductile, code provides values of behaviour factor greater than 2.0 depending upon the choice of seismic force resisting system.

Hence, according to the current European provisions, seismic design of shear walls sheathed with steel sheets or strap-braced walls could be possible by considering them as common steel structures made of Class 4 cross-sections belonging to low Ductility Class and adopting a behaviour factor no greater than 1.5. Moreover, EN 1998-1 also limits the use of low Ductility Class structures to low seismicity regions, which should have design ground acceleration not greater than 0.08g. On the contrary, seismic design of shear walls sheathed with materials other than steel is not covered by the EN 1998-1.

2.2. Earthquake Codes for LWS wall systems-non-structural applications

The first inclusion of the seismic prescriptions for non-structural components were in the 1967 Uniform Building Code [21]. Subsequently, seismic design provisions were included in a wide variety of seismic codes

covering a large number of non-structural components and systems, even if the prescriptions were focused only on the safety of critical equipment in essential facilities. Only in the last three decades, several guidelines and standards have developed more accurate seismic design provisions and evaluation procedures for non-structural components, in order to ensure proper performance during earthquakes.

Currently, the approach of the building codes, namely the European seismic code EN 1998-1 [4], and the American codes for new buildings ASCE 7 [13] and for existing buildings ASCE/SEI 41-13 [22] regarding the design of non-structural systems follow three different paths. The first code category is involved in providing prescriptive requirements for common products, such as suspended ceilings, by means of seismic protection details and specifications. The second code category assumes that the non-structural components should be designed for lateral seismic forces that are proportional to the element weight. In this regard, the equivalent lateral force method is used for acceleration-sensitive components, so that the anchorages and bracing systems should be able to withstand the earthquake accelerations. The third code category requires that the deformation-sensitive components should be designed to accommodate the design inter-storey drifts of the primary structure. However, all of the above-mentioned standards and their prescribed approaches address the problem in a generic way, without providing any specific rules for non-structural components made with LWS framing. On the other hand, FEMA E-74 [3] is a practical guide towards reducing seismic damages in different types of non-structural building components such as architectural, mechanical, electrical, plumbing, furniture fixtures, etc. In particular, Sections 6.3.2 and 6.3.4 FEMA E-74 provide guidelines

for LWS interior partition walls and ceilings, respectively by identifying various type of damages and proposing mitigation details for the components made with LWS. The report also provides connection details for LWS partition walls in order to avoid connection of stud and sheathing to track and bracing details for the suspended ceiling systems.

The two investigated typologies of LWS wall systems for non-structural applications investigated in thesis are indoor partition walls and outdoor façades, which can be characterized as deformation sensitive components. As per current requirements of EN 1998-1 [4] under seismic design situation, these walls systems should fulfil the damage limitation requirement for non-structural building elements. A common approach to check the compliance of LWS wall systems to the damage limitation requirement is to test their representative specimens under different types of loading protocol. In this regard, in-plane quasi-static reversed cyclic tests of LWS infilled façades are also carried out and results are presented (Section 5) in this thesis.

EN 1998-1 [4] defines the displacement demands on the deformation-sensitive elements by imposing an inter-story drift ratio (IDR) limit. The damage limitation requirements for non-structural elements, which corresponds to the serviceability limit state, should be satisfied by limiting the design IDR of the main structure to the code-specific values. Specifically, EN 1998-1 defines the IDR as following:

$$\frac{d_r \cdot v}{h} \tag{2-1}$$

where d_r is the design inter-storey drift evaluated as the difference of the average lateral displacements at the top and bottom of a storey and

are obtained by a structural analysis of the system based on the design response spectrum (i.e. for a rare seismic event having 475-year return period); v is the reduction factor, which takes into account the lower return periods of the seismic action associated with the damage limit state and ranges between 0.4 and 0.5, depending on the importance class of buildings; and h is the storey height. For ensuring the non-structural damage limitation requirement, the inter-storey drift ratio should be limited to the following values according to EN 1998-1:

- 0.5% for buildings having non-structural components made of brittle materials and attached to structure;
- 0.75% for buildings having ductile non-structural components;
- 1.0% for buildings having ductile non-structural components fixed in a way so as not to interfere with structural deformations.

2.3. CFS strap-braced walls

CFS strap-braced stud wall is an all-steel solution against the action of lateral forces on low to mid-rise LWS buildings (see Figure 2-1). A pair of CFS straps placed in X configuration connected to the external frame provides the main lateral load resistance. Straps are only considered active in tension due to their slenderness. Thus, any lateral load applied on the wall is absorbed only by the strap in tension, transmitting significant axial compression force to studs at the end of wall. These walls are made of series of studs, which are fitted on the horizontal tracks. External studs also called as chord studs, can usually either be back to back lipped C-channel or box cross section, in order to avoid buckling due to the compression force transmitted by the straps. Track members are usually made of un-lipped U cross sections. Generally self-drilling screws are used to attach

the straps to the gusset plates placed at the four corners of wall. Hold-down devices and shear anchors are used to connect the wall to foundation or to other floors. The wall uses the steel strap to dissipate the energy through their tensile plastic elongation, whereas the rest of the wall components are expected to remain elastic (capacity design approach).

1. Stud
2. Chord stud
3. Track
4. Hold-down
5. Shear anchorage
6. Steel strap brace
7. Connection of strap brace
8. Tension anchorage
s_s: stud spacing
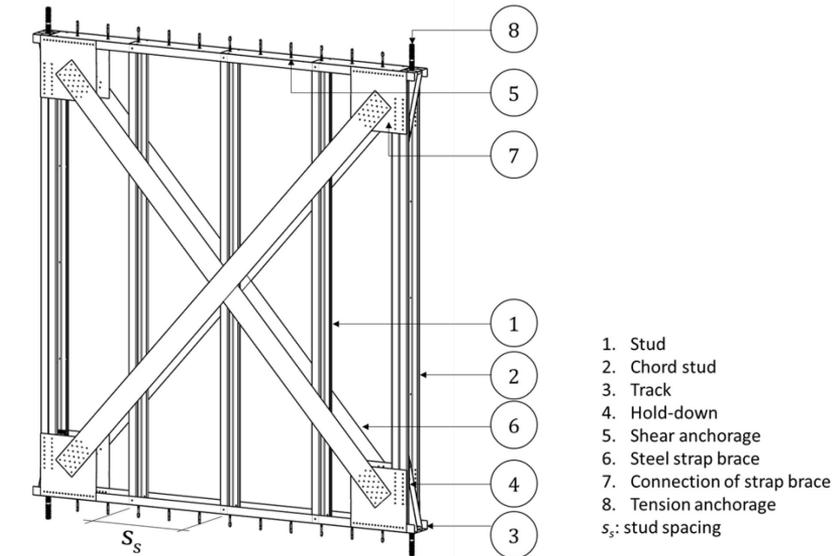
Figure 2-1 Typical Configuration of CFS strap-braced wall

2.3.1. Experimental studies

2.3.1.1.   Tests on wall specimens

Most of the experimental studies conducted in past to characterize the seismic response of CFS strap-braced walls used monotonic and quasi-static cyclic tests (Figure 2-2). The results from these experiments are often represented in the form of force drift hysteretic curves. Figure 2-3 shows a typical hysteretic response curves of CFS strap-braced wall from the in-plane quasi-cyclic test. Besides, evaluating the hysteretic curves, these experiments were mostly aimed at enhancing the wall performance by

improving the different geometrical details. In the following paragraphs, major outcomes from these researches are highlighted.

Figure 2-2 In plane quasi static cyclic test on strap-braced wal1 [7]
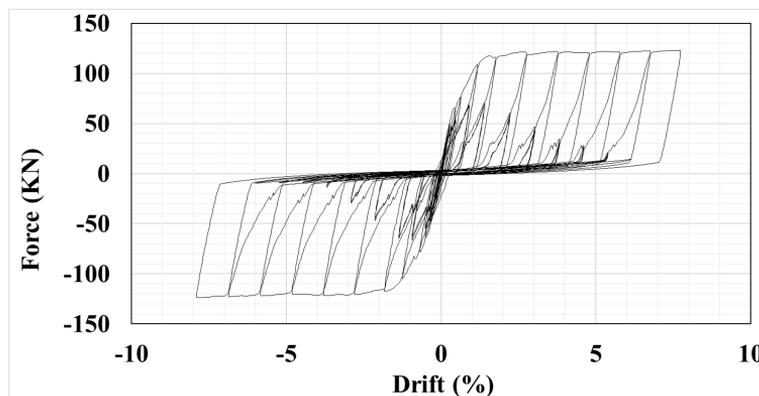
Figure 2-3 Typical hysteretic response of CFS strap-braced wall [7]

Fülöp and Dubina[23] showed the importance of following the capacity design philosophy in the wall design from their test results, in which strap-braced walls experienced brittle failures at the corner areas of the specimens like local buckling of tracks in the walls ,which were not

designed following the capacity design philosophy. Cyclic experiments were conducted on both sheathed and strap-braced CFS shear wall solutions, which showed that braced walls depict more stable hysteresis loops than sheathed shear walls but on the other hand, they also show severe pinching of the hysteretic loops.

Al-Kharat and Rogers in [24] and [25] also demonstrated the importance of capacity design approach for the design of CFS strap-braced stud walls. They tested walls designed with and without capacity design approach. In case of walls designed without following capacity design approach [24], lower values of R were reported and walls were unable to maintain ductile behaviour. In particular, R values of 3.65, 2.11 and 1.72 for low to high strength walls were obtained, which were considerably lower than ASCE 7 [13] value of 4 for USA. However, they mentioned that it was not even possible to achieve a value of 4 for R factor even if capacity design approach was followed for tested walls. In the later phase of their experimental campaign [25], they tested fifteen CFS strap-braced stud wall specimens designed following a capacity design approach. A value of 2.6 for $R = R_d \cdot R_o$ ($R_d = 2.0$ and $R_o = 1.3$) was obtained based on the experimental results where, R_d and R_o are the ductility and over strength related response modification factors. Velchev et al. [26] tested a series of weld and screw-connected CFS strap-braced stud wall specimen of various length and brace sizes in order to verify AISI S213 [27] seismic provisions for them. They found a value of R equal to 2.6 suitable for walls with aspect ratio 2:1 and 1:1 in AISI S213 [27], which was code of practice for seismic design guidelines for LWS buildings in North America at that time. They also cautioned on the use of walls with higher aspect ratios (height to width ratio) than 4:1, which could develop flexural forces in

chord studs, as also shown by Mirzaei et al. in [28]. In fact, the latest North American standard for seismic design of CFS systems addressed this issue by requiring a frame analysis of the wall using an assumption of joint fixity.

Various other research studies investigated different geometrical options for bracing and corner connection details. Moghimi and Ronagh [29] tested twenty full-scale wall specimens under quasi-static cyclic loading according to different position of bracings (connecting bracing at intermediate studs instead of chord studs) and using a bracket or gusset plates at corners. Their results indicated the improvement of lateral performance of the walls by using brackets, which removed slackness in bracing, whereas a modified bracing configuration resulted in a reduction of lateral load resistance of the wall. Zeynalian and Ronagh [30] reported higher values for R factor (greater than 4 as in ASCE 7 [13]) for CFS strap-braced stud walls with brackets based on the analysis of finite element models of walls having varying bracket lengths. Casafont et al. [31] conducted tests on connections made at different locations in strap-braced walls. Based on the test results it was found that net section failure is the only failure mode in bracing which allows them to utilize their full plastic capacity, and screws are much better option than bolts and other connecting devices due to their smaller diameters, which in turn increase the net section area.

Fiorino et al [32] proposed a seismic design method for the design of CFS strap-braced stud walls, which matches the current framework of EN 1998-1 [4] in terms of behaviour factor definition and capacity design rules prescriptions. They validated the design method through monotonic

and cyclic tests [7] on elastic and dissipative walls. Their experimental results [7] were also in good agreement with the results obtained from other researchers [24,25].

2.3.1.2.   Tests on building specimens

A more rational approach for investigating the seismic response of any LFRS is through the shake-table test of it building representations (Figure 2-4), which are conducted out under the action of acceleration time histories representative of the seismic hazard exposed to the building. These tests not only reveal the hysteretic response curves and different failure mechanism as by the quasi-static cyclic tests but also give useful information on building dynamic characteristics and the interaction of LFRS with different components of the building.
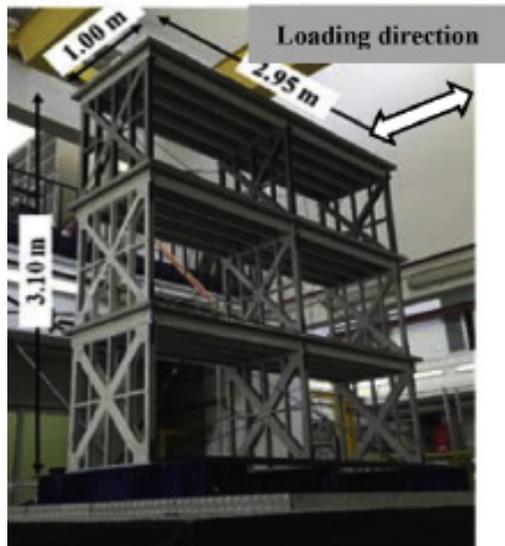
Figure 2-4 Shake-table test on building representation of CFS strap braced walls [33]

Kim et al. [34] tested a double storey strap-braced bare CFS frame structure with box shaped columns. The test results highlighted the

effectiveness of strap-bracings as a reliable seismic force resisting systems in the LWS buildings. Another key takeaway from the tests was using a fix end connected studs of the strap-braced wall, which also contributed to the shear resistance and providing energy dissipation during regions of the earthquake response where the braces provided no strength or stiffness due to their slenderness. Furthermore, the experimental results were also used to validate the R=4 provided in ASCE 7 [13] for strap-braced walls using the methodology of FEMA report 355F [35], which uses IDA procedures to evaluate system performance. Experimental result [34] were used to calibrate the numerical models of one to six storey buildings. It was recommended to use $R = 4$ for LWS buildings with strap-braced walls provided that these structures should have the top story lateral resistance more than the design value of resistance. This exception was due to the fact that top stories of four and six storey buildings experienced excessive story drifts in dynamic analysis.

Very recently, the performance of strap-walls designed with an elastic concept, i.e. capacity design philosophy not being followed and the behaviour factor is 1.5 as per current prescriptions [4] for LWS LFRS in Europe, was analysed by performing the shake-table tests [36] on two reduced-scale (1:3) three-storey two-bay prototypes. Two prototypes differed with each other with respect to the floor typology: composite steel-concrete floors (Concrete solution) or floors made of wood-based panels (Wood solution). Preliminary results of this research showed that the global response was almost linear for both mock-ups, with maximum inter-storey drifts recorded at the 3rd level (3.62% for Concrete solution and 2.44 % for Wood solution) and the observed damages were strap yielding and bolt loosening for both solutions, whereas local buckling of chord

studs occurred only for mock-up with wood-based floors. Floors behaved as rigid in their plane according to the ASCE 7 [13] definition for both solutions.

2.3.2. Numerical studies

In the past, several researchers developed numerical models of CFS strap-braced walls. Numerical modelling is often done to not only, further explore the experimental results but to also to serve as a benchmark for the parametric studies. Models developed in the past ranged from simple analytical to very complex finite element representations. This section summarizes the main intent behind the development of these models and their main features.

Pastor and Rodríguez-Ferran [37] presented a differential model of hysteretic behaviour for CFS strap braced walls, which can capture the slackness due to buckling of braces as well as strength and stiffness degradation. However, their model assumes that wall is able to maintain its load carrying capacity under excessive lateral displacements without ever reaching to failure.

Kim et al. [38] also developed the analytical models for CFS strap braced stud walls in DRAIN-2DX [39] program. In their model, they used beam column element with plastic hinges lumped at both end for the studs. Addition of plastic hinges at the end of studs was due to the fact that they had fixed connections in earlier tested specimen of walls [34] and it accounted for additional bending stiffness of studs. For straps, they used inelastic truss bar elements. However, original hysteretic model of this element in DRAIN-2DX [39] did not capture severe pinched behaviour of

CFS strap braced stud walls, therefore they added a gap property to truss element to capture the complete behaviour.

Comeau et al. [40] evaluated the seismic performance factors for CFS strap braced stud walls using Incremental Dynamic Analysis (IDA) based on FEMA P695 [12] methodology. Bilinear spring elements with strain hardening and slackness characteristics were used to model hysteretic response on walls in Ruaumoko [41] software. Mirzaei et al. [28] developed an elastic analytical model with fixed connections except for the end of braces, in order to study the effect of wall aspect ratio on the moment generated in chord studs due to frame action.

In addition to above mentioned analytical models, several finite element models were also developed. Gad et al. [42] developed FE models in ANSYS [43] for Plasterboard lined CFS frame without bracing in order to study effect of presence of different boundary conditions and aspect ratio on ultimate capacity of wall using nonlinear static analysis. Later on, they combined these models with models of braced frame developed by Barton [44]. In the combined model, straps were modelled as series of three nonlinear springs: strap-frame connection, solid strap and strap tensioner unit system.

Zeynalian and Ronagh [30] developed finite element models of CFS strap braced stud walls with additional brackets at corner of walls. A nonlinear static analysis was conducted in ANSYS [43] with varying the length of brackets for each model in order to optimize their seismic response.

To sum up, numerical models presented in Pastor and Rodríguez-Ferran [37], Kim et al. [38] and Comeau et al. [40] lacked the ability to

capture brittle failure modes for CFS strap braced stud walls. Available models develop for CFS strap braced stud walls did not represent all wall structural components, except models presented in Kim et al. [38]. In addition, finite element models presented in Gad et al. [42] and Zeynalian and Ronagh [30] only represented the static behaviour of CFS strap braced stud walls and cannot be used in analysis of complete buildings due their complexity. In this context, there is a need to develop a numerical model which can capture brittle and ductile failure modes, can properly represents the contribution of all components to lateral force resistance under dynamic and cyclic loads and is computationally efficient to be used in models of complete 3D buildings. Such type of model is developed within the work presented in this thesis.

2.4. CFS shear walls

Shear wall is one of the most common type of structural system to provide the lateral resistance in LWS buildings, which resists lateral forces through the interaction between steel frame and sheathing panels. These shear walls are essentially composed of a CFS frame sheathed with panels and connected with the tensile and shear anchorage for transmitting lateral forces to the floor or foundation. Gypsum and wood based panels are among one of the many types of panels used in such constructions [8,23,45,46], which can be either nailed or screwed to the main steel frame (Figure 2-5). CFS gypsum sheathed shear walls are normally used in conjunction with other primary seismic force resisting system in buildings, whereas their use as unique seismic force resisting system is limited to low rise buildings [18] due to their limited ductility arising from the brittle behaviour of gypsum panels [18] in comparison with the wood-based panels or the steel sheets. Since the scope of this thesis is limited to the

seismic performance evaluation of LWS buildings braced with CFS gypsum or wood sheathed shear walls, this section only explains the experimental and numerical studies conducted on these types of LFRS-s.

1. Stud
2. Chord stud
3. Track
4. Hold-down
5. Shear anchorage
6. Wood or gypsum based panel
7. Screw at panel edge
8. Screw in the panel field
9. Sheathing joint
10. Tension anchorage
s_s: stud spacing
s_f: screw in the panel field
s: screw at panel edge

Figure 2-5 Typical Configuration of CFS shear wall

2.4.1. Experimental studies

2.4.1.1. Tests on wall specimens

CFS shear walls are essentially made of sheathing panels or boards connected via screws or other type of connectors to the main steel frame and dissipate energy mainly through tilting or bearing at sheathing connections. Over the time, a huge number of experimental studies on the seismic response of CFS shear walls braced with sheathing board or panels have been carried out. The diversity of these experimental studies comes from the range of sheathing material: gypsum or wood panel, sheathing connections, wall geometry, etc, being used in different parts of the world. One of the outlining goals behind these experiments is always to evaluate

the design strength values for different wall configurations. Besides this, tests are also used to judge the ductility and energy dissipation capacity of the wall and propose new geometrical details based on the test results to improve the wall seismic response. Due to highly diverse and huge experimental database, only few studies are explained here, whereas others [47–53] are explained elsewhere [54].

Figure 2-6 In plane quasi static cyclic test on CFS gypsum sheathed shear walls (Deformed shape) [8]

Pioneer studies on wood and gypsum sheathed shear walls were conducted by Serrette and his colleagues, which also served as the background documents concerning guidelines of the these shear walls in North American standard for seismic design of CFS structural systems AISI S400 [18]. These studies [55–60] included the monotonic and cyclic test on full or small-scale wall assemblies with varying connection spacings, studs spacing and combination of sheathing materials on different faces of the wall. In his subsequent work, Serrette and Chau [61] also proposed formulation to estimate deflection of the shear walls that

incorporates empirical factors to account for nonlinear behaviour of different wall components.

Apart from these researches, various other researchers also explored the lateral in plane response of individual wood and gypsum sheathed shear wall specimens with double [8,62,63] or single [29,64] side sheathed or in some cases the gypsum panel combined with another type of the panel [8,29,62,65] through the monotonic [8,62–64,66] or the cyclic [8,29,62,65–67] tests. Furthermore, these experimental investigations on the seismic response of CFS gypsum sheathed shear walls revealed that the wall strength is not affected by the aspect ratio [62] and that it remains constant per unit length up until an aspect ratio of 2:1 [18] and it is a function of the individual sheathing connection strength, and it can be reasonably predicted through the analytical methods [68–70] already present in the literature for timber shear walls [65]. Moreover, the strength of the wall can be increased by increasing the thickness of the panel or by sheathing the both faces of the frame [63] and by increasing the number of sheathing connections.

A reasonable amount of research [23,52,53,71] using the monotonic or cyclic tests to predict the response of long walls with an aspect ratio (height to length ratio) as low as 0.2 has also been carried out. In some cases [52,71], wall capacities obtained from the tests on long shear walls with opening are also compared against an empirical design method known as "Perforated Shear walls" [72] for wood frame shear walls to check the method validity for CFS frame shear walls. The calculated shear capacities of walls using the empirical design method [72] appeared valid, but conservatively estimates the ultimate capacity. It was also concluded

from these tests that long, fully-sheathed shear walls were significantly stiffer and stronger but less ductile than walls with openings

One of the most significant work was done by Fülöp and Dubina [23] on the investigation of the effect of loading type (monotonic or cyclic loading), the presence of openings and interior gypsum cladding on the lateral response of shear walls. The key highlights of the research were the definition of acceptable damage levels corresponding to various performance objectives for the different configurations of tested walls. Another important work was presented by Serrette and Nolan [73], on the cyclic performance of CFS shear walls sheathed with wood panel using pins. The experimental results provided reasonable evidence on the acceptable seismic performance of this system, which supported the argument of standardizing the use of steel pins as a connecting system in CFS shear walls.

Peck et al. [62] studied the effects of blocking, intermediate fastener spacing, aspect ratio, and loading pattern on a lateral response of gypsum sheathed shear walls through monotonic and cyclic testing. They concluded that the reduction of intermediate fastener spacing can significantly improve unblocked wall capacity and enhance the post peak response of wall. Similarly, Ye et al. [45,74] studied the effect of combining layers of gypsum board with other type of board panels and the use of reinforced end studs. The results indicated that use of double layer of wall board panels significantly improves the shear capacity, and the difference in sheathing material can influence the shear behaviour of screw connections. The screws normally experience a tilting failure mechanism,

which can be restrained by the concrete in reinforced end studs, hence leading to an improved seismic behaviour.

As mentioned earlier, gypsum panels are normally combined with other type of sheathing material to have much improved seismic behaviour. Mohebi et al. [75] combined single sided steel sheathed shear walls with layers of either gypsum or fibre cement board panels, which resulted in an almost 80% increase in shear strength of the wall. Tests conducted under CFS NEES project [76] also included an extensive in plane testing program of wood (OSB) sheathed shear walls with gypsum panels present on the interior face of walls in some cases. More information on the CFS NEES project [76] is given in next section.

2.4.1.2.   Tests on building specimens

Shake-table tests provide a rational means of investigating the seismic response of any type of LFRS. Unlike the case of CFS strap braced walls which had the building specimens made entirely of the LFRS, the building specimens tested in past for CFS shear walls not only include the LFRS but also other structural elements of LWS building like gravity load bearing walls, and non-structural elements like partitions and ceiling systems.

Figure 2-7 Shake-table test on building representation of CFS gypsum sheathed shear walls [77]

A North American research project called as CFS-NEES [76] focused on how to improve the understanding and performance of CFS buildings with wood structural panels and floors was in progress for last couple of years and finished recently. The key highlight of the project was the shake-table testing of a two-storey commercial building, which demonstrated eighteen times stiffer response, due to the presence of gravity load resisting and non-structural components, than the actual designed response, calculated only considering the contribution of shear walls. In particular, the presence of gravity load resisting systems caused an increase of 4 times and the addition of non-structural elements increased further 4.5 times the lateral stiffness of the building. Another outcome from the project was the use of a ledger framing system, in which the frame of shear walls also includes a ledger track which increases the shear wall resistance

by approximately 10%, but modestly decreases its energy dissipation capacity [66].

In Europe, shake-table tests were also conducted within the ELISSA project, which included the experimental seismic performance evaluation of modular lightweight steel buildings sheathed with gypsum panels [78] (Figure 2-7). Shake-table tests on a full-scale two-storey 2.7 m × 4.7 m (plan dimensions) × 5.3 m (high) building was carried out [77]. The building was designed with a behaviour factor of 3.0 and an over strength factor of 1.8. The building was tested in two different conditions. In the first condition (bare construction), it included mainly structural components of walls, floors and roof, whereas in the second condition (complete construction) it was completed with all non-structural components. In order to evaluate the dynamic properties (fundamental vibration period and damping ratio), white-noise tests were carried out on both the bare structure and complete construction, whereas earthquake tests were conducted on the complete construction in order to evaluate the seismic performance. The main findings of this experimental activity showed that the characteristics of the building were significantly altered by the non-structural systems, with a decrease of the fundamental period of about 20%, corresponding to an increase of the lateral stiffness equal to about 4 times. The maximum inter-storey drift was very small (0.80% for 1st level and 0.52% for 2nd level) and the residual inter-storey drifts were negligible, evidencing a very modest inelastic behaviour. Floors behaved as rigid in their plane, according to the ASCE 7 [13] definition. The damage was very small in both structural parts and finishing materials. In particular, only after the earthquake tests with scaling factor more than

100%, presence of gypsum dust and small detachment of cover paper at some corner joints on the internal faces of walls was observed.

2.4.2. Numerical studies

The dynamic behaviour of CFS shear walls is characterized by a remarkable nonlinear response with a strong pinching of the hysteresis loops and degradation of the strength and stiffness in subsequent loops as shown in Figure 2-8. In past, various researchers proposed numerical models to simulate this type of response. They can be broadly categorized into equivalent truss, equivalent shell and detailed finite element (FE) models based on the approach used in their development and the resulting inherent complexity. An equivalent truss model [79–84] relies on equivalent nonlinear truss elements or linear truss elements combined with nonlinear springs to simulate the behaviour of a shear wall. A shell model [85] uses shell elements with equivalent mechanical and physical properties, which are representative of complete wall behaviour, to simulate the nonlinear behaviour of a shear wall. Detailed FE models [86–90] follow a more realistic approach by simulating the nonlinear response of a complete shear wall through modelling of main structural elements, including all individual sheathing connections, which are the main energy dissipating mechanism in walls. Following paragraphs highlight the modelling approach used in different studies for developing the numerical models for CFS shear walls.
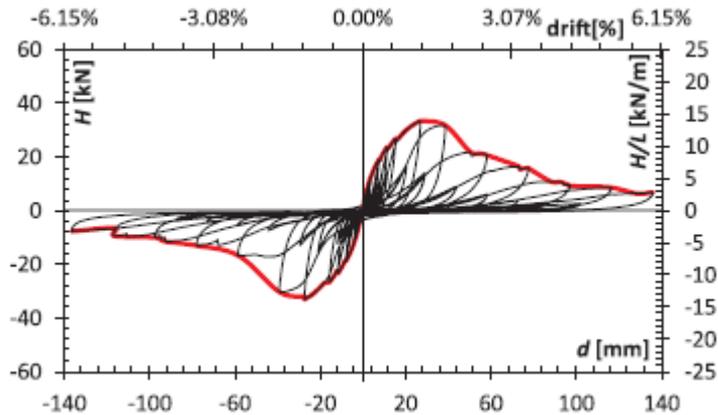
Figure 2-8 Typical hysteretic response of CFS shear wall [8]

Fülöp and Dubina [79] developed an equivalent truss model using DRAIN-3DX [91] software for CFS shear walls sheathed with corrugated steel sheets or OSB (wood) panels. They represented the nonlinear behaviour of the shear wall through pair of diagonal trusses having a fibre-hinge accommodating the desired hysteretic behaviour, which was calibrated using the experimental results [23].

Within the CFS-NEES project [76] explained in previous section, Leng at al [81] developed the computational models for the tested building structure. The models developed for the shear walls used nonlinear truss elements in a X configuration paired with an elastic wall frame, to represent the wall response under dynamic loading. In particular, *Pinching4 material* [92] was used for nonlinear truss elements, which possess the ability to simulate the pinched hysteretic response typical of CFS shear walls. In addition to using piching4 material for truss elements, they also tried to use an Elastic Perfectly Plastic material, which failed to provide better results than pinching4 material model. Moreover, for modelling the response of complete building they divided the shear walls

into the sub panels. The lateral stiffness of each individual sub panel was modelled by pair of two diagonal truss elements having a picnhing4 material.

Kechidi and Bourahla [82] presented an equivalent truss model developed in Opensees [93] software for wood and steel sheathed CFS shear walls. They used a pair of rigid truss elements in a X configuration with an equivalent non-linear *Zero Length element* in the mid of truss elements having user-defined material to represent the wall behaviour. The user defined material was a uniaxial material, which used only the physical and mechanical characteristics of the wall as input to simulate the wall hysteretic response. The criteria governing the hysteretic behaviour of the uniaxial material was selected based on relevant experimental results.

Bourahla et al. [83] presented a simple model to account for the overall lateral stiffness and strength of the shear walls in the complete building models in SAP2000 software [94]. Model used a nonlinear equivalent shear link having a pivot hysteretic model connected to rigid triangular shell elements. They achieved a quite good match in terms of comparison of dynamic properties of numerical model of complete building with the results obtained from its ambient vibration testing.

The nonlinear hysteretic response of shear walls can also be represented by a set of differential equations which define the material rule for a nonlinear spring representing the behaviour of the shear wall. One such model was presented by Nithyadharan and Kalyanaraman [84], which used Bouc-Wen-Baber-Noori [95] smooth differential model in order to simulate the response of CFS shear walls braced with calcium silicate panels.

Martinez et al. [85] followed a more simplified modelling approach by simulating the behaviour of CFS wood sheathed shear walls using an equivalent orthotropic shell elements in SAP2000 software [94]. The equivalent properties of shell elements were adjusted to account for the global behaviour of the shear wall.

Buonopane et al. [86] presented a detailed finite element model developed in OpenSees software [93] representing the main energy dissipating component (sheathing connections) in CFS wood sheathed shear walls through radially-symmetric nonlinear spring elements placed at each sheathing connection location. Rigid behaviour of OSB or gypsum sheathing panels was modelled through the *rigid diaphragm*, whereas the CFS frame was modelled using *elastic beam column elements*. *Pinching4 material* [92] was used for the nonlinear spring elements, which was calibrated based on the experimental results of sheathing connection tests.

Zhou et al. [88] developed a detailed finite element model for CFS wood sheathed shear walls in ANSYS software [43] and compared their performance against the results of monotonic tests on shear walls. They modelled the frame and sheathing with the *Shell181 element* and used coupling methods to handle the panel-to-steel profile connections that allowed only rotation in connections, restricting any translation.

Telue and Mahendran [89] also developed detailed finite element models for CFS wood sheathed shear walls for the evaluation of their monotonic response using ABAQUS [96] software. They used ABAQUS *S4R5 shell* to model the CFS frame and *B31 beam elements* to model sheathing connections.

Chu Ding [90] at Virginia Tech developed a user element (UEL) for sheathing connections in ABAQUS based on the pinching4 material available in OpenSees. Then using the developed UEL for connections, a high-fidelity model of CFS OSB (wood) sheathed shear was developed. Frame and sheathing were both modelled as shell elements. Performance of models was quite good under the monotonic loading while for cycling loading, models experienced divergence in the solution. In order to overcome this, they locked the direction of faster deformation once it enters the plastic zone, which lead to the convergence of solution.

To sum up, the models explained earlier are able to predict the in-plane static and dynamic response of CFS shear walls with good accuracy. Models developed following an equivalent truss or shell approach [79,80,84,85] use the shear wall test results for the calibration purposes. Although these equivalent models require full scale wall test data as input, their modelling simplicity allows to use them in simulating the nonlinear dynamic response of whole buildings [86,87,97,98] under given ground motions. On the other hand, detailed FE models allow the simulation of the shear wall response using the results of sheathing connection tests, but due to their high computational complexity, they cannot be used for whole building modelling.

2.5. LWS wall systems for non-structural applications

Partition walls made with a CFS frame are one of most common type of system for dividing the floor space for different functional requirements. They are normally made by attaching the gypsum-based panels to CFS frame through screws in a similar manner as of shear walls used in LWS buildings. Though in contrast to the shear walls, the metal

frame of partition walls is made of relatively thinner profiles, screws are widely spaced and the tensile anchorage is absent. Likewise, façade walls made with LWS frame elements follow a similar construction arrangement as of partitions. The main difference between the façade and the partition walls is the type of wall boards used on the exterior faces of the wall. Usually, cement-based boards which can offer improved environmental performance are used. In some cases, the façade wall can also be made of two parallel steel frames separated by a vacuum for improved environmental performance, resulting in an overall thicker façade wall (Figure 2-9).

1. 12.5 mm thick standard gypsum boards
2. Track profile (75×40×0.6 mm unlipped channel sections)
3. Stud profile (75×50×7.5×0.6 mm lipped channel sections spaced at 300 or 600 mm on centre)
4. 6×35 mm plastic dowels for fixed connections or 8×80 mm plastic dowels for sliding connections, spaced at 500 mm on centre at the wall top and bottom and 600 mm on centre at the wall ends
5. 3.5×25 mm bugle head phosphated self-piercing screws spaced at 700 mm on centre
6. 3.5×35 mm bugle head phosphated self-piercing screws spaced at 250 mm on centre
7. Paper tape fixed with gypsum-based plaster
8. Self-adhesive paper tape (only for fixed connections)

a)

1. Self-adhesive paper tape (only for fixed connections)
2. Paper tape fixed with gypsum-based plaster
3. 3.9×38 mm wafer head with full thread phosphated self-piercing screws spaced at 250 mm on centre
4. 3.5×25 mm bugle head phosphated self-piercing screws spaced at 700 mm on centre
5. 12.5 mm thick impact resistant gypsum boards
6. 12.5 mm thick standard gypsum board
7. Track profile (50×40×0.6 mm unlipped channel sections)
8. 6×35 mm plastic dowels for fixed connections or 8×80 mm plastic dowels for sliding connections, spaced at 500 mm on centre at the wall top and bottom and 600 mm on centre at the wall ends
9. Stud profile (50×50×7.5×0.6 mm lipped channel sections spaced at 300 or 600 mm on centre)
10. Track profile (75×40×0.8 mm unlipped channel sections)
11. Stud profile (75×50×7.5×0.8 mm lipped channel sections spaced at 600 mm on centre)
12. 4.2×39 mm wafer head with milling ribs zin coated self-drilling screws spaced at 200 mm on centre
13. 12.5 mm thick outdoor cement boards
14. Glass fibre tape with an alkaline-resistant coating and cement-based plaster

b)

Figure 2-9 a) Single frame partition wall b)Dual frame façade [99]

This section provides a summary of current studies available in literature on the experimental and numerical seismic characterization of LWS indoor partitions and façade. There are no studies available in literature, which use either experimental and numerical approach to characterize the seismic behaviour of individual units of LWS façades. The experimental study presented in this thesis on LWS façades is a pioneer study on this topic.

2.5.1. Experimental studies

In past, most of the researchers used quasi static cyclic and shake-table testing to characterize the seismic response of LWS indoor partition walls. The tests include the experiments on individual specimens of partitions or complete building specimens equipped with various type of non-structural components including the partitions. Tests using the shake-table or the special floor acceleration simulator (Table 2-2) on full-scale single or multi-storey buildings were carried out on the systems made of LWS indoor partition walls, outdoor façades and suspended ceilings, while in plane tests (Table 2-3) under the action of quasi-static reversed cyclic and dynamic loading protocols were carried out on wall specimens or wall specimens combined with out of plane façades. The main objectives of these studies addressed following issues: (i) dynamic identification (evaluation of fundamental frequency and damping ratio); (ii) evaluation of dynamic amplification; (iii) assessment of force vs drift curve response; (iv) effect of non-structural components on the response of the structure; (v) comparison among different constructional arrangements; (vi) damage description; (vii) comparison between experimental and analytical response; (viii) assessment of fragility curves by correlating damage states (DS) to the drift.

Very recently, with an aim to expand and improve the knowledge of seismic response of non-structural LWS drywall components, an experimental study was also conducted at University of Naples Federico II, Italy with in a project carried out with an Industrial partner: Knauf. The results from the experimental study are also used to calibrate the numerical models of partition developed in this thesis. In particular, the main objective of the study was to investigate the seismic performance of

drywall components, i.e. LWS indoor partition walls, outdoor façades and suspended ceilings. The research activity covered different topics: tests on materials and components [100,101]; in-plane [102] and out-of-plane [103] tests on partition walls; dynamic shake table tests on prototypes made of partition walls, façade walls and suspended continuous ceilings [99] (Figure 2-10).

Figure 2-10 Knauf project. a) Out-of-plane partition wall tests (tall partition wall); b) In-plane partition wall tests (Type 1 specimen); c) In-plane partition wall tests (Type 2 specimen) d) Shake-table tests

Table 2-2 Existing studies using the shake table or floor acceleration simulators

Study	No. of specimens	No. of storey	Type of test [1]	Fragility curves	DS-IDR correlation
[104]	2	1	Shake-table: X	No	No
[105]	1	4	Shake-table: X+Y	No	No
[106]	1	1	UB-NCS [2]: X	No	Yes
[107]	1	1	Shake-table: X, X+Y	No	No
[108]	16	1	UB-NCS [2]: X	Yes	Yes
[109]	1	5	Shake-table: X	No	Yes
[110]	1	2	Shake-table: X+Y	Yes	Yes
[99]	5	1	Shake-table: X	Yes	Yes

[1] X, Y: horizontal directions, [2] UB-NCS: Floor acceleration simulator [106]

Table 2-3 Existing studies on the in-plane behaviour

Authors	No. of specimens	Dimensions (width x height mm)	Type of loadings	Fragility curves	DS-IDR correlation
[111]	54	2400 x 2400	Quasi-static reversed cyclic and dynamic	No	No
[112]	4	3950 or 2975 x 2800 or x 2800	Quasi-static reversed cyclic and dynamic	No	No
[113]	16	4880 x 2440	Quasi-static reversed cyclic	No	Yes
[114]	2	2400 x 2400	Quasi-static reversed cyclic	No	No
[115]	2	3400 x 2550	Quasi-static reversed cyclic	No	No
[116]	6	5100 x 5000	Quasi-static reversed cyclic	Yes	Yes
[102]	12	2400 x 2700	Quasi-static reversed cyclic	Yes	Yes

The current state of the art on LWS façades is very limited. In fact, the only relevant study in the literature was conducted by Wang et al. [117], which included the shake table tests on five-storey reinforced concrete building equipped with LWS façades. The tested façades were not infilled in the structural elements and were connected to the floor slabs through steel clips. Different types of damages in the façades were identified along with the drifts they occurred and are classified in to different Damage states (DS-s). The study was only limited to the one type of façades, with the same type of panels, wall steel frame and connection to the surroundings on all stories. Contrarily to the study of Wang et al. [117] on façades that are not infilled, the experimental study on façades presented in this thesis explicitly focuses on the in plane seismic performance of infilled façades, and investigate the effect of different construction parameters on their performance.

It is also worth mentioning, that there are only slight differences between the LWS façades and the partitions, if they are completely infilled in a structural frame. In such cases, the only difference could be an additional finishing layer or the type of panels on the exterior faces, which are usually made of materials more resistant to outdoor environment in case of façades. To this end, one can also compare the behaviour of façades with the partitions. However, most of the studies on LWS partitions do not also focus on the individual geometrical parameters of the walls to study their effect on wall seismic performance, as it is done in this thesis for façades. The geometrical parameters investigated in the presented experiments are explained in Section 5.

2.5.2. Numerical studies

Prominent advances in the numerical modelling of hysteretic behavior of LWS partition walls made with thin steel profiles and gypsum-based panels have taken place in past to support the prediction of their seismic response. The hysteretic response of these partitions is characterized by severe pinching of force displacement cycles and degradation of strength and stiffness in subsequent loading cycles as shown in Figure 2-11.
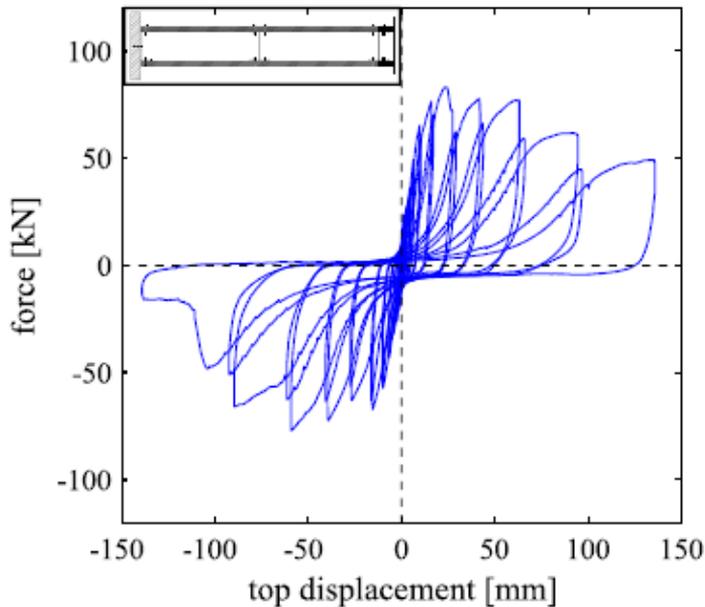
Figure 2-11 Typical LWS partition hysteretic response [118]

The models developed for the LWS partition walls in past can be grouped in two categories: simplified spring model and the detailed FE models. Simplified spring models usually relied on a single spring element lumped with the global hysteretic behaviour of the wall while the detailed FE models represented the different components of the partition wall with individual nonlinear elements of various types. The two groups of models

serve the different purpose. Simplified spring models are useful for the building level simulations and assist in a more rational building performance based seismic design (PBSD). This is mainly due to their simplicity, which allows an easy integration of them in a building model for even a large number of non-structural components. Contrarily, the detailed FE model have proven themselves handy in predicting the different damage mechanism of the walls, which subsequently can be used to develop the fragility curves of the walls for different damage states. Moreover, FE models are also used to perform parametric analyses, that can be used by researchers to invent new construction details for improving the damage fragility of the walls.

Simplified spring type models were developed by Tasligedik et al. [119], Wood and Hutchinson [120], Davies et al. [121] and Magliulo et al. [122]. The model developed by Tasligedik et al. [119] used Ruaumoko2D software [41] to simulate the experimental results of the LWS partition walls tested infilled in a special pinned reinforced concrete frame. A similar approach was followed by Davies et al. [121] in Ruaumoko2D software for the LWS partition walls tested with the out of plane return walls [123] on specially design non-structural component simulator. One of the key highlight of the study by Davies et al. [121] was the demonstration of the influence of partition walls on the dynamic properties of building through a simulation of four-story steel moment-resisting frame medical facility model equipped with the calibrated partition wall models. These analyses of the building showed that including the contribution of LWS gypsum partition walls to the lateral force resisting system increases the building collapse safety margin by 32%. Building on the same experimental database [123] as used by Davies et al. [121], Wood

and Hutchinson [120] also developed a simplified spring model in OpenSees software. In their work, they also introduced different error metrics to evaluate the accuracy of the models. The model developed by Magliulo et al. [122] was used to predict the shake-table response one storey mock-up fitted with LWS partitions.

One of the most detailed model developed ever to date was presented by Rahmanishamsi et al. [124] for LWS partition walls considering all the critical components using the OpenSees software [93]. In that model, the nonlinear behaviours of the connections were represented by hysteretic load-deformation springs, which have been calibrated using the component-level experimental data. The studs and tracks were modelled adopting beam elements with their section properties accounting for nonlinear behaviour. The gypsum boards were simulated by linear four-node shell elements. A relatively less complicated model was also developed by Petrone et al. [125] using the SAP2000 software for the LWS partitions tested by them. The frame to sheathing connections were modelled as nonlinear link elements, which was calibrated using the test results on the sheathing connections. However, the model [125] did not possess as far reaching capabilities to predict the damage mechanism in the walls as the model presented by Rahmanishamsi et al. [124].

Simplified spring model for LWS partition walls are also presented in thesis. These partitions were tested under in plane quasi-static cyclic loading in the past [102] at University of Naples "Federico II", Italy. The presented model differs with the already existing models in literature in a sense that, it also provides a set of particular parameters for the different groups of walls, which vary in terms of construction details: sliding/fixed

connections of the wall to the surrounding structural elements or the presence/absence of out of plane return walls. Though the work presented by Wood and Hutchinson [120] and Davies et al. [121] also showed simplified models for the walls with similar groups as in this case, but the principal difference is the presence of the building structural elements on the sides of the tested partitions, which were not present for the walls tested in [120,121] and used for subsequent model calibration. Sliding connections to the surrounding structural elements [102] are usually provided in the walls to allow them to accommodate lateral drifts in earthquakes without causing major damages. A typical practice is to provide these connection only on the wall top, while the walls tested in [102] and modelled here as shown in Section 6 also had the sliding connections on the sides to accommodate much higher wall drifts, which makes the models presented in this thesis also different from the other models [119–122], which do not have the modelled wall configurations with sliding connections on sides too.

2.6. FEMA methodology

Behaviour factor plays a vital role in the seismic design of a building following the capacity design approach. It allows the designer to reduce the seismic actions by a factor greater than one, which accounts for building inherent ductility and over strength. Behaviour factor for any structural system can be evaluated preliminary through either a test-based approach or a numerical analysis. However, as highlighted by Macillo et al. [8], test-based methodology does not explicitly consider the load-deformation hysteresis "shape", characterized by the pinching for CFS wall systems. A more elaborate methodology to evaluate the behaviour factor is outlined by FEMA document P695 [12], which uses nonlinear

analysis techniques, and explicitly considers uncertainties in ground motion, modelling, design, and test data to achieve an acceptably low probability of collapse of the building equipped with the LFRS. Methodology has been used in past for different LWS structural typologies, like CFS steel sheathed shear walls [97,98], CFS special bolted moment frames [126] and CFS strap-braced walls [40]. The use of this methodology is extended to CFS strap-braced walls, CFS gypsum sheathed shear walls and CFS wood sheathed shear walls in this thesis to evaluate their behaviour factor according to European design philosophy. The methodology has already been applied to CFS strap braced walls to evaluate their response modification factor for Canadian design by Comeau et al. [40]. However in [40], the design approach used to design archetypes followed the Canadian design philosophy, which is different than the European design philosophy and hence the evaluated value of R cannot be used as behaviour factor in Eurocodes. Moreover, the model developed by Comeau et al. [40] were stick model which neglected the overall three dimensional building behavior having CFS strap braced walls both at perimeter and inside the building, gravity studs, floors etc.

ATC 63 Federal Emergency Management Agency (FEMA) report entitled P695 "Quantification of Building Seismic Performance Factors" [12] provides the standard procedural methodology to quantify the seismic performance of a lateral force resisting systems. Figure 2 shows the general framework of the methodology. This methodology has been written in compatibility with the United States construction standards therefore it is tailored, wherever necessary, to be used with European construction standards: Eurocodes in this thesis. Methodology (Figure 2-12) follows an iterative approach by assuming an initial value of behaviour factor (q) for

the design of set of archetypes, whose performance is quantified through non-linear static analysis and non-linear dynamic collapse simulations under a suite of earthquake records and their safety is evaluated in terms of acceptable collapse margin ratios. Methodology then defines the acceptable performance criteria for the archetypes, which must be fulfilled in order to confirm the initial assumption of behaviour factor and the adopted design method. Chapter 3 and 4 explain in detail each step of the methodology followed for the investigated LFRS-s.
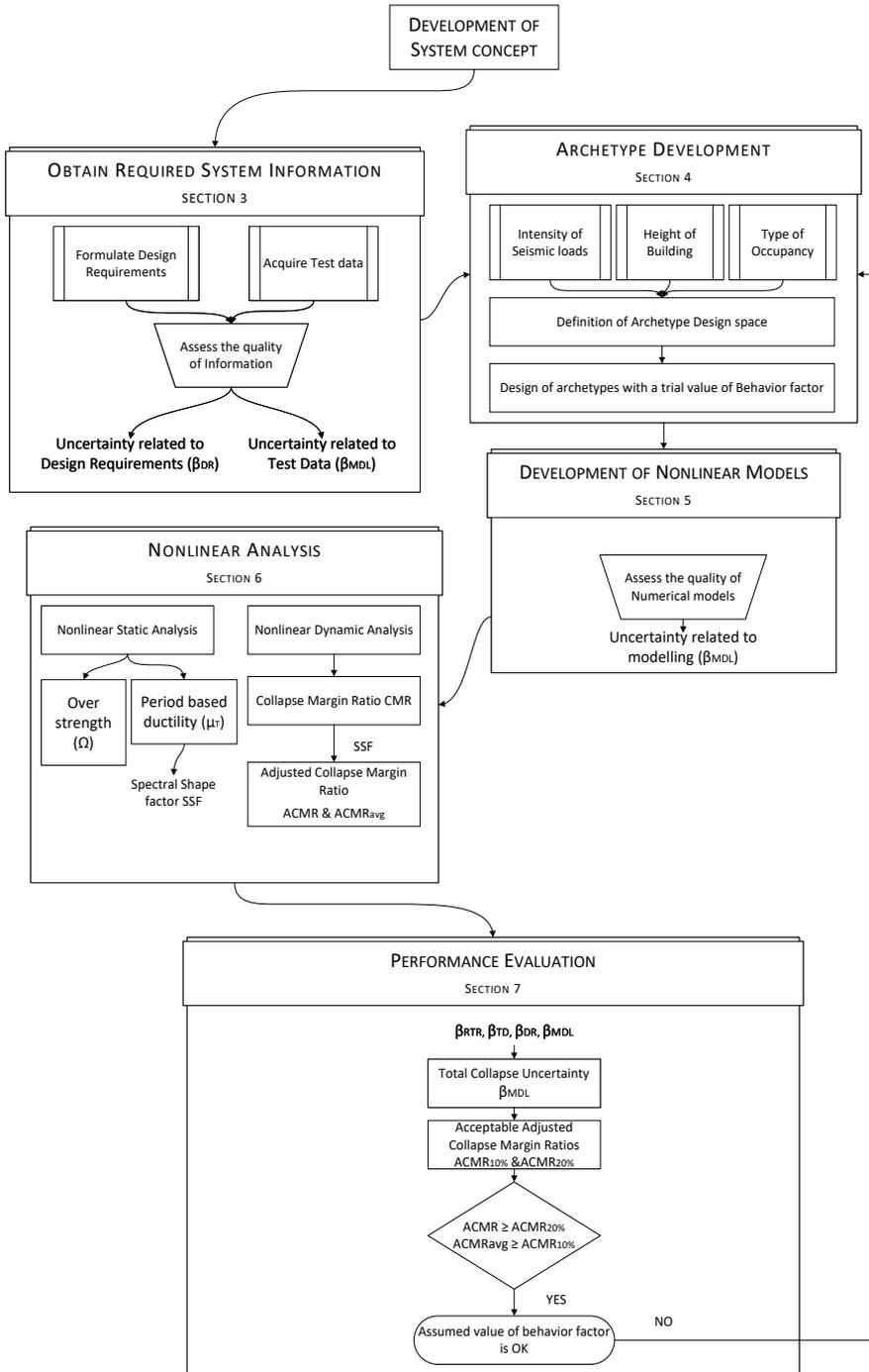
Figure 2-12 General framework of FEMA P695 methodology (Section numbers are the corresponding numbers in [12]*)*

The last step in the methodology is the performance evaluation of the archetypes, which is used to establish the acceptability of trial value of behaviour factor used in the design. This step uses the input parameters from various previous steps of the methodology, hence making it more complex to understand. Therefore, this step is further illustrated with an in-depth diagram (Figure 2-13) showing the function of different parameters used in the step.
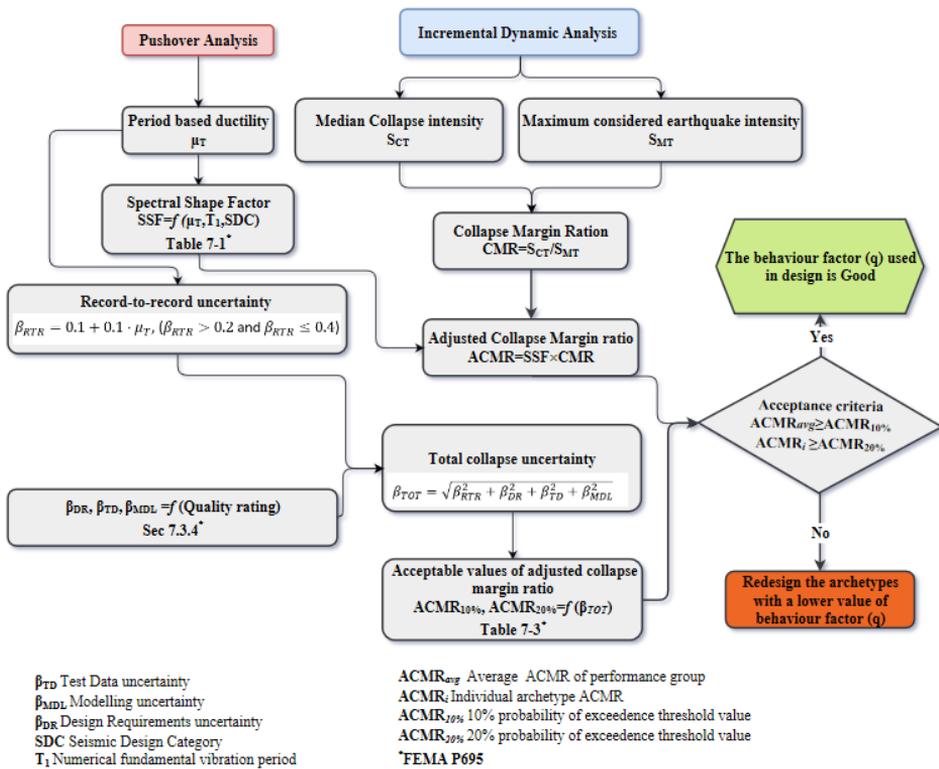
Figure 2-13 Overview of performance evaluation process

3. Seismic performance evaluation of LWS buildings with CFS strap-braced walls

CFS strap-braced stud wall (Figure 3-1) is an all-steel solution against the action of lateral forces on low to mid rise LWS buildings. Current edition of European earthquake design standard: EN 1998-1 [4] does not provide any seismic design guidelines for LWS buildings with CFS strap-braced walls as the main LFRS. Though there is an alternative approach to design such buildings by considering them a traditional hot rolled X-braced frame as explained in Section 2.1.1 but that approach certainly does not make use of any energy dissipation capacity of the building and will result in a structure with a limited ductility. This section judges the suitability of the proposed design method and a behaviour factor for CFS strap-braced walls using the FEMA P695 methodology [12], which is explained in Section 2.6. The arrangement of subsections in this chapter follows the order of different steps in the methodology (see Figure 2-12). The initial step of the methodology involves the development of system concept, which focuses on understanding the functioning of the investigated LFRS and is explained in Section 2.3. The next step involves the explanation of the experimental data and the design method. The utilized test data is

explained alongside the modelling of single wall response (Section 3.2.1), while the design method is illustrated in Section 3.1.4.
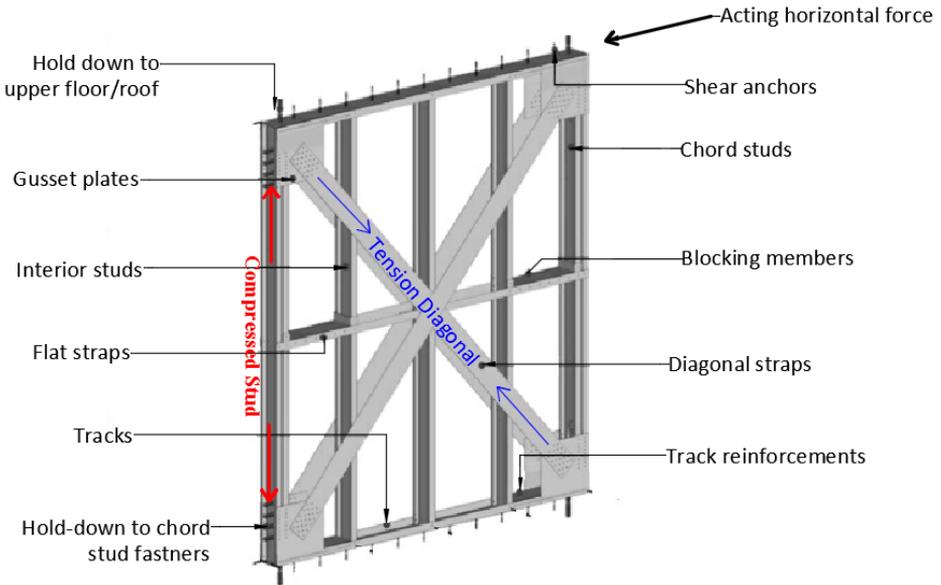
Figure 3-1 Typical Configuration of CFS strap-braced stud wall

3.1. Archetypes selection and design

FEMA P695 [12] methodology requires to define a set of structural system archetypes. An archetype is a "Prototypical representation of a seismic force resisting system". A set of archetypes which represent a range of design parameters and building configurations is called Archetype design space. Furthermore, methodology requires to divide the Archetype design space into performance groups based on the major differences in Structural configuration and gravity loads.

An Archetype design space comprising of 14 archetype buildings differing in location, height, plan configuration and type of occupancy is

defined. Complete design space is considered as one performance group because archetypes do not represent significant changes in the structural configuration and gravity loads, that could affect the behaviour of LFRS (CFS strap-braced walls). Table 3-1 lists all of the archetypes included in the design space. The difference of archetypes in terms of occupancy, height and the intensity of seismic loads are further explained in upcoming subsections.

Table 3-1 Archetype design space CFS strap-braced walls (q=2.5)

Archetype ID	Type of Occupancy	Number of Storeys	Seismic Loads Intensity
R2L	Residential	2	Low
R2M			Medium
R2H			High
R3L		3	Low
R3M			Medium
R3H			High
R4L		4	Low
R4M			Medium
O1L	Office	1	Low
O1M			Medium
O1H			High
O2L		2	Low
O2M			Medium
O2H			High

3.1.1. Type of Occupancy

Archetypes are categorized in to residential or office type occupancies. The choice of occupancy affects the live load acting on the floors. In Europe, EN 1991-1-1 [127] provides live loads for different type of occupancies of buildings. A value of 2.0 KN/m^2 and 3.0 KN/m^2 is prescribed for floors of residential and office buildings respectively. In case of roof, live loads depend on the accessibility of roof. In case of residential archetype, roof is considered accessible, which resulted in a live

load of 2.0 KN/m^2. For office archetypes, roof is considered not accessible except for normal maintenance and repair, which resulted in lower value of 0.4 KN/m^2 for live loads on roof. Figure 3-2 shows the typical plan of residential and office archetypes designed for medium intensity seismic loads. The number and position of CFS strap-braced stud walls corresponds to three storeys residential and two storeys office archetypes.
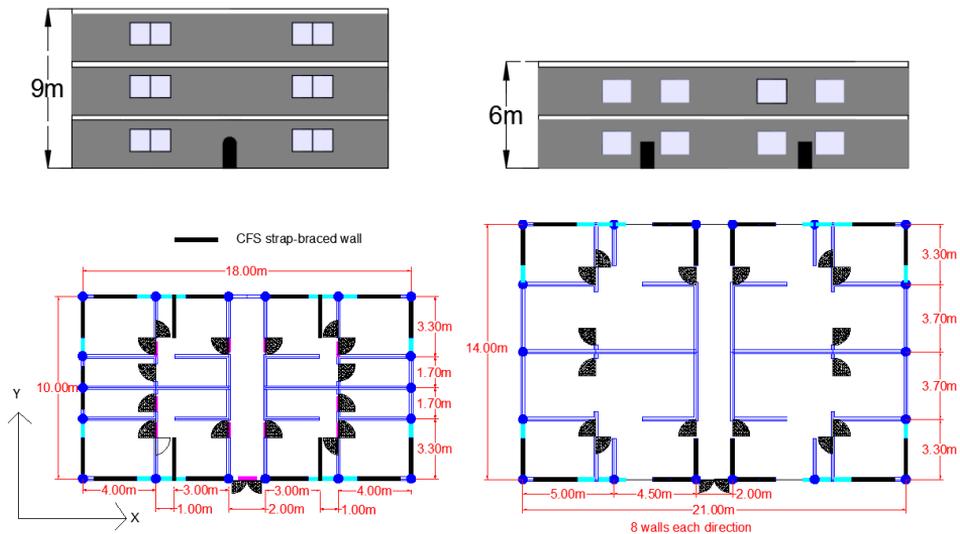
Figure 3-2 Plan and Elevation of a) Three storey residential archetype designed for medium intensity seismic design loads b) Double storey office archetype designed for medium intensity seismic loads

3.1.2. Height of buildings

Cold-formed steel elements are used in low to mid rise LWS buildings. This trend is reflected in the selection of archetypes in current study by limiting the maximum height of archetype to 12 m. Maximum height limitation is confirmed later in the design process of archetypes, when a 12 m archetype situated in a high seismic location resulted in an

excessive base shear, which could not be resisted by the highest strength CFS strap-braced walls used in this study. Keeping in view the height limitations, one, two, three and four storey archetypes are defined. The total storey height is 3.0 m, including 2.7 m high walls and 0.3 m thick floors.

3.1.3. Intensity of Seismic loads

Archetypes buildings are assumed to be located in three locations with low, medium and high seismicity. Low, Medium and High seismic locations have a reference peak ground acceleration ($a_{g,R}$) with 10% probability of exceedance in 50 years of 0.15g, 0.25g and 0.35g, respectively. Soil class C is assumed for all locations. Archetype design space comprised of only residential and office buildings which can be classified as ordinary buildings according to EN 1998-1 [4]. Therefore, an important class of II is assigned to all archetypes. Design peak ground acceleration (a_g) for each location was computed using equation (3-1):

$$a_g = a_{g,R} \cdot \gamma_I \tag{3-1}$$

where γ_I is importance class of building and has a value of 1.0 for ordinary buildings. An initial assumption of a value of 2.5 for the behaviour factor is made based on experimentally evaluated q values by Iuorio et al. [7]. Finally, design response spectrum is defined based on the guidelines of EN 1998-1 [4].

FEMA P695 [12] is written in consensus with United States Loading provisions for Building structures (ASCE 7 [13]), which defines the earthquake loading in terms of Seismic Design Category (SDC). In contrast to seismic loads defined according to No-collapse and Damage

Limitation requirement of EN 1998-1 [4], ASCE 7 [13] defines two levels of earthquake: Design Earthquake (DE) and Maximum Considered Earthquake (MCE). DE is defined in ASCE 7 [13] as 2/3 times of MCE, while MCE is defined as the earthquake having 2% probability of exceedance in 50 years, i.e. a return period of 2475 years. According to some studies [128], DE can be considered as an earthquake of 10% probability of exceedance in 50 years for some areas in United States, which corresponds to No-collapse requirement of EN 1998-1 [4]. Since FEMA P695 methodology uses MCE in its formulations, therefore it is necessary to define a level similar to MCE for locations used here for the archetypes, which can be obtained by simply multiplying the elastic response spectrum of EN 1998-1 by 1.5. Figure 3-3 shows the three design response spectrums of EN 1998-1 used in this study and the Seismic Design categories (SDC) of ASCE 7 based on the Design Earthquake (DE). All three seismic loads intensities in this study can be categorized as SDC D (min) to SDC D (max).
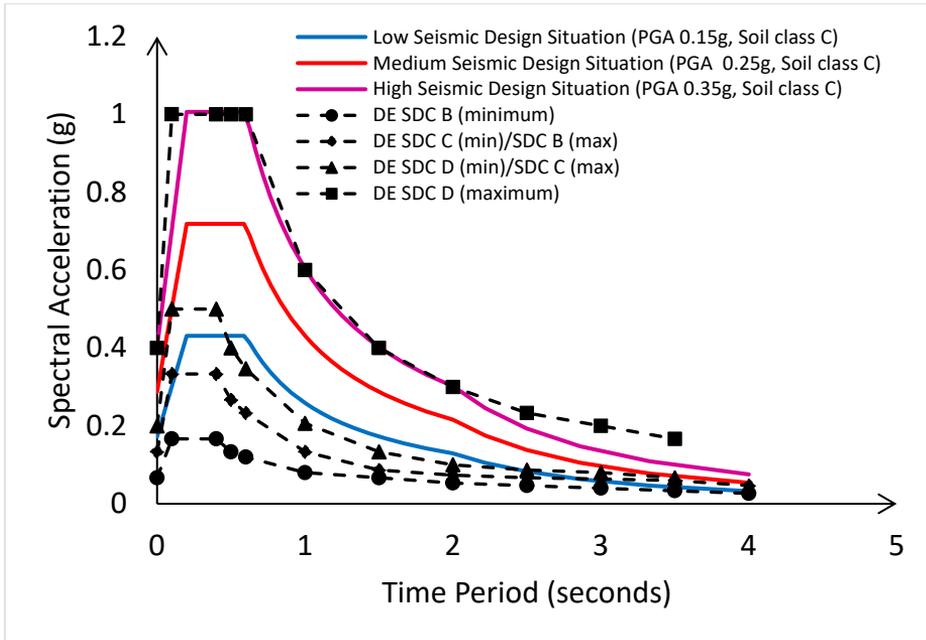
Figure 3-3 Comparison of the Elastic Design Response Spectrum of EN 1998-1 and the Seismic Design Categories based on Design Earthquake of ASCE 7 for archetypes with CFS strap-braced walls

3.1.4. Design of Archetypes

Design of all archetypes is carried out according to the relevant parts of Eurocodes. Gravity loads comprised of dead load of the structure itself (Table 3-2), live loads due to the occupancy of the structure stated in Section 3.1.1, a constant snow load of 1.0 KN/m^2 and a constant suction wind load of 0.35 KN/m^2 on roof. Gravity loads are then combined according to the fundamental combinations of EN 1990 [129]. In order to resist the gravity loads, a composite structural scheme made of cold-formed steel trapezoidal sheathing with light weight concrete and a steel mesh reinforcement is adopted for the roof and floors. Lipped channel cross sections made of Continuous hot dip zinc coated carbon steel sheet of structural quality S350GD+Z (f_y: 350MPa;f_u: 420MPa) are used for

joists and studs, which are spaced 600 mm apart. Table 3-3 lists the dimension of cross sections used for the joist and stud elements. Design of all gravity load resisting elements is carried out in accordance with the prescriptions of EN 1993-1-1 [130] and EN 1993-1-3 [14].

Table 3-2 Dead loads for archetypes

DEAD LOADS (kN/m^2)		
Floor Loads		
Concrete and Cold-Formed profile for slab		1.97
Finishes	Flooring (0.2 kN/m^2) Floating Concrete (0.48 kN/m^2) Internal Partitions (0.8 kN/m^2)	1.48
Joist		0.16
Ceiling		0.10
Total		3.71
Roof Loads		
Concrete and Cold-Formed trapezoidal sheathing for slab		1.97
Finishes	Flooring (0.2 kN/m^2) Floating Concrete (0.48 kN/m^2) Isolation and Roofing Water Proof (0.2 kN/m^2)	0.88
Joist		0.16
Ceiling		0.10
Total		3.10
Wall Internal		
Stud and Track		0.20
Gypsum Wall board		0.20
Insulation		0.05
Total		0.55
Wall External		
Stud and Track		0.20
Insulation and Plaster		0.14
Cover Plaster board		0.16
Gypsum wall board		0.10
Total		0.60

Table 3-3 Cross section dimensions of gravity load resisting elements

Structural Element	Cross section dimensions [a]		
Joists	Residential Archetypes		C 300x50x10x3 mm
	Office archetypes		C 300x50x10x3.5 mm
Studs	Residential Archetypes	1st and 2nd storey	C 150x50x20x3 mm
		3rd and 4th storey	C 150x50x20x1.5 mm
	Office archetypes	1st storey	C 150x50x20x3 mm
		2nd storey	C 150x50x20x1.5 mm

a.   *C-section: outside-to-outside web depth* x *outside-to-outside flange size* x *outside-to-outside lip size* x *thickness*

For the earthquake design of Archetypes, EN 1998-1 [4] is used in conjunction with design formulas for CFS strap-braced stud walls presented in [131]. Lateral loads on the archetypes compose of earthquake loading and a wind load of $0.7\ KN/m^2$ acting on the outside walls. Earthquake loads were always the leading action and hence were never combined with wind actions. EN 1990 [129] combination of actions for seismic design situation (equation (3-2)) is used for earthquake design of archetypes.

$$G_k + \psi_{E,i} \cdot \varphi \cdot Q_K + A_{Ed} \qquad (3\text{-}2)$$

where, G_k is the dead load of building; $\psi_{E,i}$ and φ are the combination coefficients having a value of 0 and 1 for roof and 0.3 and 0.5 for floors, respectively; Q_K is the variable action, which is a live load for all archetypes, and A_{Ed} is the design value of seismic action. Since all of the archetypes followed the criteria of regularity in plan and elevation of

EN 1998-1 [4], therefore lateral force method is used to compute equivalent earthquake horizontal forces. Design base shear (V_d) for each archetype is calculated according to equation (3-3)

$$V_d = S_d(T_1) \cdot m \cdot \lambda \qquad (3-3)$$

where T_1 is the fundamental period of vibration of building approximated according to equation 4.6 of EN 1998-1 [4] ($T_1 = C_t H^{\frac{3}{4}}$, with $C_t = 0.05$ and H = building height); $S_d(T_1)$ is the ordinate of the elastic design spectrum (see Figure 3-3) at period T_1; m is the total seismic mass of building; λ is a correction factor. Fundamental period of vibration T_1 was equal to 0.11, 0.19, 0.26 and 0.32 seconds for one, two, three and four storey archetypes, respectively. Design base shear was then distributed over the height of building using equation (3-4).

$$F_i = V_d \cdot \frac{(z_i m_i)}{\Sigma z_j m_j} \qquad (3-4)$$

where F_i is the horizontal force acting on i^{th} storey; m_i and m_j are the seismic masses of ith and j^{th} storeys respectively; z_i and z_j are the heights of the masses m_i and m_j above the level of application of the seismic action, respectively. In order to account for the accidental torsional effects in buildings, EN 1998-1 [4] requires to multiply the forces obtained from equation (3-4) by a factor δ computed according to equation (3-5).

$$\delta = 1 + 0.6 \cdot \frac{x}{L_e} \qquad (3-5)$$

where x is the distance between walls located at the perimeter of building to the centre of mass of the building in plan, measured perpendicularly to the direction of the seismic action and L_e is the distance

between the two outermost walls, measured perpendicularly to the direction of the seismic action. The computed value of δ was 1.3.

Lateral resistance to seismic loads is provided through CFS strap-braced walls. Three wall configuration of low (W1), medium (W2) and high (W3) dissipative capacity are designed following the formulations proposed in [131] and listed in Table 3-4.

Table 3-4 Design wall strength associated to each wall component

Strength of the wall component	Failure modes	Design Formula
$H_{c,c}$- wall strength associated to the diagonal to strap connection	Bearing failure in the strap-$F_{b,Rd}$ Shear failure of a screw-$F_{v,Rd}$	$n_d \cdot n_s \cdot \min\left(F_{b,Rd}, F_{v,Rd}\right) \cos$
$H_{c,d}$ -wall strength associated to the yielding of the diagonal strap	Yielding of a steel strap-$N_{pl,Rd}$ Net section failure of a strap-$N_{u,Rd}$	$n_d \cdot \min\left(N_{pl,Rd}, N_{u,Rd}\right) co$
$H_{c,g}$- wall strength associated to the net section failure of the gusset plate	Net section failure of a gusset plate-$F_{n,Rd}$	$n_d \cdot F_{n,Rd} \cos\theta$
$H_{c,s}$- wall strength associated to the buckling of the studs	Buckling of a chord stud-$N_{s,Rd}$	$\dfrac{N_{s,Rd} - N_{Ed,G}}{h} L$
$H_{c,t}$- wall strength associated to the buckling of the track	Buckling of a track-$N_{t,Rd}$	$N_{t,Rd}$
$H_{c,a}$- wall strength associated to the tension and shear anchors	Strength of a tension anchor-$N_{a,Rd}$ Strength of a shear anchor-$V_{a,Rd}$	$\min\left(\dfrac{N_{a,Rd} + N_{Ed.G}}{h} L;\ n_a V_{a,Rd}\right)$

n_d is the total number of straps in tension; n_s is the total number of screws in a strap-to-frame connection; $N_{Ed,G}$ is the axial force due to gravity loads; θ is the angle of strap with respect to horizontal; L is the length of the wall; H is the height of the wall

For each wall component, one or more failure mechanism can be identified and then strength associated with the weakest failure mode define the design lateral strength of the wall. Therefore, the lateral design strength of the wall (H_c) can be computed according to Equation (3-6):

$$H_c = \min (H_{c,c}, H_{c,d}, H_{c,g}, H_{c,s}, H_{c,t}, H_{c,a}) \qquad (3\text{-}6)$$

Same lateral resistance was provided in both directions of archetypes through use of same number and type of walls. Table 3-5 lists the structural elements used for W1, W2 and W3 walls, while Table 3-6 lists the design values of lateral wall strength associated to each wall component. Table 3-7 summarizes the number and type of wall configuration placed in both directions per storey of each archetype.

Table 3-5 Structural elements used for W1, W2 and W3 CFS strap-braced stud walls

	W1	**W2**	**W3**
Width x Height	2400x2700 mm	2400x270 0mm	2400x270 0mm
Chords studs	Back to back channel section (S350) C150x50x20x1.5 mm [a]	Back to back channel section (S350) C150x50x20x3 mm [a]	Back to back channel section (S350) C150x50x20x3 mm [a]
Straps	70x2mm[b] (S235)	140x2mm[b] (S235)	170x2.5mm[b] (S235)
Diagonal to frame connection	No.15 4.8 x 16 mm screws [c]	No.25 6.3 x 40 mm screws [d]	No.35 6.3 x 40 mm screws [d]
Tension anchors	M24 class 8.8 bolt rods	M24 class 8.8 bolt rods	M24 class 8.8 bolt rods
Shear anchors	M8 class 8.8 bolts spaced at 300 mm on centre	M8 class 8.8 bolts spaced at 300 mm on centre	M10 class8.8 bolts spaced at 300mm on centre
Hold down to chord stud fastener	4 M16 class 8.8 bolts	4 M16 class 8.8 bolts	4 M20 class8.8 bolts

a.   *C-section: outside-to-outside web depth* x *outside-to-outside flange size* x *outside-to-outside lip size* x *thickness.*
b.   *Width* x *thickness.*
c.   *Nominal diameter* x *length, modified truss head self-drilling screws.*
d.   *Nominal diameter* x *length, hexagonal flat washer head self-drilling screws.*

Table 3-6 Design values of lateral wall strength associated to each wall component of CFS strap-braced stud wall

Strength Associated with each component	W1 Design Resistance (kN)	W2 Design Resistance (kN)	W3 Design Resistance (kN)
$H_{c,d}$[a]	42.84	85.68	130.60
$H_{c,c}$[b]	74.07	146.80	221.30
$H_{c,g}$[c]	110.13	173.29	212.3
$H_{c,s}$[d]	137.53	346.81	346.81
$H_{c,d}$[e]	110.50	323.98	323.98
$H_{c,a}$[f]	69.77	112.44	176.81
H_c[g]	42.84	85.68	130.60

a.   wall strength associated to the yielding of steel straps.
b.   wall strength associated to the diagonal to strap connection
c.   wall strength associated to the net failure of strap connections
d.   wall strength associated to the buckling of studs
e.   wall strength associated to the buckling of tracks
f.   wall strength associated to the tension and shear anchors
g.   Design wall strength

Table 3-7 Number and type of wall configuration placed in both directions per storey of each archetype

High Seismic Loads				Medium Seismic Loads				Low Seismic Loads			
Storey	Storey Shear (KN)	Wall Configuratio	No. of walls	Storey	Storey Shear (KN)	Wall Configuratio	No. of walls	Storey	Storey Shear (KN)	Wall Configuratio	No. of walls
R2H				R2M				R2L			
1	681	W2	8	1	486	W2	6	1	291	W2	4
2	398	W2	8	2	284	W1	6	2	170	W1	4
R3H				R3M				R3L			
1	1096	W3	10	1	783	W3	8	1	469	W2	6
2	881	W3	10	2	629	W2	8	2	377	W2	6
3	452	W2	10	3	323	W1	8	3	193	W1	6
				R4M				R4L			
				1	1072	W3	10	1	643	W2	8
				2	951	W3	10	2	570	W2	8
				3	707	W2	10	3	424	W2	8
				4	342	W1	10	4	205	W1	8
O2H				O2M				O2L			
1	1108	W3	10	1	792	W3	6	1	475	W2	6
2	639	W2	10	2	457	W2	6	2	274	W2	6
O1H				O1M				O1L			
1	495	W2	6	1	353	W2	6	1	212	W1	6

3.2. Non-linear Model Development for Archetypes

OpenSees [93] software is used to develop the non-linear models for the designed archetypes. A 3D model for each archetype was developed. Initially, models of single walls are developed based on already available experimental data [7] and their ability to accurately capture hysteretic behaviour was evaluated. Then, these models are used to develop complete 3D model of archetypes and analysed using Incremental dynamic analysis procedures [132] for performance evaluation.

3.2.1. Models of Single walls

A non-linear model was developed for each configuration of CFS strap-braced stud wall shown in Table 3-5. W1 and W2 walls have the same design characteristics as that of WLD (Figure 3-4 a) and WHD (Figure 3-4 b) walls tested by Iuorio et al. [7]. Therefore, their experimental results are relied on to calibrate the models. Iuorio et al. [7] tested three configurations (twelve tests) of CFS strap braced stud walls designed according to elastic (non-dissipative) and dissipative design approaches. Walls lateral response is investigated by carrying out tests under monotonic and cyclic loading. Additionally, they performed several tests on steel materials, elementary connections and joints between strap and gusset plate in order to study the component influence on global wall behaviour.

a): WLD
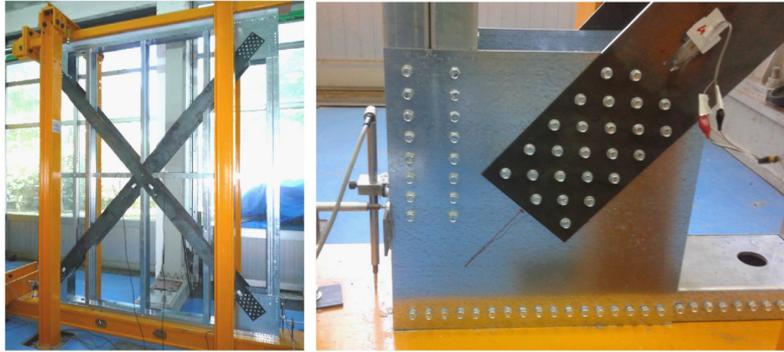
b): WHD

Figure 3-4 general view and corner detail of walls tested by Iuorio et al.[7].

Figure 3-5 shows the generic OpenSees model developed for the walls. Truss element with a Uniaxial elastic material is used to represent the chord studs. Chord stud failure due to tension or global buckling is simulated using OpenSees MinMax material in conjunction with uniaxial elastic material. Threshold values of strains in MinMax material, which govern the occurrence of failure of studs in tension ($\varepsilon_{t,Rk}$) and compression ($\varepsilon_{b,Rk}$) are calculated using equation (3-7) and (3-8).

$$\varepsilon_{t,Rk} = \frac{N_{t,Rk}}{A \cdot E} \qquad\qquad (3\text{-}7)$$

$$\varepsilon_{b,Rk} = \frac{N_{b,Rk}}{A \cdot E} \tag{3-8}$$

where, $N_{t,Rk}$ and $N_{b,Rk}$ are the nominal resistances corresponding to the tensile and buckling failure of chord studs., respectively, E is the Young's modulus of steel and A is gross cross section area. $N_{t,Rk}$ and $N_{b,Rk}$ are obtained according to prescriptions given in EN 1993-1-1 [130] and EN 1993-1-3 [14]. The buckling resistance of chord studs $N_{b,Rk}$ is calculated considering the minimum of in plane and out of plane flexural, and flexural-torsional buckling resistance.
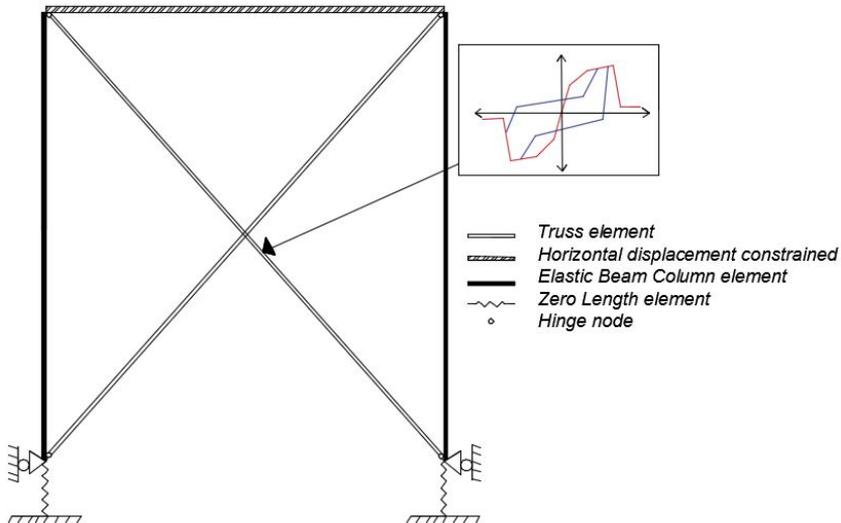
Figure 3-5 Generic OpenSees model for CFS strap-braced stud wall

Truss elements having Pinching4 material is used to model straps, which are the main source of energy dissipation in CFS strap-braced walls. More details about the calibration of strap's pinching4 material will follow in Section 3.2.2. Zerolength elements of a unit area are modelled at the bottom of stud's end in order to add stiffness contribution of the hold down anchors to foundation or floor. ElasticMultiLinear material with a stiffness

of 30 kN/mm in tension, defined on the basis of experimental results [7] and a very high stiffness (10,000 kN/mm) in compression is used for Zerolength elements. Tensile failure of anchors is captured by using OpenSees MinMax material in conjunction with ElasticMultiLinear material. Tensile strain in MinMax material for anchors is set to not exceed the nominal tensile strain $\varepsilon_{a,Rk}$ of anchors preventing any tensile rupture in them while there is no strain limit in compression. Nominal tensile strain in anchors $\varepsilon_{a,Rk}$ is calculated using equation (3-9):

$$\varepsilon_{a,Rk} = \frac{N_{a,Rk}}{k_a} \qquad\qquad (3\text{-}9)$$

where $N_{a,Rk}$ is the nominal tensile resistance of anchors and k_a is the stiffness of tension anchor equal to 30kN/mm. In order to check consistency of the developed model against the test results, non-linear quasi static analysis using cyclic load is performed. Same cyclic protocol as used in the reference tests [7] is imposed at the top of walls. Figure 3-6 shows the force vs displacement response curves and cumulative energy dissipation of developed single wall models for W1, W2 and W3 configuration against their respective experimental results.
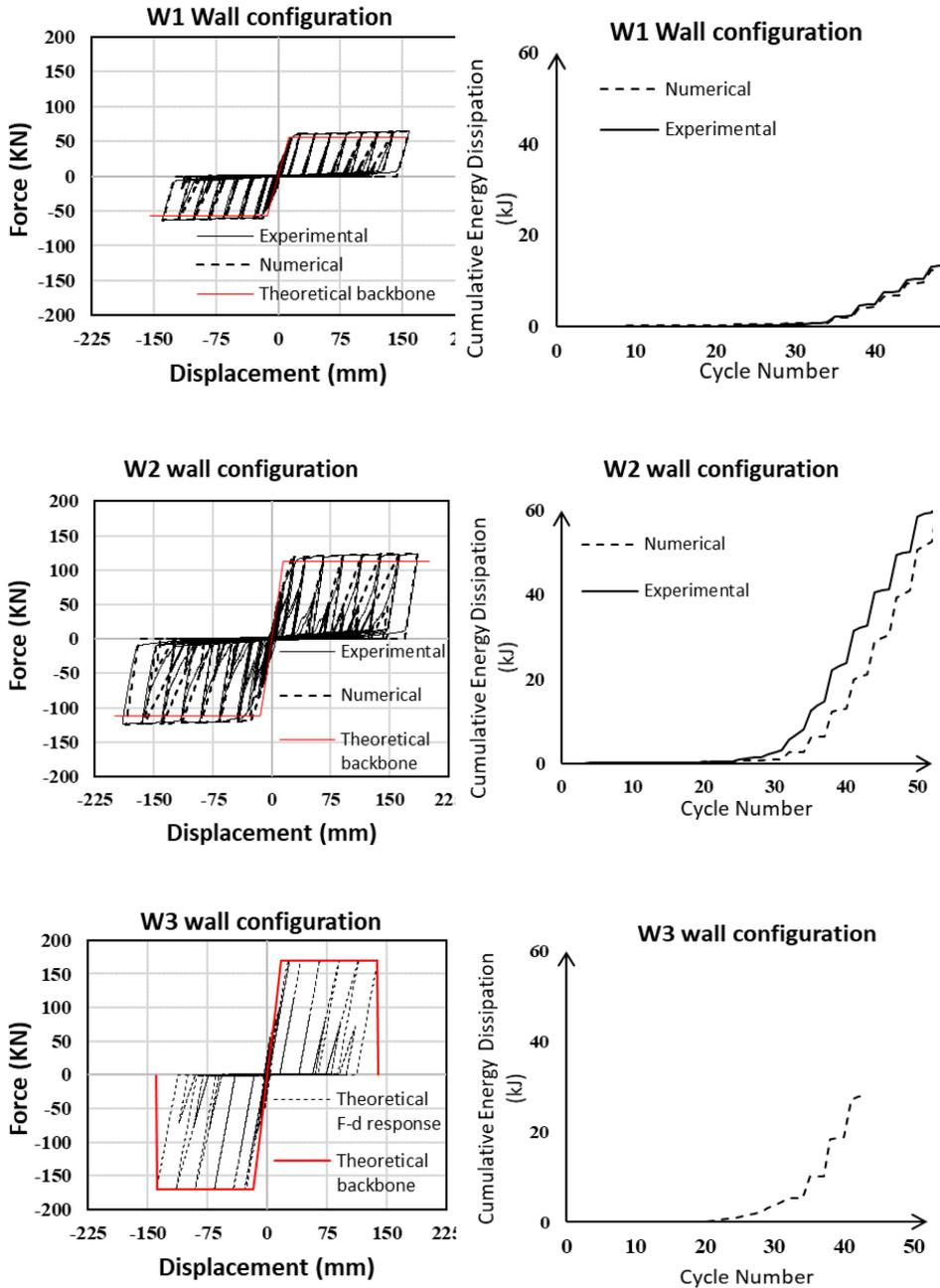
Figure 3-6 Comparison of hysteretic behaviour and cumulative energy dissipation of numerical models against their respective experimental results along with their backbone envelopes

3.2.2. Hysteretic characterization

Behaviour of CFS strap-braced stud walls is characterized by pinched hysteretic response which is captured using pinching4 material [92]. Pinching4 material is a uniaxial material that can represent pinched load deformation response with an ability to exhibit degradation under cyclic loading, defined through a set of 39 parameters. These parameters include 16 parameters for the definition of the backbone envelope (ePf1, ePd1, ePf2, ePd2, ePf3, ePd3, ePf4, ePd4, eNf1, eNd1, eNf2, eNd2, eNf3, eNd3, eNf4, eNd4), 6 parameters for defining the cyclic behaviour (uForceP, uForceN, rDispP, rDispN, rForceP, rForceN), which are the ratios of the deformation at which unloading/reloading occurs to the maximum (d_{max})/minimum (d_{min}) historic deformation demand, 5 parameters for governing the strength degradation (gF1, gF2, gF3, gF4, gFLim), 5 parameters for controlling the unloading stiffness degradation (gK1, gK2, gK3, gK4, gKLim), 5 parameters for controlling the reloading stiffness degradation (gD1, gD2, gD3, gD4, gDLim), and 2 parameters for limiting the maximum degradation in each cycle (gE, dmgType). In particular, the 4-point backbone envelope is defined considering an average envelope curve obtained considering the positive and the negative branches. Therefore, symmetric values of these parameters are used for both the positive and the negative branches and only 8 independent parameters are defined (ePdi=eNdi, ePfi=eNfi). Similarly, symmetric values of the parameters defining the cyclic behaviour are also used for both the positive and negative branches of hysteretic path. The key parameters of the material are illustrated in Figure 3-7. These parameters are selected based on the available experimental results [7]. In particular, experimentally calibrated 4-points multi-linear backbone envelope in both positive and negative directions define the material law. Cyclic parameters are selected and calibrated in a way to achieve good

match with respect to experimental results [7], in terms of force vs. displacement relationship and dissipated energy.
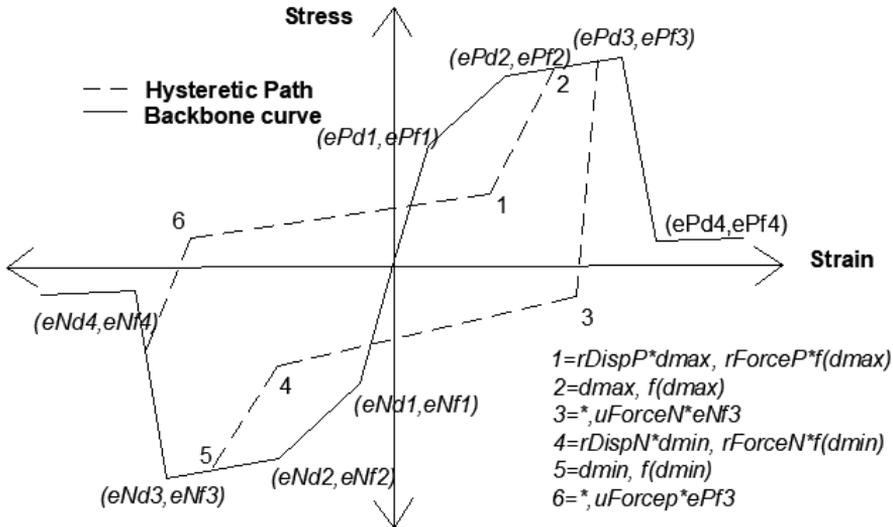
Figure 3-7 OpenSees definition of Pinching4 material

Since there is no experimental data available for W3 wall configurations, therefore its backbone curve is predicted theoretically based on the wall strength and the stiffness, evaluated according to the procedure described in [131] and using the experimental mechanical properties of materials and components obtained in [7]. In particular, the first point of the theoretical backbone curve is positioned at the middle of the elastic branch defined by the theoretical predicted stiffness, whereas the second point is positioned at the end of elastic branch, defined by the theoretical predicted wall strength. The third point is defined by the theoretical predicted wall strength and a displacement corresponding to the 5% of the inter-storey drift ratio. Finally, the fourth point defines the

vertical drop of strength after the displacement corresponding to the 5% inter-story drift ratio. The parameters governing cyclic behaviour of W3 wall (uForce, rForce and rDisp) are same as that of W2 wall. The accuracy of the theoretical procedure to predict wall response is validated by applying the same procedure to W1 and W2 wall, for which there were experimental results [7] already available. Table 3-8 shows the comparison of theoretical stiffness and strength for W1, W2 and W3 wall in comparison with their available experimental values.

Table 3-8 Comparison of theoretical and experimental wall strength and stiffness

Wall type	$H_{c,exp}$[a] (kN)	$H_{c,th}$[b] (kN)	$H_{c,th}/H_{c,exp}$	k_{exp}[c] (kN/mm)	k_{th}[d] (kN/mm)	k_{th}/k_{exp}
W1	60	56	0.93	5.11	4.37	1.16
W2	120	112	0.93	8.38	7.52	1.13
W3	-	170.5	-	-	9.72	-

[a] Experimental wall strength
[b] Theoretical wall strength, associated with the yielding of steel straps
[c] Experimental wall stiffness
[d] Theoretical wall stiffness computed according to formulations in [131]

Theoretical backbone envelopes for W1, W2 and W3 wall models are also shown in Figure 3-6. It must be noted that the maximum displacement that the theoretical model of W3 wall could achieve is set to not exceed the 5% inter storey drift. For this reason, in Figure 3-6 the total cumulative energy dissipated by wall W2 (at cycle 52) is more than that dissipated by wall W3 (at cycle 40), while for the same cycle 40 the cumulative energy dissipated by wall W2 is less than that dissipated by wall W3 (12 kJ for wall W3 vs 18 kJ for wall W3. This 5% drift is the minimum drift that other two wall configurations (W1 and W2) achieved in the experiments [7]. This limit is reflected in the model parameters by

strain at the 3rd point of backbone curve (*ePd3*). Table 3-9 summarizes the properties of *Pinching4 material* used for W1, W2 and W3 wall configurations. A more detailed description of model of single wall is also presented in [133].

Table 3-9 Pinching04 Material properties for W1, W2and W3 configuration of CFS strap-braced stud wall

Wall ID	W1	W2	W3
Parameters for backbone curve			
ePf1 (N/mm2)	45150	90301	128302
ePf2 (N/mm2)	89548	180601	256604
ePf3 (N/mm2)	97826	186621	256604
ePf4 (N/mm2)	7525	7525	7525
ePd1 (mm/mm)	0.00092	0.00147	0.0016
ePd2 (mm/mm)	0.00276	0.00405	0.0032
ePd3 (mm/mm)	0.02851	0.03623	0.02483
ePd4 (mm/mm)	0.02869	0.03642	0.02501
Parameters for cyclic behaviour			
uForce	0	0	0
rDisp	0.8	0.7	0.7
rForce	0.01	0.01	0.01

3.2.3. 3D non-linear model of Archetype

After modelling the single walls, complete three-dimensional models of archetypes are created. Elastic beam column elements are used to model gravity load carrying studs. Floor elements (joist, tracks and composite floor) behave as rigid elements in model due to their very high stiffness. Moment releases are created between studs and rigid floors in order avoid any transfer of moments from floor. Figure 3-8 shows a 2D schematic representation of a braced bay in double storey residential building designed for low intensity seismic loads.
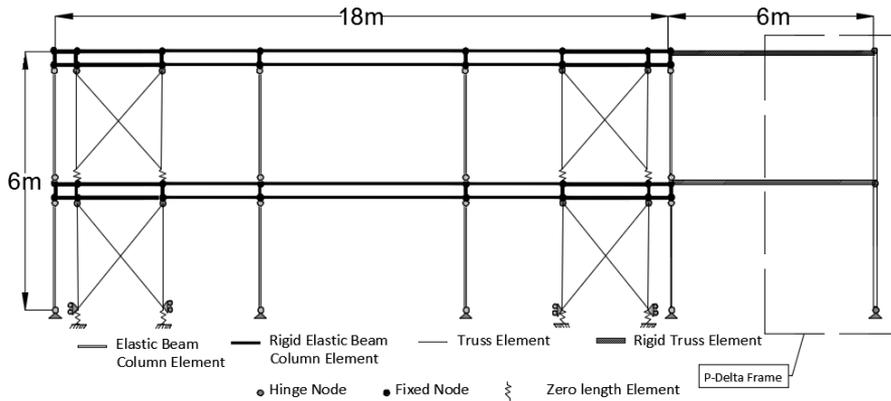
Figure 3-8 2D Schematic representation of a braced bay in Double storey residential building designed for low intensity seismic loads

Building total lateral displacement is composed of displacement due to the action of seismic loads and the global lateral displacement of building due to gravity loads also known as P-delta effect. To capture P-delta effect, a rigid frame is connected to the building in the direction of seismic action. In particular, P-delta frame is composed of columns made of axially rigid elastic beam column elements with low flexure stiffness having co-rotational coordinate transformation. Columns are pinned at both top and bottom and are linked to the main building using rigid truss elements. A similar detail is adopted for the inclusion P-delta effects in the model of CFS buildings with steel sheathed braced shear walls by Shamim and Rogers in [98]. Gravity load computed according to loading combination in equation (3-2) is applied to the P-delta columns at floor level. Preliminary non-linear static analysis performed on two storey archetypes revealed that inclusion of P-delta effects in model results in a reduced base shear. Therefore, it is decided to add P-delta frame in all subsequent archetype models.

Gravity loads are computed according to loading combination of equation (3-2). Gravity load is applied on the chord studs of walls and the gravity load carrying columns based on the proportion of their tributary areas. Seismic mass is applied at the four corners of the building. Additionally, a conservative Rayleigh damping of 2% is adopted in the model. This assumption is based on the data provided by Shamim and Rogers [98], although a value of 5% was used in other studies by Kechidi et al. [97], Dubina [134] and Shamim and Rogers [80]. Before proceeding to the non-linear analyses, gravity analysis is performed to check the internal forces in members and modal analysis is conducted to investigate the mode shapes and their respective time periods for each archetype.

3.3. Non-linear Analysis

3.3.1. Non-linear Static Analysis

FEMA P695 [12] methodology requires to perform non-linear static analysis to estimate archetype over-strength and to compute period based ductility, which is used to evaluate the effect of spectral shape of different earthquake records on the building performance. Non-linear static analysis is conducted for each archetype under the gravity load combination of equation (3-2) and lateral forces distributed over the height of building using the equation (3-4) or (3-10).

$$F_i = V_d \cdot \frac{(s_i m_i)}{\Sigma s_j m_j} \qquad\qquad (3\text{-}10)$$

Where s_i and s_j are the displacements of seismic masses m_i and m_j in the fundamental mode shape, respectively.

Archetype over strength (Ω) is computed according to equation (3-11), which is the ratio of design base shear (V_d) to the maximum base shear resistance (V_{max}) of archetype obtained through non-linear static analysis.

$$\Omega = \frac{V_{max}}{V} \qquad\qquad (3\text{-}11)$$

Period based ductility (μ_T) is defined as the ratio of ultimate roof displacement (δ_u) to the effective roof yield displacement ($\delta_{y.eff}$) (equation 3-12). Ultimate roof displacement (δ_u) was taken as the roof displacement at the point of 20% strength loss ($0.8V_{max}$) in non-linear static analysis, while effective roof yield displacement ($\delta_{y.eff}$) is computed according to equation (3-13).

$$\mu_T = \frac{\delta_u}{\delta_{y.eff}} \qquad\qquad (3\text{-}12)$$

$$\delta_{y.eff} = C_0 \cdot \frac{V_{max}}{W} \cdot \left[\frac{g}{4\pi^2}\right] (max(T, T_1))^2 \qquad\qquad (3\text{-}13)$$

where, where C_0 relates the fundamental-mode (SDOF) displacement to roof displacement obtained according to equation 6-8 of FEMA P695 [12]; V_{max}/W is the maximum base shear normalized by building weight W; g is the gravity constant; T is the fundamental period of archetype expressed as a function of height of building and computed in Section 3.1.4; and T_1 is the fundamental period of the archetype model computed using linear static analysis and summarized in Table 3-10.

Since the models of archetypes are three dimensional, therefore a non-linear static analysis is carried out in both directions under the respective distribution of lateral forces. Subsequently, over strength and period based ductility of each archetype is obtained by taking the average

of values obtained for both directions based on FEMA P695 [12] recommendation. Figure 3-9 shows the different pushover curves of the two-storey archetype designed to withstand high seismic load. It is evident that models behaved almost similar in both directions under lateral force distribution computed according to equation (3-4) or (3-10). Pushover curves for the rest of archetypes are shown in Annex A. The steep decline in the shear strength after peak (V_{max}) can be attributed to the shape of backbone curve. Table 3-10 summarises the fundamental time period obtained through linear dynamic analysis, the design base shear (V_d), the maximum base shear resistance in X and Y direction under lateral force contribution computed according to equation (3-4) or (3-10) (A or B) ($V_{max,X,A}$, $V_{max,X,B}$, $V_{max,Y,A}$, $V_{max,Y,B}$) , average ultimate roof displacement (δ_u), average effective roof yield displacement ($\delta_{y.eff}$) the average over strength factor Ω and the period based ductility μ_T obtained through non-linear static analysis for each archetype.

Table 3-10 Results from linear dynamic and non-linear static analysis

| Archetype ID	T (sec)	V_d (kN)	$V_{max,X,A}$ (kN)	$V_{max,X,B}$ (kN)	$V_{max,Y,A}$ (kN)	$V_{max,Y,B}$ (kN)	Over strength Ω	$\delta_{y.eff}$ (mm)	δ_u (mm)	μ_T
R2L	0.46	292	415	415	413	413	1.42	17	182	10.7
R3L	0.50	470	724	724	719	718	1.54	22	209	9.5
R4L	0.68	644	998	996	996	997	1.55	41	197	4.8
O1L	0.32	212	381	381	381	381	1.80	9	281	31.2
O2L	0.38	475	730	730	730	730	1.54	12	142	11.8
R2M	0.36	486	650	650	648	648	1.33	16	202	12.6
R3M	0.47	783	1180	1160	1180	1150	1.49	31	208	6.7
R4M	0.48	1073	1800	1795	1780	1785	1.67	37	222	6
O1M	0.25	352	749	749	749	749	2.13	11	315	28.6
O2M	0.31	792	1081	1081	1081	1081	1.37	12	162	13.5
R2H	0.37	681	1000	998	990	990	1.46	26	172	6.6
R3H	0.35	1096	1790	1780	1770	1770	1.46	26	187	7.2
O1H	0.25	494	749	749	749	749	1.52	11	315	28.6
O2H	0.33	1108	1800	1800	1800	1800	1.62	23	159	6.9
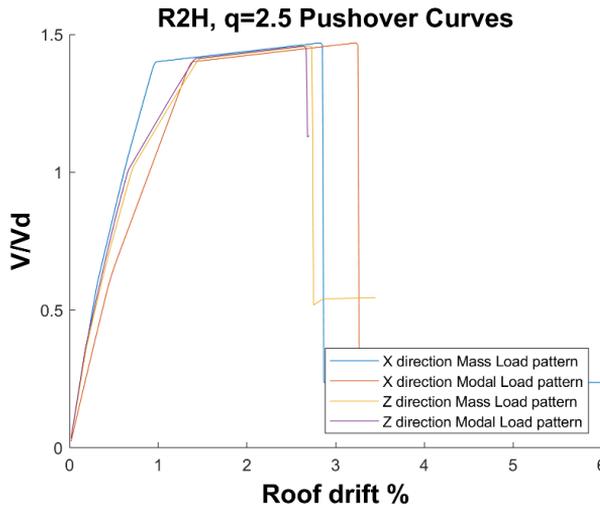
Figure 3-9 Pushover curves of a two-storey archetype designed to withstand high seismic load (R2H)

3.3.2. Non-linear Incremental Dynamic Analysis (IDA)

After completing the non-linear static analysis, the next step is to perform non-linear dynamic analysis to assess the median collapse capacities, S_{CT}, and collapse margin ratios, CMR, for each archetype. Methodology [12] prescribes to use Incremental dynamic analysis procedures [132], in which individual ground motions are scaled to increasing intensities until the archetype model reaches a collapse point. The collapse point is a damage measure, which essentially represents a local or global collapse. Damage measure in a CFS structure with strap-braced stud walls can either be defined by buckling of studs, tensile rupture of anchors, excessive yielding elongation of straps in walls, net section failure at connections or excessive inter story drifts. An archetype model is considered collapsed on the occurrence of any of these aforementioned damages. Brittle failure modes of buckling of studs and tensile rupture of anchors are already incorporated in the wall model (see Section 3.2.1). In order to avoid excessive elongation of straps, the displacement at third

point of the backbone curve of all walls was limited to 5% drift. This 5% drift reflects the minimum drift level that W1 and W2 walls are able to achieve in the experiments [7]. Also, archetype global collapse is defined in terms of maximum inter storey drift ratio of 5%.

Table 3-11 Far field ground motion records of *FEMA P695*

ID	Location, Year	Epicentral Site to Source distance (km)	PGA_{max} (g)	Magnitude	Component 1	Component 2	Normalization Factor
1	Northridge, 1994	13.3	0.52	6.7	NORTHR/MUL009	NORTHR/MUL279	0.65
2	Northridge, 1994	26.5	0.48	6.7	NORTHR/LOS000	NORTHR/LOS270	0.83
3	Duzce, Turkey, 1999	41.3	0.82	7.1	DUZCE/BOL000	DUZCE/BOL090	0.63
4	Hector Mine,1999	26.5	0.34	7.1	HECTOR/HEC000	HECTOR/HEC090	1.09
5	Imperial Valley, 1979	33.7	0.35	6.5	IMPVALL/H-DLT262	IMPVALL/H-DLT352	1.31
6	Imperial Valley, 1979	29.4	0.38	6.5	IMPVALL/H-E11140	IMPVALL/H-E11230	1.01
7	Kobe, Japan, 1995	8.7	0.51	6.9	KOBE/NIS000	KOBE/NIS090	1.03
8	Kobe, Japan, 1995	46	0.24	6.9	KOBE/SHI000	KOBE/SHI090	1.1
9	Kocaeli, Turkey, 1999	98.2	0.36	7.5	KOCAELI/DZC180	KOCAELI/DZC270	0.69
10	Kocaeli, Turkey, 1999	53.7	0.22	7.5	KOCAELI/ARC000	KOCAELI/ARC090	1.36
11	Landers. 1992	86	0.24	7.3	LANDERS/YER270	LANDERS/YER360	0.99
12	Landers, 1992	82.1	0.42	7.3	LANDERS/CLW-LN	LANDERS/CLW-TR	1.15
13	Loma Prieta, 1989	9.8	0.53	6.9	LOMAP/CAPP000	LOMAP/CAP090	1.09
14	Loma Prieta, 1989	31.4	0.56	6.9	LOMAP/G03000	LOMAP/G03090	0.88
15	Manjil, Iran, 1990	40.4	0.51	7.4	MANJIL/ABBAR--L	MANJIL/ABBAR--T	0.79
16	Superstition Hills, 1987	35.8	0.36	6.5	SUPERST/B-ICC000	SUPERST/B-ICC090	0.87
17	Superstition Hills, 1987	11.2	0.45	6.5	SUPERST/B-POE270	SUPERST/B-POE360	1.17
18	Cape Mendocino, 1992	22.7	0.55	7	CAPEMEND/RIO270	CAPEMEND/RIO360	0.82
19	Chi-Chi, Taiwan, 1999	32	0.44	7.6	CHICHI/CHY101-E	CHICHI/CHY101-N	0.41
20	Chi-Chi, Taiwan, 1999	77.5	0.51	7.6	CHICHI/TCU045-E	CHICHI/TCU045-N	0.96
21	San Fernando, 1971	39.5	0.21	6.6	SFERN/PEL090	SFERN/PEL180	2.1
22	Friuli, Italy, 1976	20.2	0.35	6.5	FRIULI/A-TMZ000	FRIULI/A-TMZ270	1.44

Two sets of ground motion records for collapse assessment are provided in FEMA P695: Far-Field record set and the Near-Field record set. Methodology prescribes to use the Far-Field record set for structures, which are designed for Seismic Design Category (SDC) B, C and D according to ASCE 7 [13]. The three seismic design levels defined according to EN 1998-1 [4] in this study can be related to SDC D of ASCE 7 [13] (see Figure 3-3). Therefore Far-Field record set is used for the performance evaluation, which consists of twenty-two component pairs of horizontal ground motions from sites located greater than or equal to 10 km from fault rupture. Table 3-11 lists the 22 pair of strong ground motions (44 records) provided by FEMA P695 [12]. The records given by FEMA have only one record from Italy and four in total from Europe and can represent collapse in buildings founded on any type of soil across all seismic regions of the world. The record set given by FEMA do not represent much higher difference with the European Seismic hazard map [135] in terms of PGA of records. Therefore, the use of these records is valid for Europe.

All 22 earthquake records are normalized based on Peak Ground Velocity (PGV) using the normalization factors, which are provided in [12] and listed in Table 3-11. These normalization factors are intended to remove the unwarranted variability between records due to inherent differences in event magnitude, distance to source, source type and site conditions, without eliminating overall record-to-record variability. Normalized ground motions are then matched to the archetype design response spectrum through the scaling of median response spectrum of all records within the range of their fundamental periods. As a result, a scaling factor for each archetype is obtained.

Following Incremental Dynamic Analysis approach, all 44 scaled records are applied to archetype models in both directions with the intensity increasing from 20% (Scaling factor (SF) = 0.2) to 600% (Scaling factor = 6.0) with increments of 20%. Since median of all records is already matched to the design response spectrum, therefore SF = 1.0 is associated with the design earthquake level. As explained in section 3.1.3, maximum considered earthquake of ASCE 7 [13] can be obtained by multiplying design earthquake of EN 1998-1 [4] by 1.5, therefore SF = 1.50 is associated to the Maximum Considerer Earthquake (MCE) level. Collapse Margin Ratio (CMR) is the ratio of median collapse intensity S_{CT} to the maximum considered earthquake S_{MT}. The median collapse intensity S_{CT} is defined in terms of Scaling Factor of the earthquake intensity, at which half of the ground motions in the record set cause collapse of an archetype model while, S_{MT} is taken as 1.50. Figure 3-10 shows the IDA curves for three-storeys residential (R3M) and double storey office (O2M) archetypes designed for medium intensity seismic loads.
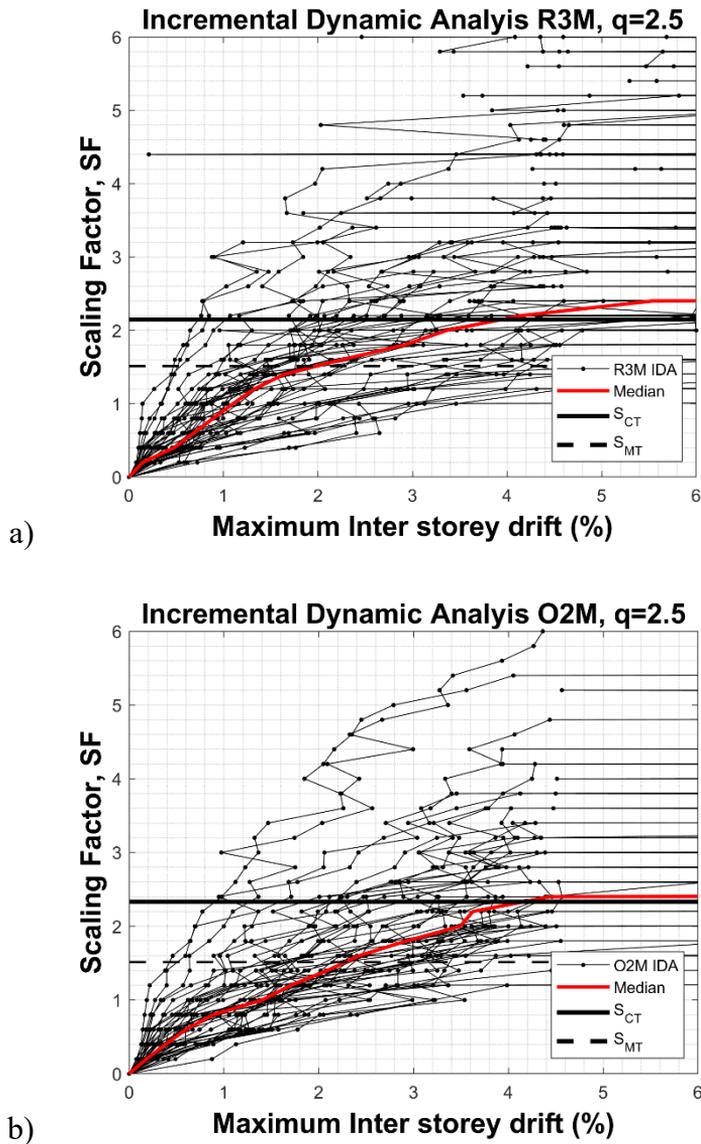
Figure 3-10 IDA curves for a: three storeys residential (R3M) and b: double storey office (O2M) archetypes designed for medium seismic loads

3.4. Performance Evaluation of Archetypes

Using the results of non-linear analyses on archetype models, the acceptability of trial value of behaviour factor ($q = 2.5$) used in design is

evaluated using the performance evaluation criteria of FEMA P695 [12]. The Adjusted Collapse Margin Ratio (ACMR) for each archetype is computed using equation (3-14).

$$ACMR = CMR \cdot SSF \tag{3-14}$$

where SSF is a Spectral Shape Factor, which is the function of period based ductility (μ_T), Fundamental period (T) of an archetype model and seismic design category and can be calculated according to Table 7-1a and 7-1b of FEMA P695 [12]. Different sources of uncertainty are also accounted for the performance evaluation process that could contribute to variability in collapse capacity. In particular, the main source of uncertainty includes: record to record uncertainty (β_{RTR}), design requirements uncertainty (β_{DR}), test data uncertainty (β_{TD}) and modelling uncertainty (β_{MDL}). The total uncertainty is then computed using equation (3-15).

$$\beta_{TOT} = \sqrt{\beta_{RTR}^2 + \beta_{DR}^2 + \beta_{TD}^2 + \beta_{MDL}^2} \tag{3-15}$$

Record to record uncertainty (β_{RTR}) is due to variability in the response of archetypes model to different ground motion records. FEMA P695 recommends to use β_{RTR} equal to 0.40 for structures that have period-based ductility, μ_T, greater than 3. Since, all of the archetype models have period-based ductility, μ_T, greater than 3, therefore, β_{RTR}, is taken as 0.4. The other uncertainty parameters β_{DR}, β_{TD} and β_{MDL}, are the qualitative measures. FEMA P695 [12] provides the following qualitative scale to quantify them: (a) Superior, $\beta = 0.10$; (b) Good, $\beta = 0.20$; (c) Fair, $\beta = 0.35$; and (d) Poor, $\beta = 0.50$. Design procedure for CFS strap-braced stud walls presented in [131], and validated against the experimental results in

[7] is adopted. This design procedure provide safeguard against unanticipated failure modes. However, confidence in these design requirements is medium because they are only validated via single wall cyclic tests. On this basis, design requirements used in this study are rated as 'Good' ($\beta_{DR} = 0.2$). Tests conducted in [7] are used as the experimental evidence for CFS strap-braced walls and rated as 'Good' ($\beta_{TD} = 0.2$). These tests are conducted at material, component and assembly level and provided evidence on the seismic behaviour of CFS strap-braced stud walls and all relevant failure modes. Archetype modelling is also rated as 'Good' (($\beta_{MDL} = 0.2$) because all models are calibrated based on the experimental results and have the ability to simulate post peak shear strength and the brittle failure mechanisms. Internal forces arising in members due to P-delta effects are also accounted for in them. Finally, total uncertainty, β_{TOT}, is computed using equation (3-15) to be 0.53.

In order to evaluate the collapse fragility of each archetype for performance evaluation, fragility curves are generated using lognormal probability distribution [136]. Fragility curves are then adjusted to account for the effect of spectral shape of different earthquake records using SSF and the total uncertainty β_{TOT}. In Figure 3-11, the scatter plot represents the simple probability of collapse at a particular scaling factor computed using equation (3-16).

$$P(C|x) = \frac{n(x)}{n} \qquad\qquad (3\text{-}16)$$

Where $P(C|x)$ is the probability of collapse of building at a scaling factor x, $n(x)$ is the number of ground motion at scaling factor x that caused collapse and n is total number of ground motions. Basic Fragility

curve is obtained by fitting lognormal cumulative distributive function to scatter plot of simple probability [136]. Shifted fragility curve is obtained by multiplying the Basic curve with SSF and uncertainty adjusted fragility curve is calculated using β_{TOT} as the standard deviation in lognormal cumulative distributive function.
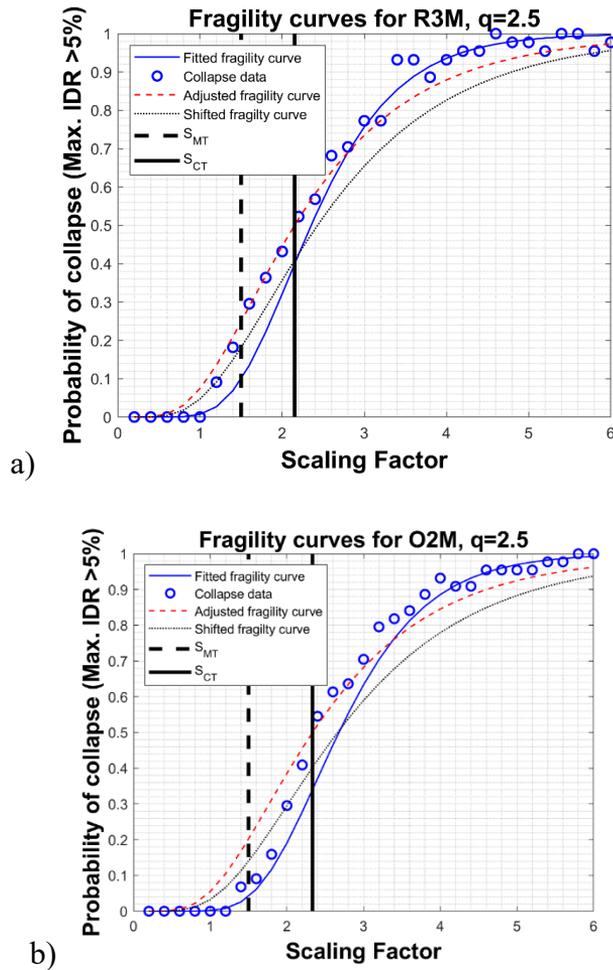

a)

b)

Figure 3-11 Fragility curves for a) three storeys residential (R3M) and b): double storey office (O2M) archetypes designed for medium seismic loads

The last step in the performance evaluation process is to measure the acceptability of Adjusted Collapse Margin Ratios (ACMR) of

archetypes based on the total system collapse uncertainty, and established values of acceptable probabilities of collapse. Table 7-3 of FEMA P695 [12] provides acceptable values of adjusted collapse margin ratio, $ACMR_{10\%}$ and $ACMR_{20\%}$ of 1.97 and 1.57, respectively based on total collapse uncertainty β_{TOT}. Using acceptable values of adjusted collapse margin ratio, two performance criteria are defined: the average value of adjusted collapse margin ratio, $ACMR_{average}$, for each performance group should be greater than $ACMR_{10\%}$, and the individual values of adjusted collapse margin ratio, $ACMR_i$, for each archetype within a performance group should be greater than $ACMR_{20\%}$. All of the archetypes have the $ACMR_i$ greater than $ACMR_{20\%} = 1.57$, except single storey office archetype designed for high seismic loads ($ACMR_{O1H} = 1.53$) which has a ACMR value close to $ACMR_{20\%}$. Overall, the average adjusted collapse margin ratio $ACMR_{average}$ of complete design space, which is taken as one performance group, is greater than $ACMR_{10\%} = 1.97$ ($ACMR_{average} = 2.05$). Accordingly, it can be concluded the initial assumption of behaviour factor, $q = 2.5$, and the design method is appropriate for archetype buildings. Table 3-12 summarizes the performance evaluation of complete archetype design space.

Table 3-12 Performance evaluation of Archetype design space according to FEMA P695

Archetype ID	S_{CT}	S_{CT}	SSF	CMR	ACMR	ACMR 20%	Pass /Fail	ACMR avg	ACMR 10%	Pass /Fail
R2L	3.4	1.5	1.14	2.27	2.58	1.57	Pass			
R3L	3.67	1.5	1.14	2.45	2.79	1.57	Pass			
R4L	3.7	1.5	1.13	2.47	2.79	1.57	Pass			
O1L	2.87	1.5	1.14	1.91	2.18	1.57	Pass			
O2L	3.4	1.5	1.14	2.27	2.58	1.57	Pass			
R2M	2.27	1.5	1.14	1.51	1.73	1.57	Pass			
R3M	2.18	1.5	1.13	1.45	1.64	1.57	Pass			
R4M	2.53	1.5	1.12	1.69	1.89	1.57	Pass	2.05	1.97	Pass
O1M	2.4	1.5	1.14	1.6	1.82	1.57	Pass			
O2M	2.5	1.5	1.14	1.67	1.9	1.57	Pass			
R2H	1.95	1.5	1.3	1.3	1.69	1.57	Pass			
R3H	1.94	1.5	1.31	1.29	1.69	1.57	Pass			
O1H	1.72	1.5	1.33	1.15	1.53	1.57	Near Pass			
O2H	2.16	1.5	1.3	1.44	1.87	1.57	Pass			

4. Seismic performance evaluation of LWS buildings with CFS shear walls

CFS Shear wall is one of the most common type of structural system to provide the lateral resistance in LWS structures, which provides the resistance through the interaction between the steel frame and the sheathing panels. These shear walls are essentially composed of a CFS frame sheathed with panels and connected with the tensile and shear anchorage for transmitting lateral forces to the floor or foundation. Current edition of the European earthquake design standard: EN 1998-1 [4] does not provide any seismic design guidelines for LWS buildings with CFS shear walls as the main LFRS. In order to bridge this gap, this chapter explains the probabilistic seismic performance evaluation, following the FEMA P695 methodology, of LWS building archetypes equipped with CFS wood or gypsum sheathed shear wall as the main LFRS, which are designed following a particular value of a behaviour factor and a proposed design method. The successful evaluation of the LWS building archetypes against the performance evaluation criteria of FEMA P695 will build the confidence in the used design method and the value of behaviour factor, which subsequently can become part of the new edition of EN 1998-1. Similar to Section 3, the arrangement of subsections in this chapter also follows the order of different steps in the FEMA P695 methodology (see Figure 2-12). The initial step of the methodology involves the development of system concept, which focuses on understanding the functioning of the investigated LFRS and is explained in Section 2.4. The next step involves the explanation of the experimental data and the design method. The utilized test data is explained alongside the modelling of single wall

response (Section 4.1.5), while the design method is illustrated in Section 4.1.5.

4.1. Archetypes selection and design

A set of 14 archetypes (Table 4-1) are selected for the seismic performance evaluation of the LWS buildings with the CFS gypsum sheathed shear walls as the primary lateral force resisting system. All of these archetypes are designed according to relevant parts of the Eurocode [4,137], while using a trial value of 2.0 for the behaviour factor.

Table 4-1 Archetype design space CFS gypsum sheathed shear walls (q=2.0)

Archetype ID	Type of Occupancy	Type of Floor/ Roof	H [m]	$a_{g,R}$[1] [ms^{-2}]	T[2]	q	V_d[3]	No of walls in each direction
R1L		Composite	3	0.98	0.11	2	129	4
R2L		Composite	6	0.98	0.19	2	175	6
R3L		Composite	9	0.98	0.26	2	322	11
R4L		Composite	12	0.98	0.32	2	469	16
R1M	Residential	Composite	3	1.96	0.11	2	258	9
R2M		Composite	6	1.96	0.19	2	350	12
R3M		Light weight	9	1.96	0.26	2	528	18
R1H		Composite	3	2.94	0.11	2	387	13
R2H		Composite	6	2.94	0.19	2	525	18
O1L		Composite	3	0.98	0.11	2	101	4
O2L		Composite	6	0.98	0.19	2	332	11
O1M		Composite	3	1.96	0.11	2	203	7
O2M	Office	Light weight	6	1.96	0.19	2	504	17
O1H		Light weight	3	2.94	0.11	2	304	11

[1] reference peak ground acceleration [4]
[2] fundamental period of vibration of building [4], $T=C_tH^{3/4}$, with C_t =0.05 and H = building height
[3] design base shear [4]

Unlike the case of CFS gypsum sheathed shear walls, two sets of archetypes are designed for CFS wood sheathed shear walls. Initially a set

of 18 archetypes (Table 4-2) is designed with a trial value of behaviour factor equal to 4.0. However, this set of 18 archetypes failed the performance evaluation criteria as shown in Section 4.4, which led to the development of second set of archetypes with a lower value of behaviour factor. The second set of archetypes has 12 cases (Table 4-3) designed with a trial value of behaviour factor equal to 2.5. This iteration of behaviour factor is in line with the methodology of FEMA P695, which prescribes to keep doing these iterations until an archetype design space having a particular value of behaviour factor passes its performance evaluation criteria.

Table 4-2 Archetype design space CFS wood sheathed shear walls (q=4.0)

Archetype ID	Type of Occupancy	Type of Floor/ Roof	H [m]	$a_{g,R}$[1] [ms^{-2}]	T[2]	q	V_d[3]	No. of Walls A (1:1)	No. of Walls B (2:1)
R2L		Light weight		0.98	0.19	4.0	75.58	4	0
R2M		Light weight	6	1.96	0.19	4.0	151.17	2	6
R2H (1)		Light weight		2.94	0.19	4.0	226.75	6	2
R2H (2)		Light weight		2.94	0.19	4.0	226.75	0	14
R4L		Light weight		0.98	0.32	4.0	173.40	4	4
R4M	Residential	Light weight	12	1.96	0.32	4.0	346.80	12	0
R4H (1)		Light weight		2.94	0.32	4.0	520.19	14	4
R4H (2)		Light weight		2.94	0.32	4.0	520.19	0	32
R6L		Light weight		0.98	0.44	4.0	271.42	8	0
R6M (1)		Light weight	18	1.96	0.44	4.0	542.84	14	4
R6M (2)		Light weight		1.96	0.44	4.0	542.84	0	32
O1L		Light weight		0.98	0.11	4.0	41.84	0	4
O1M		Light weight	3	1.96	0.11	4.0	83.67	4	0
O1H		Light weight		2.94	0.11	4.0	125.51	4	0
O2L	Office	Light weight		0.98	0.19	4.0	121.53	4	0
O2M		Light weight		1.96	0.19	4.0	243.06	8	0
O2H (1)		Light weight	6	2.94	0.19	4.0	364.59	12	0
O2H (2)		Light weight		2.94	0.19	4.0	364.59	0	24

[1] reference peak ground acceleration [4]
[2] fundamental period of vibration of building [4], T=C_tH$^{3/4}$, with C_t =0.05 and H = building height
[3] design base shear [4]

Table 4-3 Archetype design space CFS wood sheathed shear walls (q=2.5)

Archetype ID	Type of Occupancy	Type of Floor/ Roof	H [m]	$a_{g,R}$[1] [ms^{-2}]	T[2]	q	V_d[3]	No. of Walls A (1:1)	No. of Walls B (2:1)
R2L	Residential	Light weight		0.98	0.19	2.5	118.93	0	8
R2M		Light weight	6	1.96	0.19	2.5	237.86	4	8
R2H		Light weight		2.94	0.19	2.5	356.79	4	14
R4L		Light weight	12	0.98	0.32	2.5	277.43	8	0
R4M		Light weight		1.96	0.32	2.5	462.39	14	0
R6L		Light weight	18	0.98	0.44	2.5	434.27	14	0
O1L	Office	Light weight		0.98	0.11	2.5	55.74	0	4
O1M		Light weight	3	1.96	0.11	2.5	111.49	0	8
O1H		Light weight		2.94	0.11	2.5	167.23	2	8
O2L		Light weight		0.98	0.19	2.5	191.22	6	2
O2M		Light weight	6	1.96	0.19	2.5	382.45	12	0
O2H		Light weight		2.94	0.19	2.5	573.67	6	28

[1] reference peak ground acceleration [4]
[2] fundamental period of vibration of building [4], $T=C_tH^{3/4}$, with $C_t =0.05$ and H = building height
[3] design base shear [4]

The archetypes differ with each other in terms of the occupancies, building heights (H) and seismic hazards. For CFS wood sheathed shear walls, an additional parameter: aspect ratio of the wall is also considered, since it is found to have significant impact on the building performance. The choice of these design parameters certainly reflects the probable use of the investigated structural system in a building and are recommend parameters by the FEMA P695 methodology. Though, there could be some resemblance in terms of kind of design parameters to the other studies [97,98], but they are the key governing parameters for any type of structural system. The resulting archetypes are also unique in their floor plans, different intensity of seismic loads and a completely different set of guidelines used for designing them. The complete design space is considered as one performance group for both LFRS-s due to the fact that the changes in structural configuration and gravity loads among different archetypes will not alter the behaviour of seismic force resisting system, significantly. The differences among the archetypes and reason behind the

selection of different parameters is further explained in following subsections.

4.1.1. Type of occupancy

Two type of occupancies are considered for the archetypes: residential and office. The major differences among the two occupancies is different intensity of live loads they cause. In particular, Eurocode EN 1990 [138] defines a live load of 2.0 kN/m^{2}and 3.0 kN/m^2 for residential and office type of occupancies, respectively. The two occupancies also differ with each other in terms of accessibility to roof. In case of the residential occupancy, roof is considered accessible with an expected live load equal to the floors i.e. 2.0 kN/m^{2,} while the roof of office archetype is considered inaccessible except for normal maintenance and repair, which resulted in 0.4 kN/m^2 expected live load defined based on EN 1990 [138]

4.1.2. Height of buildings

The height of the archetypes reflected the current trend of LWS buildings use in the seismic areas, which is only limited to the low-rise buildings. In case of gypsum sheathed shear walls, 3.0 to 12.0 m high archetypes are selected for the residential buildings, while the maximum height of archetype is limited to 6.0 m for the office buildings. On the other hand, the archetypes with CFS wood sheathed shear walls have the heights ranging from 6.0 to 18.0 m for residential buildings, while for office archetypes maximum height is limited to 6.0 m. Total height of each storey for both type of occupancies is 3.0 m including a floor depth of 0.3 m.

One of the most important factors limiting the application of CFS shear walls as the primary LFRS in LWS buildings is the building height. Even the North American standard S400 [13,17] currently stipulates a height

limit of 20 m for CFS wood sheathed shear walls for the buildings designed to resist high seismic hazard. To verify this height limit and to check whether this limit can be further relaxed, a 12.0 m high archetype is also designed for CFS gypsum sheathed shear walls. However, the design of the 12.0 high archetype is only limited to site with low seismic hazard due to the large base shear calculated in case of the high or medium seismic hazard, which demanded to have a larger number of shear walls, more than the maximum viable number considering architectural demands. The maximum number of walls limited by architectural demands in case of CFS gypsum sheathed shear walls, that could be placed on each storey, is eighteen per direction of the application of seismic actions. For wood sheathed shear walls, the building heights are limited to 18 m for the similar reason as of gypsum sheathed shear walls. In fact, an 18 m high archetype located in a location with high seismic hazard is not present in the archetype design space (Table 4-2), primarily due to its large design base shear. The office building archetypes have always building height limited to 6 m due to the large design base shear for building heights beyond this limit.

As mentioned earlier, a second set (Table 4-3) of archetype design space is also designed for CFS wood sheathed shear wall with a lower value of behaviour factor. However, two archetypes case (R4H and R6M) are omitted in the second design space (Table 4-3), if it is compared with the design space shown in Table 4-2. The primary reason for omitting these cases is also the large design base shear, which is increased after reducing the value of behavior factor (from 4.0 to 2.5) and cannot be resisted even if the maximum number of shear walls is used. More information on the calculation of design base shear is given in Section 4.1.5.

4.1.3. Intensity of seismic loads

Three anonymous geographical sites with low, medium and high seismic intensity levels representative of the type of the seismic hazard exposed to European continent are assumed as location of the archetypes. The main European earthquake standard EN 1998-1 [4] defines seismic hazard as a reference peak ground acceleration $a_{g,R}$ with a 10 % probability of exceedance in 50 years corresponding to ultimate limit state. According to European seismic hazard map [135], the Low, Medium and High seismic hazard are assigned with $a_{g,R\ level}$ of 0.1g, 0.2g and 0.3g, respectively. All the archetypes are assumed to be built on Soil class C and belong to an Importance class II according to EN 1998-1 [4]. Figure 4-1 shows the 5 % damped elastic design response spectrum of the three sites. It also shows that the SDC B_{max}, D_{min} and D_{max} according to ASCE 7 can be associated to Low, Medium and High seismic intensity levels used in this study, respectively. More explanation on the association of respective SDC-s to the seismic intensity levels used in this study can be found in Section 3.1.3.
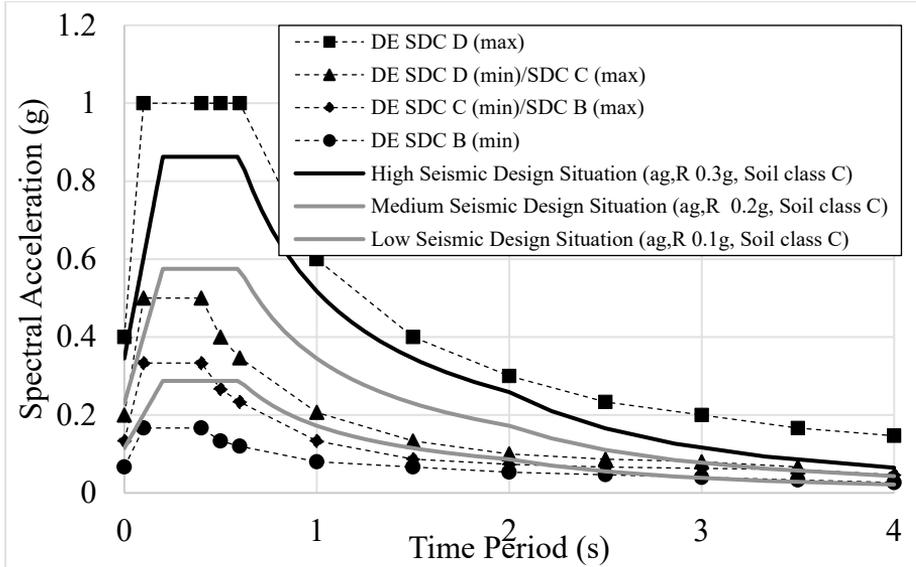
Figure 4-1 Comparison of the Elastic Design Response Spectrum of EN 1998-1 [6] and the Seismic Design Categories based on Design Earthquake of ASCE 7 [9] for archetypes with CFS shear walls

4.1.4. Aspect ratio of walls

In case of wood sheathed shear walls, two walls with an aspect ratio (height to width ratio) equal to 1.0 (Wall A) and 2.0 (Wall B) [66] are selected in the design phase to resist the seismic loads. While in case of gypsum sheathed shear walls, only one wall with an aspect ratio equal to 1.0 is selected. This is primarily due to the absence of experimental data on gypsum sheathed shear walls with aspect ratio 2.0, which can be used to calibrate the wall model. Though there are experimental results available on the gypsum sheathed shear wall with an aspect ratio of 0.5 [8] that can be used for calibrating the wall model, but the wall had few imperfect sheathing connections, which resulted in the reduction of wall in plane resistance. Therefore, it was decided to avoid such experimental results and only use one gypsum sheathed shear configuration wall with an aspect

ratio equal to 1.0. More information on the selection of wall configurations and their design is provided in next section.

In practice, LWS building could have walls with many aspect ratios spread across its plan. A similar practice is adopted in the design of archetypes with wood sheathed shear walls. In order to understand the effect of aspect ratio on the building performance, few special cases are also designed in the archetype design space of wood sheathed shear walls (R2H (2), R4H (2), R6M (2) and O2H (2)), which have only Wall B (aspect ratio 2) spread across their plan. In fact, from the examination of hysteretic envelopes of walls with aspect ratio 1.0 and 2.0, the wall with aspect ratio 2.0 appears to show better load carrying capacity up to higher drifts in comparison with the wall with aspect ratio of 1.0. In order to further confirm this trend of increase in the wall deformation capacity with an increase in the wall aspect ratio, experimental results from other researches [58,139] on the similar wall configuration are also investigated, which also revealed a similar trend as shown in Figure 4-2 and Table 4-4. Figure 4-2 compares the hysteretic envelopes of the experimental tested walls used here [66] to other similar tested specimens while Table 4-4 shows a quantitative comparison between the experimental results used here and the results from other researchers. Table 4-4 shows that by increasing the wall aspect ratio, the ultimate displacement (d_u) of wall increases by 42-48% while the post peak ductility defined as the ratio of ultimate displacement (d_u) to the displacement at the peak strength (d_p) increases by 14-19%. However, in case of the conventional definition of the ductility, which is taken as the ratio between the ultimate displacement (d_u) and the elastic displacement (d_e), a decrease of 20-37% is observed with increase in wall aspect ratio. This opposite trend for the conventional definition of

ductility may be attributed to far higher decrease in the elastic displacement with the decrease in wall aspect ratio. Nonetheless, for the LFRS seismic performance evaluation, the most important parameter is wall's ultimate displacement (d_u), as it controls building global drift. The d_u and d_e are the displacement at the 80 % post peak and 20 % pre peak strength on the wall experimental backbone envelope. The four special cases of archetypes: R2H (2), R4H (2), R6M (2) and O2H (2), compare the performance of building archetypes with only aspect ratio 2.0 wood sheathed shear wall against the archetypes having both aspect ratio 1.0 and 2.0 wall. These four special cases investigate, how the use of only aspect ratio 2.0 wall (Wall B) in building can improve its collapse performance as it as better load carrying capacity beyond peak strength.
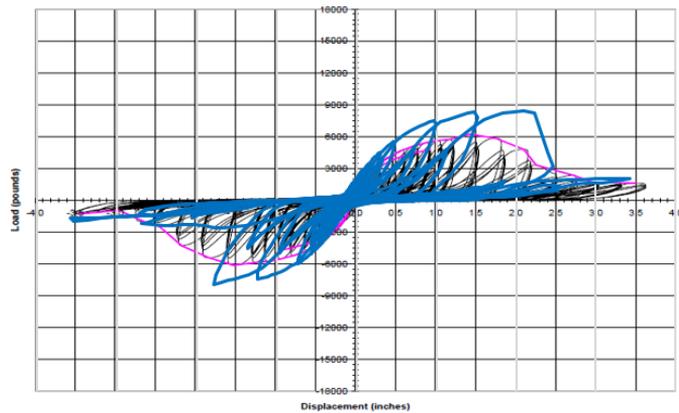
a) Aspect ratio 1.0 (Wall A)
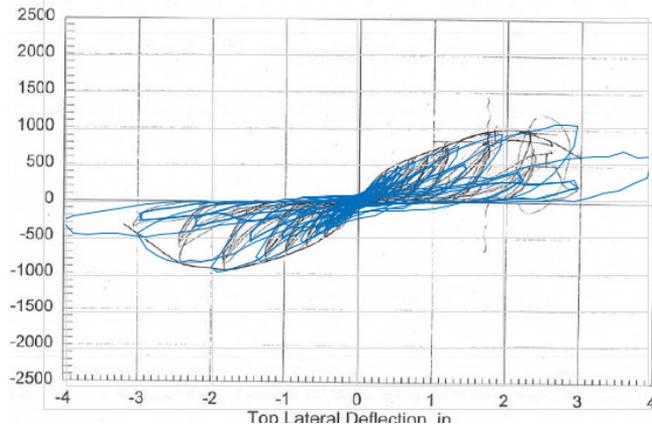
b) Aspect ratio 2.0 (Wall B)

Figure 4-2 Comparison of hysteretic envelopes for wall A and B (blue-used in this study [66]

Table 4-4 Quantitative comparison of aspect ratio 1 and 2 tested specimens of CFS wood sheathed shear wall

Wall Aspect ratio	Fe [kN]	de [mm]	Fp [kN]	dp [mm]	Fu [kN]	du [mm]	du/dp [-]	du/de [-]
2.0 [66]	7.27	10.62	18.18	61.00	14.54	77.56	1.30	7.39
1.0 [66]	14.84	5.83	37.11	49.23	29.68	54.20	1.09	9.25
2.0 [58]	6.82	9.93	17.05	48.26	13.64	69.85	1.45	7.04
1.0 [139]	11.12	4.45	27.80	37.47	22.24	47.63	1.27	11.84

Figure 4 shows the architectural plan with maximum number of shear walls for both residential and office type archetypes.
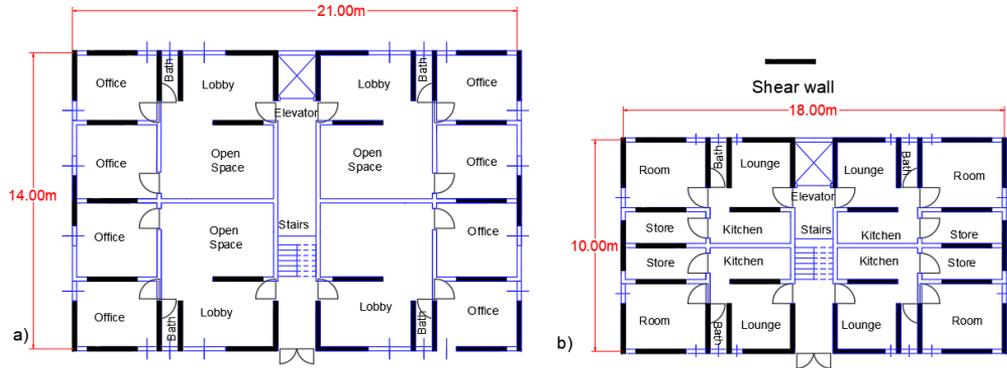
4.1.5. Design of archetypes

Figure 4-3 Plan of a) two storey office archetype designed for medium intensity seismic design loads (O2M); b) double storey residential archetype designed for high intensity (R2H) for CFS gypsum

The archetypes are structurally designed according to the relevant parts of Eurocodes. Two different types of floors are used in case of gypsum sheathed shear walls: a lightweight steel floor sheathed with panels (light solution) and a composite steel concrete deck (ordinary solution). The use of lightweight floors is only limited to the archetypes which resulted in excessive design base shear, if an ordinary floor is used in them. The use of light floor also allowed to expand the number of archetypes, which would otherwise not be possible if a composite steel concrete deck is used as the only solution for floors. In case of wood sheathed shear walls, a lightweight steel floor is used for all archetypes. The resulting dead loads on the floors due to light or ordinary floor solutions, ceilings and vertical partitions are 1.30 or 1.80, 0.10 and 0.80 kN/m^2, respectively, while on the roof dead loads due to light or ordinary roof solutions and ceilings are 1.40

or 2.30 and 0.10 kN/m^2, respectively. In addition to dead loads, a snow load of 1.00 kN/m^2 and a suction wind load of 0.35 kN/m^2 is assumed to be acting on the roof of archetypes. Fundamental load combinations of EN 1990 [138] are used to add up all of the gravity loads. The design of archetypes against the gravity load is carried out using EN 1993-1-3 [14], which provides supplementary rules for CFS members and sheathing. In particular, C 150 × 50 × 20 × 1.5 mm or C 150 × 50 × 20 × 3 mm (C-section: outside-to-outside web depth × outside-to-outside flange size × outside to-outside lip size × thickness) profiles spaced 600mm on centre made of continuous hot dip zinc coated carbon steel sheets of structural quality S350GD + Z (yield nominal stress: 350 MPa; ultimate nominal stress: 420 MPa) are used for studs.

The lateral loads acting on the archetypes included a wind load of 0.70 KN/m^2 and earthquake loads as explained earlier, among which earthquake loads were always the leading action and hence were never combined with wind actions. The prescription of EN 1998-1 [4] are used to obtain the design seismic loads acting on the building. In seismic design situation, load combination given in expression (4-1) according to EN 1998-1 [4] and 1990 [138] is used to combine gravity and earthquake loads.

$$G_k + \psi_{E,i} \cdot \varphi \cdot Q_k + A_{Ed} \tag{4-1}$$

where, G_k is the dead load of building; $\psi_{E,i}$ and φ are the combination coefficients having a value of 0 and 1 for roof and 0.3 and 0.5 for floors, respectively; Q_k is the leading variable action among live, snow and wind loads, which is live load, as it is greater than the wind and snow loads for all archetypes; and A_{Ed} is the design value of the seismic action, which in

this case is the seismic design base shear V_d. Lateral force method in EN 1998-1 [4] is used to compute the design base shear, because all of the archetypes meet the criteria of regularity in structural plan and elevation. The mass of archetypes is the sum of first two terms in the expression (4-1). The seismic design base shear (V_d) is distributed over the height of structure corresponding to seismic mass of each floor according to Equation (4-2).

$$F_i = V_d \cdot \frac{(z_i m_i)}{\Sigma z_j m_j} \qquad (4\text{-}2)$$

where F_i is the horizontal force acting on i^{th} storey; m_i and m_j are the seismic masses of ith and j^{th} storeys respectively; z_i and z_j are the heights of the masses m_i and m_j above the level of application of the seismic action, respectively. Distribution of design base shear corresponding to the first modal shape according to Equation (4-3) is also calculated, which has linearly increasing displacement over the height of archetype.

$$F_i = V_d \cdot \frac{(s_i m_i)}{\Sigma s_j m_j} \qquad (4\text{-}3)$$

where s_i and s_j are the displacements of seismic masses m_i and m_j in the fundamental mode shape, respectively. Both types of lateral force distribution are used in pushover analysis of archetypes as explained in upcoming sections in order to obtain the worst-case scenario response. Moreover accidental torsional effects in archetypes are also considered, which are taken into account as per EN 1998-1 [4] requirements of multiplying the forces obtained from Equation (4-2) or (4-3) by a factor δ computed according to Equation (4-4).

$$\delta = 1 + 0.6 \cdot \frac{x}{L_e} \qquad (4\text{-}4)$$

where x and L_e are the distances measured perpendicularly to the direction of the seismic action between walls located at the perimeter of archetypes to the centre of mass in plan and between the two outermost walls, respectively. The computed value of δ is 1.3.

To resist the lateral loads, CFS gypsum sheathed shear walls or CFS wood sheathed shear walls are used as the primary LFRS in each direction of application of the earthquake loads. The design process involves selecting the configuration and the length of shears walls and eventually the total number of walls that would be needed to resist the design base shear. A 2.40 m wide and 2.30 m high shear wall configuration (Figure 4-4 a) which is already tested by author (Figure 4-5 a) and has shown acceptable performance under the both cyclic [8] and shake-table [140] testing is selected as the only configuration used for archetypes with gypsum sheathed shear walls. While in case of archetypes with wood sheathed shear walls, two walls with an aspect ratio equal to 1.0 (height x width: 2.74 x 2.44) (Figure 4-4 b) and 2.0 (height x width: 2.74 x 1.22) are selected. These 2 walls have been tested by the researchers [66] in USA within the CFS NEES project [76]. The only difference between wood sheathed shear walls of aspect ratio 1.0 and 2.0 is their geometry. Figure 4-4 shows the mechanical and material details for both types of shear walls while Figure 4-5 show these walls, while they were being tested.
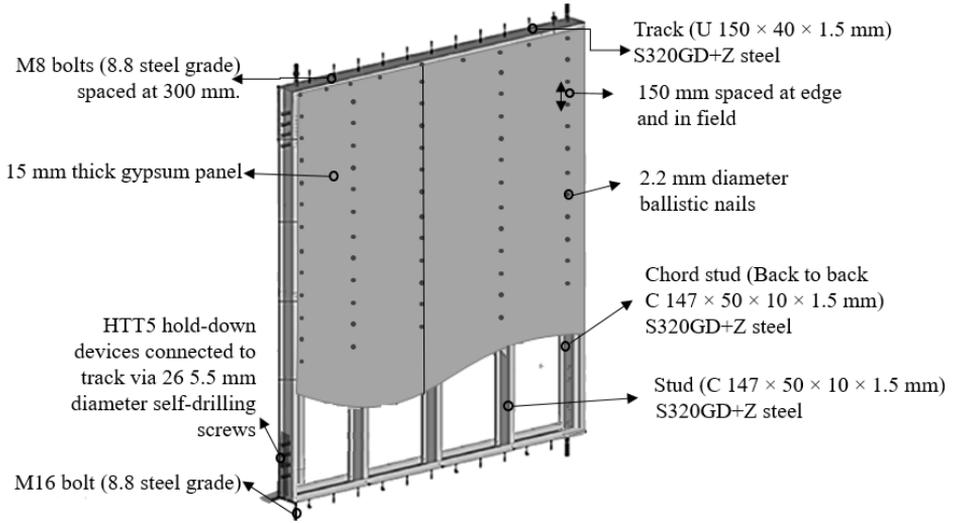
a)   CFS gypsum sheathed shear wall [8]
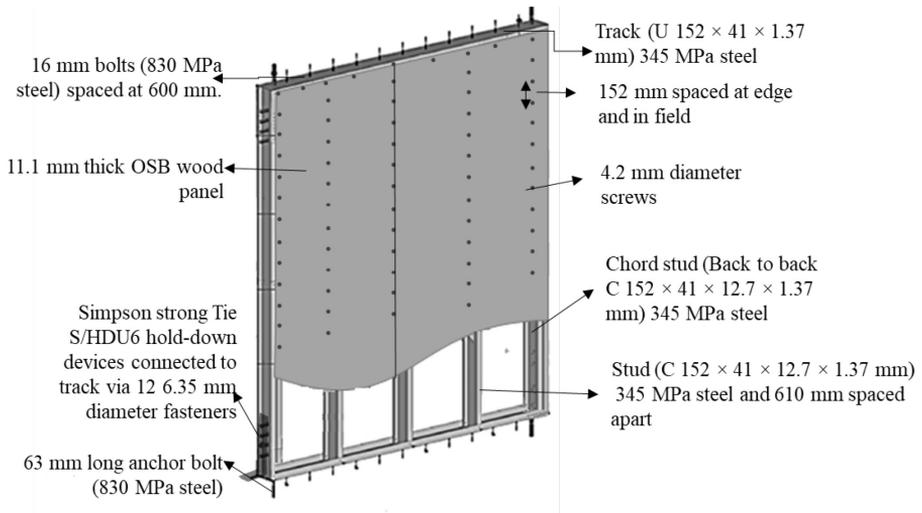
b)   CFS wood sheathed shear wall [66]

Figure 4-4 Shear wall configurations

a) CFS gypsum sheathed shear walls aspect ratio 1.0

b) CFS wood sheathed shear walls: Wall A (left), Wall B (right)

Figure 4-5 Shear walls being tested [8,66]

The reason behind the selection of these configurations of shear walls is the presence of experimental evidence which would be needed in calibrating its numerical response. However, it must be noted that the selected wall configurations are not the strongest possible wood sheathed shear wall configurations. Strength of the shear wall can be increased by reducing the sheathing connections spacing at the wall perimeter, thickness of the steel frame elements and diameter of the screws. Anyhow, the selection of shear wall configurations in this paper is strictly linked to the availability of their experimental data. Once the configuration of wall is selected, the number of shear wall needed in each direction of application of earthquake load can be obtained by dividing the seismic design base shear with the design strength of the wall. Equal number of walls are provided on each floor of the archetype in order to avoid irregularity in the stiffness along the height of archetypes.

The design of the walls is carried out following the capacity design approach, which ensures the ductile behaviour of structural system by providing appropriate over-strength in non-dissipative components of the system. Sheathing connections are the main dissipative components, and the strength of walls associated with sheathing connections can be evaluated through various formulations available in literature for timber shear walls [68–70]. Authors used the lower bound method proposed by Källsner and Girhammar [68] for timber shear walls, which estimates the lateral strength per wall unit length (F_{Rd}) according to Equation (4-5).

$$F_{Rd} = \frac{n}{s} F_{Rd,c} \qquad (4\text{-}5)$$

where, $F_{Rd,c}$ is design shear strength of single panel-to-steel connection and can be evaluated according to Equation (4-6), n is the number of sides sheathed with structural panels and s is the spacing of panel-to-steel connections along the wall top track. In case of gypsum sheathed shear walls, the selected configuration of the shear wall is sheathed on both sides (n=2) with a 15 mm thick gypsum board and connected to the steel frame via 2.2 mm diameter nails spaced at 150 mm on centre (s=150mm), while in case of wood sheathed shear walls, the selected wall configurations are sheathed on one side (n=1) with a 11.1 mm thick oriented standard board (OSB) and connected to the steel frame via 4.2 mm diameter screws spaced at 152 mm on centre at the panel edges (s=152 mm).

$$F_{Rd,c} = \frac{k_{mod} F_{Rk,c}}{\gamma_M} \tag{4-6}$$

where, $F_{Rk,c}$ is the characteristic strength of single panel-to-steel connection, which can be evaluated from tests on individual connections, k_{mod} is a coefficient dependent on loading duration and moisture content, assumed equal to 1.10 for instantaneous loading according to EN 1998-1 [4] and Service class 1 of EN 1995-1-1 [141]; γ_M is the partial safety factor assumed equal to 1.00 considering the seismic actions as an accidental load combination, as suggested for dissipative structures by EN 1998-1 [4] and EN 1995-1-1 [141]. It must be noted that Equation (4-6) is given in EN 1995-1 [141] which covers mainly wood structures. Characteristic shear strength of single gypsum panel-to-steel connection is evaluated to be 0.83 kN using cyclic shear tests [100] while the same is evaluated to be 1.89 kN [142] for a single connection made between OSB panel and the steel frame. Subsequently, F_{Rd} is evaluated to be 12.1 kN/m and 13.72 kN/m for CFS gypsum and wood sheathed shear wall, respectively. Hence, the strength

of one gypsum sheathed shear wall is evaluated to be 29.0 kN, which is close to the peak strength of 33.0 kN observed during the cyclic test [8] on a similar specimen. While, the shear strengths of aspect ratio 1.0 and 2.0 wood sheathed shear walls is evaluated to be 33.49 and 16.74 kN, respectively, which are close to the experimentally evaluated strength values of 36.35 and 17.93 kN [66] for walls with aspect ratio 1.0 and 2.0, respectively. An over-strength factor of 1.2 is used for the non-dissipative elements including chord studs, tracks, sheathing panels, hold-downs and shear anchorage. The design strength of these non-dissipative element can be evaluated from other relevant parts of Eurocodes.

4.2. Non-linear Model Development for Archetypes

Numerical modelling of the archetypes is needed for their seismic performance evaluation. It is expected from the building using CFS shear walls as the primary seismic force resisting system, that it would mainly develop the nonlinear mechanism only at the sheathing connections, while rest of the elements would remain elastic. Thus, the simulation of response of the shear walls is the single most important factor in the modelling of complete building response. OpenSees software [93] is used for developing the numerical models. A two-stage modelling approach is adopted. At first, numerical model for single wall is developed and calibrated based on the experimental result and then in the later stage, the model of single wall is incorporated in a complete building representing the global response of the archetypes. The choice of the type of model for single wall and different modelling options available in literature are explained in detail in Section 2.4.2. Here only the significant details and fewer comments on the efficiency of single wall models is provided.

4.2.1. Models of Single walls

A simplified model (Figure 4-6), which relies on a pair of nonlinear diagonal truss elements is used to simulate the response of a shear wall. Simplified models have already been used by researchers in similar studies [97,98,143] to simulate the response of typical LWS structural systems due to the ease through which they can be integrated with the complete building models. Another option is to model the response through a detailed FE model [86,87] which requires the modelling of individual sheathing connection, but the integration of such wall models with building models would be more complex and prone to convergence problems due to the increased complexity.
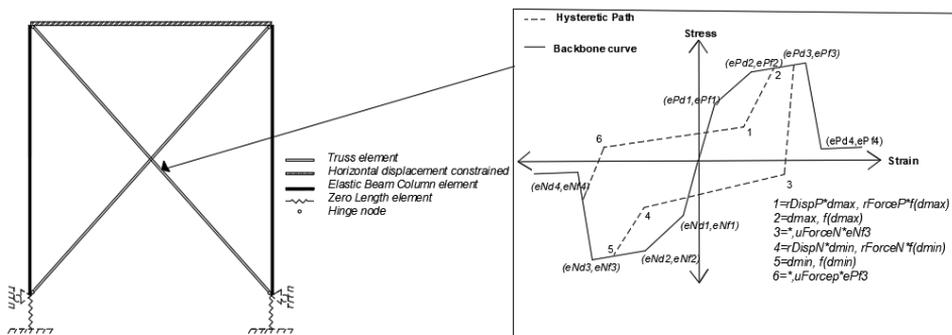

Figure 4-6 Simplified Truss model using Pinching4material

Figure 4-6 shows a typical hysteretic response of CFS wood and gypsum sheathed shear wall, which is characterized by severe pinching. The pinching of hysteresis loops is produced by tilting and bearing of nails or screws against the sheathing material in one loading direction then upon the load reversal they do not experience an equal level of tilting or bearing forces due to the loosening of sheathing connection. The loosening of sheathing connections is primarily responsible for the pinched response. Pinching4 material [92] is used to represent the nonlinearity in truss

elements having a unit area, which are the representative of the behaviour of walls as a whole. Choice of Pinching4 material is motivated by appreciable results obtained by other researchers who used it to simulate the response of CFS shear walls [80,133]. Pinching4 material is a uniaxial material that can represent pinched load deformation response with the ability to exhibit degradation under cyclic loading, defined through a set of 39 parameters. These parameters include 16 parameters for the definition of the backbone envelope (ePf1, ePd1, ePf2, ePd2, ePf3, ePd3, ePf4, ePd4, eNf1, eNd1, eNf2, eNd2, eNf3, eNd3, eNf4, eNd4), 6 parameters for defining the cyclic behaviour (uForceP, uForceN, rDispP, rDispN, rForceP, rForceN), which are the ratios of the deformation at which unloading/reloading occurs to the maximum (d_{max})/minimum (d_{min}) historic deformation demand, 5 parameters for governing the strength degradation (gF1, gF2, gF3, gF4, gFLim), 5 parameters for controlling the unloading stiffness degradation (gK1, gK2, gK3, gK4, gKLim), 5 parameters for controlling the reloading stiffness degradation (gD1, gD2, gD3, gD4, gDLim), and 2 parameters for limiting the maximum degradation in each cycle (gE, dmgType). In particular, the 4-point backbone envelope is defined considering an average envelope curve obtained considering the positive and the negative branches. Therefore, symmetric values of these parameters are used for both the positive and the negative branches and only 8 independent parameters are defined (ePdi=eNdi, ePfi=eNfi). Similarly, symmetric values of the parameters defining the cyclic behaviour are also used for both the positive and negative branches of hysteretic path. The key parameters of the material are illustrated in Figure 4-6 and their values are provide in Table 4-5. which are calibrated on the basis of experimental results [8,144].

Table 4-5 Parameters for pinching4 material

CFS gypsum sheathed shear walls													
Parameters for backbone curve													
ePf1	ePf2	ePf3	ePf4		ePd1		ePd2		ePd3		ePd4		
[kN]	[kN]	[kN]	[kN]		[m/m]		[m/m]		[m/m]		[m/m]		
4.8	19.1	23.8	9.8		0.0002		0.0024		0.005		0.0161		
Parameters for cyclic behaviour													
uForce	rDisp	rForce	gF,1,2	gF,3,4	gF,Lim	gK,1,2	gK,3,4	gK,Lim	gD,1,2	gD,3,4	gD,Lim	gE	dmgType
[-]	[-]	[-]	[-]	[-]	[-]	[-]	[-]	[-]	[-]	[-]	[-]	[-]	[-]
0	0.45	0.1	0	0	0	1.2	1.2	0.9	0.2	1.2	0.4	10	energy
CFS wood sheathed shear walls													
Parameters for backbone curve (Walls 1:1)													
ePf1	ePf2	ePf3	ePf4		ePd1		ePd2		ePd3		ePd4		
[kN]	[kN]	[kN]	[kN]		[m/m]		[m/m]		[m/m]		[m/m]		
5.5	22.3	27.9	7.5		0.00023		0.0027		0.009		0.0122		
Parameters for backbone curve (Walls 2:1)													
ePf1	ePf2	ePf3	ePf4		ePd1		ePd2		ePd3		ePd4		
[kN]	[kN]	[kN]	[kN]		[m/m]		[m/m]		[m/m]		[m/m]		
4.4	17.9	22.4	11.0		0.00020		0.0039		0.008		0.0138		
Parameters for cyclic behaviour													
uForce	rDisp	rForce	gF,1,2	gF,3,4	gF,Lim	gK,1,2	gK,3,4	gK,Lim	gD,1,2	gD,3,4	gD,Lim	gE	dmgType
[-]	[-]	[-]	[-]	[-]	[-]	[-]	[-]	[-]	[-]	[-]	[-]	[-]	[-]
0	0.5	0.1	0	0	0	0	0	0	0	0	0	10	energy

Rest of the wall elements, including chord studs and hold down devices are also modelled, which are necessary for the transfer of forces to the rest of building. However, in case of wood sheathed shear walls, hold down devices are not modelled explicitly, due to the absence of data on their response from the experiments [66]. In fact, the hysteretic response curves provided by the in plane quasi static cyclic tests [66] on wood sheathed

shear walls already had the force and deformations of hold down devices lumped in the global wall response. The chord studs present at ends of the wall transmitting the axial forces are modelled using the Truss elements with a Uniaxial elastic material, having modulus of elasticity of 210 GPa. Due to the axial forces being transmitted through them, they can either collapse due to tension or can have buckling under the compression. Moreover, the hold devices could also show brittle failure modes under the action of tensile force coming from chord studs. Though, these brittle failure modes are not deemed to happen before the ductile failure of wall due to the adoption of capacity design approach, but their inclusion in models could help in to evaluate the functionality of capacity design approach.

Opensees MinMax material is used in conjunction with Uniaxial elastic material in order to simulate the chord stud failure due to tensile rupture or the local or global instabilities. Opensees MinMax material is always used in conjunction with another material, which define its stress-strain behaviour, and it enforces the threshold values of strain, beyond which strength and stiffness of an element are set to zero. In the specific case, threshold values, which govern the occurrence of failure of studs in tension ($\varepsilon_{t,Rk}$), and compression ($\varepsilon_{b,Rk}$), were calculated using Equation (4-7) and (4-8).

$$\varepsilon_{t,Rk} = \frac{N_{t,Rk}}{A \cdot E} \qquad\qquad\qquad (4\text{-}7)$$

$$\varepsilon_{b,Rk} = \frac{N_{b,Rk}}{A \cdot E} \qquad\qquad\qquad (4\text{-}8)$$

where: $N_{t,Rk} = 247$kN and $N_{b,Rk} = 123$kN are the nominal resistances obtained according to prescriptions given in EN 1993-1-1 [130] and EN 1993-1-3 [14] corresponding to the tensile and buckling failure of chord

studs , respectively; E is the Young's modulus of steel; A is gross cross section area. Of course, the $N_{b,Rk}$ takes into account both the strength reduction due to the local buckling of cross section and the global member instabilities. In case of wood sheathed shear walls, the threshold limit in tension is the minimum of tensile strength of chord stud or hold down devices because their wall model does not have the hold down device modelled explicitly.

Hold-down devices in case of gypsum sheathed shear walls are modelled by using Zerolength elements having ElasticMultiLinear material with a stiffness $k_a = 37kN/mm$ in tension defined based on the experimental results [8]. MinMax material is used in conjunction with ElasticMultiLinear material in order to consider brittle tensile failure of the devices. For this purpose, tensile strain in MinMax material is set to not exceed the nominal tensile strain $\varepsilon_{a,Rk}$ of the hold downs, whereas there is no strain limit in compression. In particular, nominal tensile strain in anchors $\varepsilon_{a,Rk}$ is calculated using Equation (4-9).

$$\varepsilon_{a,Rk} = \frac{N_{a,Rk}}{k_a \cdot l_a} \tag{4-9}$$

where $N_{a,Rk} = 43kN$ is the nominal tensile resistance of anchors and l_a represents the unit length of the hold down device.

To verify the model's ability to simulate the response of CFS shear walls, it is analysed under the same cyclic loading protocol as used in the tests [8,144]. Figure 4-7 shows the comparison of hysteretic response of the wall model and test along with the comparison in terms of cumulative energy dissipated. It can be noticed that numerical models are able to capture the experimental hysteretic response in terms of overall shape and location of peaks and are able to dissipate energy in a similar manner to

the experimental tests. Though in case of wood sheathed shear wall with an aspect ratio 1.0, there is an overestimation of energy and forces in last few cycles. However, this overestimation is due to the few abnormal hysteretic envelopes in the negative direction of the experimental force displacement response of the wall. Such type of experimental response in not typical to the wood sheathed shear walls, as one can see from the comparison of available experimental results on aspect ratio 1 wall as shown in Figure 4-2.
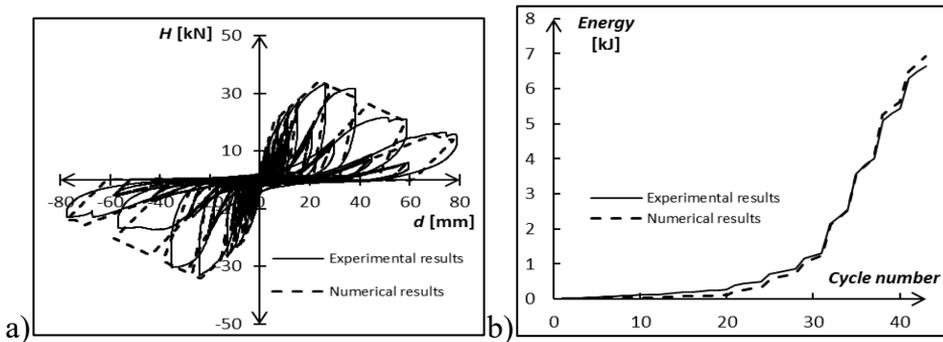
CFS gypsum sheathed shear wall
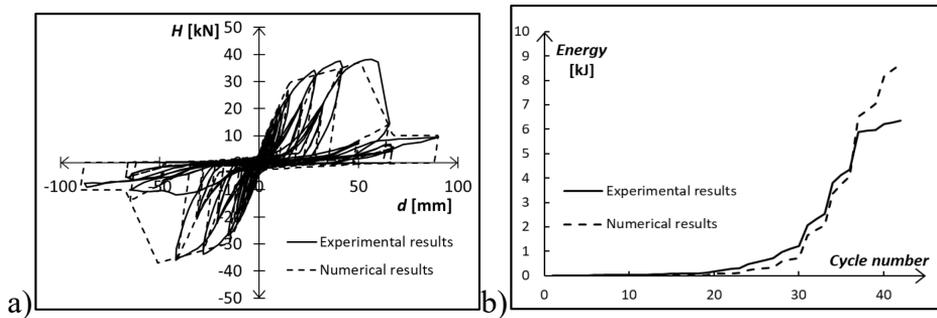
CFS wood sheathed shear walls (Aspect ratio 1:1, Wall A)
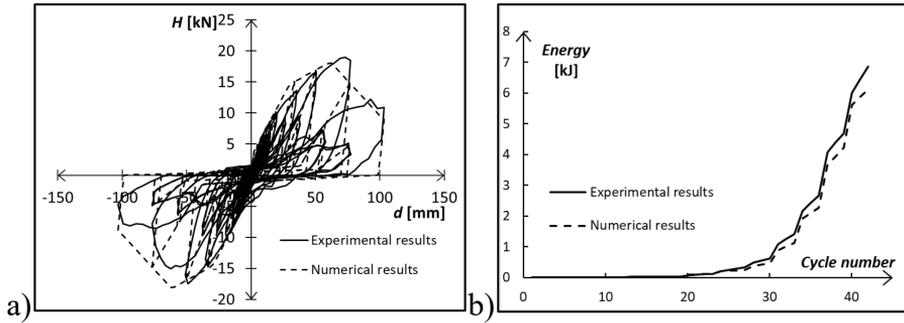
CFS wood sheathed shear walls (Aspect ratio 2:1, Wall B)

Figure 4-7 Comparison of numerical and experimental results: Hysteretic response (a), Cumulative energy dissipation (b)

4.2.2. 3D non-linear model of Archetype

A three-dimensional model representing the most important structural elements that would have significant implications on the global seismic response of the building is created for each archetype. The skeleton of a typical CFS building is made by joining the wall elements, such as studs and wall tracks, to the floor elements, such as floor tracks and joists. The gravity load bearing studs are modelled using truss elements. Not all of the gravity load bearing studs are modelled, because the presence of gravity load bearing studs does not affect much the seismic performance of the archetypes since they cannot resist any bending moments. Moreover, adding all the studs in model would make the model unnecessarily complex. Floor diaphragm could either be modelled as rigid or semi rigid depending upon its in plane stiffness. Both floor solutions are considered to offer rigid in plane behaviour owing to their high in plane stiffness. A realistic modelling approach for modelling the floors is dividing it into subpanels and calibrating their hysteretic response, as done in [9]. This approach however would require wider experimental database on floor diaphragm behaviour, is outside the scope of this study and would not

affect much the value of the behaviour factor, as it is strictly linked to collapse simulation of the seismic force resisting system. Therefore, floor elements (joist, tracks and composite floor) are modelled as the rigid elastic beam column elements. The assumption of rigid floor is also in accordance with the test results obtained from shake-table tests [140], which showed a rigid in plane response for a floor configuration similar to the light solution used in this study. Figure 4-8 shows a 3D schematic representation of a double storey residential archetype braced with gypsum sheathed shear walls.

In addition to the earthquake loads causing the lateral displacements, the gravity loads also tend to produce global lateral displacements in building due to commonly known P-delta effect, which are also resisted by the seismic force resisting system. To capture the lateral displacement arising from P-delta effect, a frame made of axially rigid Elastic beam column elements with the low flexure stiffness and having a Co-rotational coordinate transformation is connected to the building in the direction of seismic action. The axial stiffness of the columns represents the aggregate stiffness of gravity studs at a particular storey, while the flexure stiffness is 1/1000 times the axial stiffness. Nevertheless, flexure stiffness does not affect the response due to pinned end columns of the P-delta frame. P-delta effect can be simulated in OpenSees using the elastic beam column elements with the co-rotational coordinate transformation. In the actual building, the studs are truss elements, and with the truss elements, it's not possible to simulate the P-delta effect. This is the main reason of using a separate frame. Moment releases are created at the ends of columns of the P-delta frame and are linked to the main building frame using the Rigid truss elements. Moment releases at the ends of columns are intended to

avoid any transfer of moments from P-delta fame to main frame and hence only transmitting the axial force, which induce an equivalent lateral displacement in the main frame. A similar approach is also adopted for the inclusion P-delta effects in model of CFS buildings with steel sheathed braced shear walls by Shamim and Rogers in [98]. Gravity load computed according to loading combination given in Equation (4-1) is applied to the P-delta columns at floor levels.
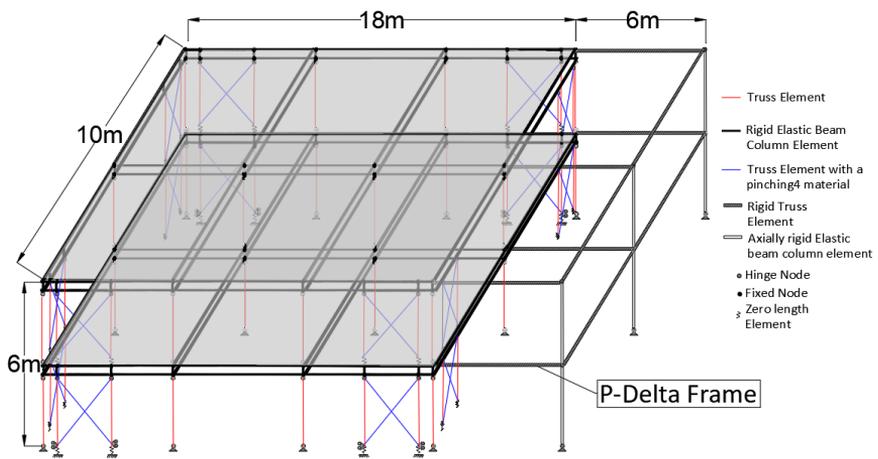

Figure 4-8 3D schematization of different elements in a model

The total gravity load divided based on the tributary area of each stud is applied as vertical point load positioned at its top. The seismic mass is distributed at the four corner nodes of each floor. In case of pushover analysis, the equivalent lateral force on each floor is applied at a single node in centre of floors. For dynamic analysis, a 2% damping ratio is used based on the Rayleigh damping model in case of archetypes braced with CFS gypsum sheathed shear walls, while a value of 5% is used for archetypes with CFS wood sheathed shear walls. These values of damping ratio reflected the measured damping values during the shake-table experiments [140,145].

4.3. Non-linear Analysis

Before proceeding to the non-linear analyses, gravity analysis is also performed to recheck the internal forces in the members and modal analysis is conducted to investigate the mode shapes and their respective vibration periods for each archetype. All of the archetypes exhibited the first mode of vibration with horizontal displacements increasing linearly along the heights. Numerical fundamental vibration period (T_1) associated with this mode shape are listed in Table 4-6, 4-7 and 4-8 along with their ratio to estimated fundamental vibration period (T) obtained from EN 1998-1 [4], which are listed in Table 4-1, 4-2 and 4-3. Numerical fundamental vibration periods (T_1) obtained from the modal analysis are 1.7 to 4.0 times higher than the estimated fundamental vibration period (T) obtained from EN 1998-1 [4], which confirms the well-known importance for evaluating vibration periods using detailed procedures such as numerical models, which take into account both the correct mass and stiffness properties, while the code estimated fundamental vibration periods (T) are just an estimate based on height and structural typology.

4.3.1. Non-linear static analysis

The ratio between the actual and the design strength of building is an over-strength factor. This factor is then used in the linear static equivalent lateral force analyses to increase the magnitude of earthquake forces in seismic standards, and hence eliminating the need for designer to perform the nonlinear analysis to calculate the ultimate response. Currently only the North American standards [13] propose a value of 2.5 for this factor, which is based on coarse estimate due to the absence of the specific research on this topic. FEMA P695 [12] methodology relies on the non-linear static (pushover) analysis to estimate archetype over-strength. The

lateral forces used in the pushover analysis are computed according to design base shear distribution given in Equation (4-2) and (4-3). Before the application of lateral force on the models, gravity loads are applied according to load combination in expression (4-1). Finally, the archetype over-strength is computed as the ratio of maximum base shear resistance (V_{max}) of archetype obtained through pushover analysis to the design base shear (V_d). Figure 4-9 shows the pushover curves of archetypes, which are the base shear (V) normalized by the design base shear (V_d) plotted against the root drift.. After achieving the maximum base shear resistance, all the archetype models have the concentration of damage at a ground storey. It is also evident that models behaved almost similar under design base shear distribution computed according to Equation (4-2) and (4-3). The shape of pushover curve can be related to the shape of backbone curve used in *Pinching4 material* for shear walls. Moreover, the pushover analysis is conducted in both planar directions of archetypes. The response in two planar directions do not differ much in terms of V_{max} in most of the cases, while the ultimate roof displacement (δ_u) presented slight differences. Ultimate roof displacement (δ_u) is taken as the roof displacement at the point of 20% strength loss ($0.8V_{max}$) in the pushover analysis [12].
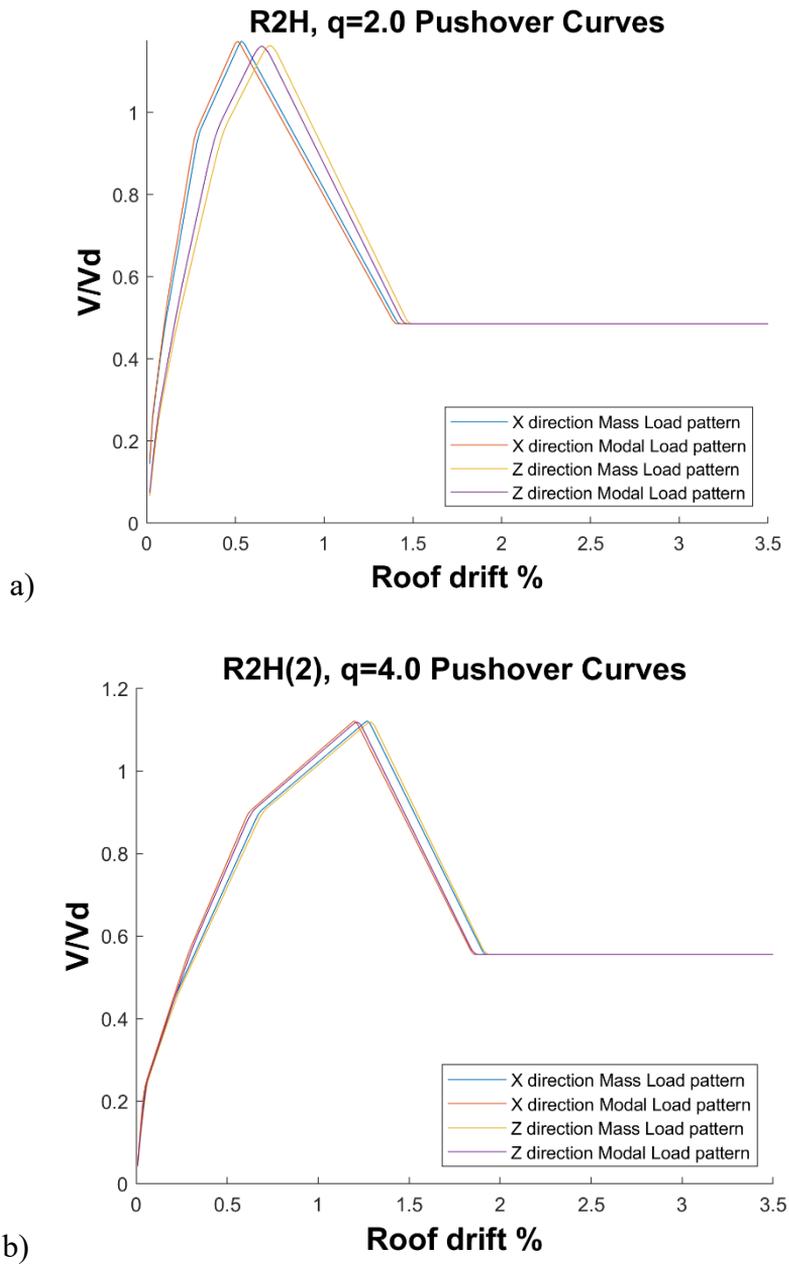
Figure 4-9 Pushover curves a: CFS gypsum sheathed shear walls archetypes; b: CFS wood sheathed shear walls archetypes

Additionally, the pushover analysis is also used to compute the period-based ductility, which is used to evaluate the effect of spectral shapes of

different earthquake records, used for the dynamic analysis, on the archetype performance. Period-based ductility (μ_T) is defined as the ratio of ultimate roof displacement (δ_u) to the effective roof yield displacement ($\delta_{y,eff}$), where effective yield roof displacement ($\delta_{y.eff}$) is computed according to Equation (4-10).

$$\delta_{y,eff} = C_0 \cdot \frac{V_{max}}{W} \cdot \left[\frac{g}{4\pi^2}\right] (\max(T, T_1))^2 \qquad (4\text{-}10)$$

where, where C_0 relates fundamental-mode (SDOF) displacement to roof displacement obtained according to Equation 6-8 of FEMA P695 [12]; V_{max}/W is the maximum base shear normalized by building seismic weight W; g is the gravity constant; T is the fundamental vibration of archetype expressed as a function of height of building and given in Table 4-1, 4-2 and 4-3; and T_1 is the fundamental vibration period of the archetype model computed using linear dynamic analysis and summarized in Table 4-6, 4-7 and 4-8.

Subsequently, the final value of the over-strength and the period-based ductility for each archetype is computed based on its average response in both directions and under both types of the load distribution patterns based on FEMA P695 [12] recommendations. Table 4-6, 4-7 and 4-8 summarize for each archetype: the design base shear (V_d), the maximum base shear resistance in both planar directions, i.e. X (long direction) and Y (short direction) under the design base shear distribution computed according to Equation (4-2) and (4-3) (A and B) ($V_{max,X,A}$, $V_{max,X,B}$, $V_{max,Y,A}$, $V_{max,Y,B}$), the average ultimate roof displacement (δ_u), average effective roof yield displacement ($\delta_{y.eff}$) the average over-strength factor Ω and the period based ductility μ_T obtained through non-linear static analysis.

Table 4-6 Results from modal and pushover analysis for CFS gypsum sheathed shear walls (q=2.0)

Archetype ID	T_1 (sec)	T_1/T	$V_{max,X,A}$ [kN]	$V_{max,X,B}$ [kN]	$V_{max,Y,A}$ [kN]	$V_{max,YB3}$ [kN]	V_d [kN]	Ω	δ_u [mm]	$\delta_{y.eff}$ [mm]	μ_T
R1L	0.28	2.5	136	136	137	137	129	1.06	44.5	6.40	6.9
R2L	0.38	2.0	204.3	204	205	205	175	1.17	50.0	7.90	6.3
R3L	0.48	1.8	408	408	408	408	322	1.27	66.3	13.9	4.8
R4L	0.65	2.0	545	545	545	545	469	1.16	48.5	23.2	1.9
O1L	0.35	3.2	137	137	130	130	101	1.33	48.5	6.10	7.0
O2L	0.48	2.5	408	408	404	404	332	1.23	58.0	12.8	4.0
R1M	0.22	2.0	341	341	338	338	258	1.32	44.5	9.40	4.6
R2M	0.34	1.8	410	410	409	409	350	1.17	49.8	12.6	3.9
R3M	0.44	1.7	615	614	614	613	528	1.16	59.3	21.4	2.7
O1M	0.31	2.8	273	273	246	246	203	1.31	52.5	9.40	4.5
O2M	0.37	1.9	614	614	599	600	504	1.21	57.3	14.9	3.3
R1H	0.20	1.8	410	410	470	470	387	1.10	51.0	10.3	4.6
R2H	0.32	1.7	616	616	616	616	525	1.17	53.3	16.3	3.0
O1H	0.27	2.5	409	409	398	398	304	1.34	58.5	10.7	4.1

Table 4-7 Results from modal and pushover analysis for CFS wood sheathed shear walls (q=4.0)

Archetype ID	T_1 (sec)	T_1/T	$V_{max,X,A}$ [kN]	$V_{max,X,B}$ [kN]	$V_{max,Y,A}$ [kN]	$V_{max,YB3}$ [kN]	V_d [kN]	Ω	δ_u [mm]	$\delta_{y.eff}$ [mm]	μ_T
O1L	0.46	4.0	73	73	73	73	42	1.73	73.00	10.1	7.3
O1M	0.29	2.5	148	148	148	148	84	1.77	55.60	8.1	6.8
O1H	0.29	2.5	148	148	148	148	126	1.18	55.60	8.1	6.8
R2L	0.56	2.9	147	147	147	147	76	1.94	74.01	16.3	4.5
R2M	0.57	3.0	175	175	166	166	151	1.14	69.00	19.6	3.5
R2H (2)	0.61	3.2	253	253	253	253	227	1.12	89.79	33.3	2.7
R2H (1)	0.37	1.9	252	252	250	250	227	1.11	76.50	12.1	6.3
O2L	0.55	2.9	144	144	147	147	122	1.19	55.38	9.7	5.7
O2M	0.45	2.3	291	291	294	294	243	1.20	61.20	13.1	4.7
O2H (2)	0.44	2.3	430	430	430	426	365	1.18	83.88	18.3	4.6
O2H (1)	0.49	2.6	434	434	434	434	365	1.19	60.55	23.0	2.6
R4L	0.99	3.1	215	215	194	194	173	1.21	81.50	30.8	2.6
R4M	0.72	2.2	441	441	441	441	346	1.27	92.25	35.1	2.6
R4H (2)	0.77	2.4	578	578	570	570	520	1.11	136.02	52.3	1.9
R4H (1)	0.77	2.4	582	582	582	582	520	1.12	102.60	53.0	2.6

R6L	1.28	2.9	290	290	290	290	271	1.07	99.46	55.2	1.8
R6M (2)	0.93	2.1	575	575	575	575	543	1.06	152.97	58.2	1.7
R6M (1)	1.01	2.3	584	584	584	584	543	1.07	119.50	69.7	2.6

Table 4-8 Results from modal and pushover analysis for CFS wood sheathed shear walls (q=2.5)

Archetype ID	T_1/T	$V_{max,X,A}$ [kN]	$V_{max,X,B}$ [kN]	$V_{max,Y,A}$ [kN]	$V_{max,YB3}$ [kN]	V_d [kN]	Ω	δ_u [mm]	$\delta_{y,eff}$ [mm]	μ_T
O1L	4.0	73	73	73	73	55	1.32	76.0	10.1	7.6
O1M	3.2	145	145	145	145	111	1.30	77.0	12.8	6.0
O1H	2.7	182	182	207	207	167	1.13	70.5	12.2	5.8
O2L	2.5	255	255	255	255	191	1.33	62.1	12.5	5.0
O2M	2.3	436	436	436	436	382	1.14	61.8	18.5	3.3
O2H	1.9	698	698	698	698	573	1.22	73.3	20.6	3.6
R2L	2.8	145	145	145	145	118	1.23	87.0	15.0	5.8
R2M	2.6	282	282	282	282	237	1.19	68.5	23.9	2.9
R2H	1.9	392	392	381	381	356	1.09	88.5	18.7	4.7
R4L	2.3	294	294	294	294	277	1.06	88.8	24.1	3.7
R4M	2.9	516	516	516	516	462	1.12	85.8	67.1	1.3
R6L	2.4	516	516	516	516	434	1.19	126.0	68.7	1.8

4.3.2. Non-linear incremental dynamic analysis (IDA)

The collapse performance of archetypes in terms of the Collapse Margin Ratio (CMR) can be assessed through incremental dynamic analysis (IDA) [132], which uses a set of ground motions scaled with increasing scaling factors to reach a magnitude that will cause the collapse. CMR is the ratio between median collapse intensity (S_{CT}) and maximum considered earthquake intensity (S_{MT}). CMR can also be perceived as a capacity to demand ratio, in which capacity and demand are represented by S_{CT} and S_{MT}, respectively. The S_{CT} is defined as the intensity at which half of the ground motions in the record set cause collapse of an archetype model, while S_{MT} is the intensity associated to the maximum considered earthquake.

The collapse of archetypes can be defined in terms of the exceedance of a threshold value of a particular damage measure representing the behaviour at either local member level or global building level. The local damage measures include buckling of studs, tensile rupture of anchors, etc, while the global building damage can be judged through checking the excessive inter storey drift levels. Most of these local type damages are not expected to happen before the failure of seismic force resisting system, due to the adoption of capacity design approach. Nonetheless, a few of local failure mechanism are modelled inherently in the model as explained earlier. The 4% inter storey drift ratio (IDR) is used as a threshold value causing the collapse at global level. In case of gypsum sheathed shear walls, the 4% IDR is selected based on a similar study on shear walls with the fibre cement board panels [146], which exhibit a comparable behaviour as walls with gypsum board panels and are classified under the same category in AISI S400 [18]. It must be noted that since the floors are rigid in plane and the archetypes are symmetrical in each direction, therefore the shear walls at any storey had equal drifts as the storey drift. The gypsum sheathed shear wall configuration used in this study was also able to sustain load carrying capacity until 6% during the experiments [8], even though the ultimate displacement was 2% defined based on its conventional definition, i.e. point corresponding to the 20% drop in strength after the peak. In case of wood sheathed shear walls, the 4% IDR is the drift level until which the individual units of shear walls had not experienced collapse during the tests [66]. By looking into similar studies [97,98,143] conducted on different types of seismic force resisting systems used in LWS building, values of IDR in a range of 2.5 to 5% can also be found.

FEMA P695 also provides the two sets of ground motion records for collapse assessment: far-field record set and the near-field record set. Methodology prescribes to use the far-field record set for structures, which are designed for Seismic Design Category (SDC) B, C and D according to ASCE 7 [13]. All of the archetypes in this study belonged to either of these categories. Far-Field record set (Table 3-11) comprises of twenty-two component pairs of horizontal ground motions (in total 44 records) from sites located greater than or equal to 10 km from fault rupture having a magnitude (Richter scale) and peak ground acceleration (*PGA*) greater than 6.5 and 0.2g, respectively. All 22 earthquake record pairs are normalized to remove the unwarranted variability between records due to the inherent differences in the event magnitude, distance to source, source type and site conditions, without eliminating the overall record-to-record variability based on the Peak Ground Velocity (PGV) using the normalization factors, which are already provided in [12] and listed in Table 3-11. Normalized ground motions are then matched to the archetype design response spectrum through the scaling of median response spectrum of all records within the range of fundamental vibration periods of archetypes. In particular the peak of median response spectra of all records is matched with design response spectra of archetype at its estimated fundamental vibration period (*T*) according to EN 1998-1 [4] and listed in Table 4-1, 4-2 and 4-3.

Finally, all the 44 scaled records are applied to archetype models in the both planar directions with a 20% increment in intensity starting from a 20% (Scaling factor (SF) = 0.2) to 600% (Scaling factor = 6.0). The SF=1.0 is the representative of design level earthquake, while SF=1.5 corresponds to MCE. This is due to the fact that the maximum considered earthquake

of ASCE 7 [13] can be obtained by multiplying the design earthquake of EN 1998-1 [4] by 1.5, as explained earlier.

The results from the analysis are represented in the form of IDA curves, in which each curve represents the response of the archetype under a particular record. The curve is made of several points, with each point representative of the maximum inter storey drift ratio achieved at a particular scaling factor. Figure 4-10 shows the IDA curves for the archetypes. From the examination of IDA curves in Figure 4-11, it can be seen that one or two record are not able to cause the collapse, even at the very high scaling factors. This problem is caused due to the scaling process explained earlier, in which median of record set is scaled to match the design response spectrum of building. However, some records could have larger variance from the median. When such records are scaled with the scaling factor obtain based on the meadian, there could be a significant mismatch between the spectral acceleration of record and design response spectral acceleration at building fundamental period of vibration, which resulted in this response.
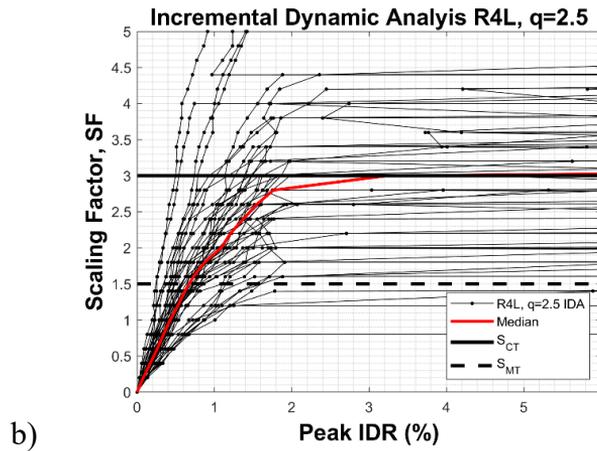

a)
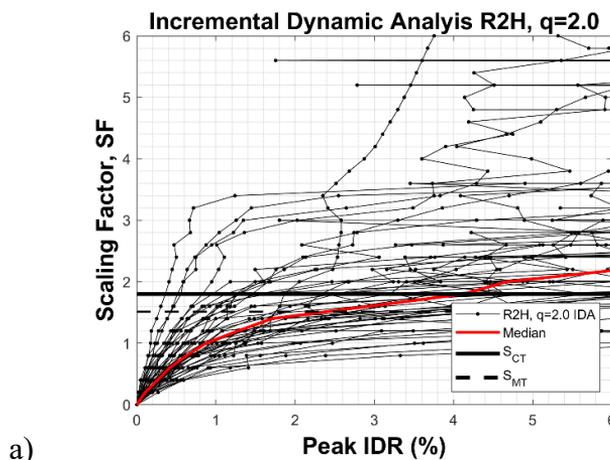
Figure 4-10 IDA curves a: CFS gypsum sheathed shear walls archetypes; b: CFS wood sheathed shear walls archetypes

4.4. Performance evaluation of archetypes

The fundamental premise of the performance evaluation process is that an acceptably low, yet reasonable, probability of collapse can be established as a criterion for assessing the collapse performance of the proposed system [12]. This is realized by checking the acceptability of the trial value of behaviour factor used in the design phase. Acceptability is measured by comparing the CMR-s against the acceptance criteria, which are based on the quality of the information used to define the system, total system uncertainty, and established limits on collapse probability.

The CMR-s obtained from the IDA analysis are adjusted to take into the spectral shapes of different records used for the analysis. The adjusted CMR (ACMR) is the product of CMR and a spectral shape factor (SSF). The SSF is a function of the period based ductility (μ_T), numerical fundamental vibration period (T_1) of an archetype model, seismic design category and, can be calculated according to Table 7-1a and 7-1b of FEMA P695 [12].

Once the ACMR of each archetype is obtained, their acceptability can be evaluated by comparing them against the performance criteria of FEMA P695. Two performance criteria are defined by the methodology [12]: the average value of adjusted collapse margin ratio, $ACMR_{avg}$, for each performance group should be greater than $ACMR_{10\%}$, and the individual values of the adjusted collapse margin ratio, $ACMR_i$, for each archetype within a performance group should be greater than $ACMR_{20\%}$. $ACMR_{10\%}$ and $ACMR_{20\%}$ values are the 10% and 20% threshold values for the probability of collapse, respectively. A higher threshold value of 20% for the probability of collapse of individual archetypes reflects the recognition of potential outliers by the FEMA methodology. The value of $ACMR_{10\%}$ and $ACMR_{20\%}$ are given in Table 7-3 of FEMA P695 and are function of total collapse uncertainty β_{TOT}.

The total collapse uncertainty β_{TOT} takes into account the different sources of uncertainty that could contribute to variability in collapse capacity. In particular, the main sources of uncertainty include: record to record uncertainty (β_{RTR}), design requirements uncertainty (β_{DR}), test data uncertainty (β_{TD}); and modelling uncertainty (β_{MDL}). The total uncertainty is then coupled from these different sources using the Equation (4-11).

$$\beta_{TOT} = \sqrt{\beta_{RTR}^2 + \beta_{DR}^2 + \beta_{TD}^2 + \beta_{MDL}^2} \qquad (4\text{-}11)$$

Record to record uncertainty (β_{RTR}) is due to variability in the response of the archetypes model to different ground motion records, which could have different frequency content and dynamic characteristic. β_{RTR} can be computed according to Equation (4-12).

$$\beta_{RTR} = 0.1 + 0.1 \cdot \mu_T, \text{ with } \beta_{RTR} > 0.2 \text{ and } \beta_{RTR} \leq 0.4 \qquad (4\text{-}12)$$

Most of the archetypes have β_{RTR} equal to 0.40, except for few cases which showed limited ductility and resulted in a lesser β_{RTR} values. The rest of the uncertainty parameters β_{DR}, β_{TD} and β_{MDL}, are the qualitative measures provided by FEMA P695 [12] on the basis of following scale: (a) Superior, $\beta = 0.10$; (b) Good, $\beta = 0.20$; (c) Fair, $\beta = 0.35$; and (d) Poor, $\beta = 0.50$. The design process used in this study ensures the ductile behaviour of seismic force resisting system, while safeguarding against the unanticipated brittle failure mechanisms and predicted the design strength in a close match to the experimental results [8,66]. Hence, the design requirements are rated as "Good" ($\beta_{DR} = 0.2$). In authors opinion, the rating could be excellent only if the seismic force resisting system is already codified in seismic standards, which in this case is not true for the Eurocodes. The test data on the performance of seismic force resisting system is rated as "Superior" ($\beta_{TD} = 0.1$), based on the fact that the different components [8,66,100,142] of the shear wall were already tested, the wall itself was tested under the both monotonic and cyclic type loadings [8,66], and last but not the least, seismic performance of the shear walls was also validated via the shake-table tests [140,147]. Archetype modelling is rated as "Good" ($\beta_{MDL} = 0.2$) because all the models are calibrated based on the experimental results and have the ability to exhibit post peak shear strength deterioration and to simulate the brittle failure mechanisms. Moreover, models also accounted for the internal forces arising in the members due to the P-delta effects. Finally, the total uncertainty, β_{TOT}, computed using Equation (4-11) is 0.49 and 0.48 for CFS gypsum and wood sheathed shear walls respectively, considering an average value of β_{RTR}, as it differs for few cases. Based on the value of β_{TOT}, $ACMR_{10\%}$ and $ACMR_{20\%}$ are obtained from Table 7-3 of FEMA

P695 [12] equal to 1.88 and 1.51, respectively in case of gypsum sheathed shear walls and 1.84 and 1.49 in case of wood sheathed shear walls.

Table 4-9 summarizes the results from the performance evaluation process of gypsum sheathed shear walls. Except three archetypes, which have $ACMR_i$ less than the $ACMR_{20\%}$, rest of the archetypes have $ACMR_i$ greater than the $ACMR_{20\%}$. These three archetypes: R3M, R2H and O1H are listed as "Near Pass" based on the fact that they still meet the acceptance criterion with an accuracy of at least 94%. In the current study, if an archetype meets the acceptance criterion by at least 90%, it is considered as "Near Pass". Similar criterion is also used for Near Passing archetypes in [97,98]. Moreover, this level of accuracy can be further be justified based on the fact that the shake-table tests of gypsum sheathed braced specimen [140] showed quite stiffer response even under an earthquake with peak ground acceleration of 1.0g. These specimens had all the finishing layers, which certainly contributed to the improved seismic performance. If the near passing archetypes are also to account for these additional finishes, their seismic response would certainly have been far better. Nonetheless, the $ACMR_{avg}$ of complete performance group clearly meets the acceptance criteria. This concludes that the initial value of behaviour factor equal to 2.0 used in design is appropriate for gypsum sheathed shear walls.

Table 4-9 Collapse performance evaluation process of CFS gypsum sheathed shear walls (q=2.0)

Archetype ID	S_{CT}	S_{CT}	SSF	CMR	ACMR	ACMR 20%	Pass /Fail	ACMR avg	ACMR 10%	Pass /Fail
R1L	2.70	1.50	1.12	1.80	2.02	1.51	Pass			
R2L	2.80	1.50	1.11	1.87	2.07	1.51	Pass	1.91	1.88	Pass
R3L	3.10	1.50	1.10	2.07	2.27	1.51	Pass			
R4L	3.33	1.50	1.08	2.22	2.39	1.51	Pass			

O1L	2.47	1.50	1.13	1.64	1.86	1.51	Pass
O2L	2.90	1.50	1.09	1.93	2.11	1.51	Pass
R1M	3.60	1.50	1.13	2.40	2.71	1.51	Pass
R2M	2.25	1.50	1.09	1.50	1.64	1.51	Pass
R3M	2.00	1.50	1.07	1.33	1.43	1.51	Near Pass
O1M	2.09	1.50	1.10	1.39	1.53	1.51	Pass
O2M	2.23	1.50	1.08	1.49	1.61	1.51	Pass
R1H	2.57	1.50	1.25	1.71	2.13	1.51	Pass
R2H	1.80	1.50	1.18	1.20	1.42	1.51	Near Pass
O1H	1.83	1.50	1.23	1.22	1.50	1.51	Near Pass

In case wood sheathed shear walls, two archetype design spaces are designed. Initially, archetypes are designed using a trial value of behaviour factor equal to 4.0. However, the archetypes in that design space failed the performance evaluation criteria of FEMA P695 as shown in Table 4-10. Most of the archetypes have $ACMR_i$ less than the $ACMR_{20\%}$ while $ACMR_{avg}$ of complete performance is also less than the $ACMR_{10\%}$. Hence, a value of 4.0 for behaviour of wood sheathed shear walls is not suitable and will result in an unsafe design. Subsequently, as the FEMA P695 methodology guides, if an archetypes design space fails the performance evaluation criteria, it should be redesigned and analysed again with a lower value of behaviour factor. The second archetype design is then designed using a trial value of behaviour factor equal to 2.5. Table 4-11 summarizes the results from the performance evaluation process of this second design space. All of the archetypes have $ACMR_i$ greater (Pass) or slightly lower (Near Pass) than the $ACMR_{20\%}$ while $ACMR_{avg}$ is also slightly lower (Near Pass) than the $ACMR_{10\%}$. The definition of near passing archetypes is same as that of gypsum sheathed shear walls. Therefore, based on these results it can be concluded that the behaviour factor of 2.5 is suitable for wood sheathed shear walls.

Table 4-10 Collapse performance evaluation process of CFS wood sheathed shear walls (q=4.0)

Archetype ID	S_{CT}	S_{CT}	SSF	CMR	ACMR	ACMR 20%	Pass /Fail	ACMR avg	ACMR 10%	Pass /Fail
O1L	3.02	1.50	1.13	2.01	2.28	1.49	Pass			
O1M	1.63	1.50	1.13	1.09	1.23	1.49	Fail			
O1H	1.09	1.50	1.30	0.73	0.94	1.49	Fail			
R2L	2.60	1.50	1.10	1.73	1.91	1.49	Pass			
R2M	1.65	1.50	1.09	1.10	1.19	1.49	Fail			
R2H (2)	1.46	1.50	1.16	0.97	1.13	1.49	Fail			
R2H (1)	1.23	1.50	1.29	0.82	1.05	1.49	Fail			
O2L	1.53	1.50	1.12	1.02	1.14	1.49	Fail			
O2M	1.33	1.50	1.10	0.89	0.98	1.49	Fail	1.35	1.84	Fail
O2H (2)	1.40	1.50	1.24	0.93	1.16	1.49	Fail			
O2H (1)	1.10	1.50	1.15	0.73	0.84	1.49	Fail			
R4L	2.40	1.50	1.07	1.60	1.71	1.49	Pass			
R4M	1.77	1.50	1.07	1.18	1.26	1.49	Fail			
R4H (2)	1.66	1.50	1.16	1.11	1.28	1.49	Fail			
R4H (1)	1.28	1.50	1.13	0.85	0.96	1.49	Fail			
R6L	2.84	1.50	1.06	1.89	2.01	1.49	Pass			
R6M (2)	2.60	1.50	1.07	1.73	1.85	1.49	Pass			
R6M (1)	2.00	1.50	1.05	1.33	1.39	1.49	Near Pass			

Table 4-11 Collapse performance evaluation process of CFS wood sheathed shear walls (q=2.5)

Archetype ID	S_{CT}	S_{CT}	SSF	CMR	ACMR	ACMR 20%	Pass /Fail	ACMR avg	ACMR 10%	Pass /Fail
O1L	3.02	1.50	1.14	2.01	2.29	1.49	Pass			
O1M	2.10	1.50	1.12	1.40	1.57	1.49	Pass			
O1H	1.60	1.50	1.28	1.07	1.37	1.49	Near Pass			
O2L	2.45	1.50	1.11	1.63	1.81	1.49	Pass			
O2M	1.60	1.50	1.09	1.07	1.38	1.49	Near Pass			
O2H	1.67	1.50	1.21	1.11	1.35	1.49	Near Pass			
R2L	3.40	1.50	1.12	2.27	2.54	1.49	Pass	1.79	1.84	Near Pass
R2M	2.08	1.50	1.08	1.39	1.50	1.49	Pass			
R2H	1.74	1.50	1.24	1.16	1.44	1.49	Near Pass			
R4L	3.00	1.50	1.09	2.00	2.18	1.49	Pass			
R4M	2.11	1.50	1.03	1.41	1.45	1.49	Near Pass			
R6L	3.70	1.50	1.05	2.47	2.59	1.49	Pass			

In order to understand the effect of aspect ratio of wood sheathed shear walls on the building seismic performance, few special cases are also designed in the archetype design space designed with a behavior factor of 4.0. As explained earlier, experiments have shown that the shear walls with an aspect ratio 2.0 have shown better ductility capacity than the walls with an aspect ratio 1.0. In particular archetypes: R2H (2), R4H (2), R6M (2) and O2H (2) have only shear wall with an aspect ratio 2.0 spread across their plan. To understand the effect of the better ductility of walls with an aspect ratio 2.0 walls, these building archetypes can be compared with the similar archetypes: R2H (1), R4H (1), R6M (1) and O2H (1), which have both aspect ratio 2.0 and 1.0 walls spread across their plan. In fact, by comparing the ACMR of these cases of archetypes with each other, R2H (2), R4H (2), R6M (2) and O2H (2) have shown on average a 28% higher ACMR's than the respective archetypes: R2H (1), R4H (1), R6M (1) and O2H (1).

The collapse probability of each archetype is further examined via fragility curves generated through lognormal probability distribution [136] applied on the IDA results. Fragility curves also provide useful means of quantifying the vulnerability of the building. Though, collapse fragility evaluation not integrally the part of the FEMA P695 methodology, however it is shown here to serve as a reference for future studies, which could relate these fragility curves to different performance levels of building and henceforth could be useful in the performance based seismic design. In Figure 4-11, the scatter plot represents the simple probability of collapse at a particular scaling factor computed using Equation (13).

$$P(C|x) = \frac{n(x)}{n} \tag{13}$$

where $P(C|x)$ is the probability of collapse of the building at a scaling factor x, $n(x)$ is the number of ground motion at a scaling factor x that caused the collapse and n is the total number of ground motions. Basic Fragility curve is obtained by fitting the lognormal cumulative distributive function the scatter plot of simple probability [136]. Fragility curves are also adjusted to account for the effect of spectral shapes of different earthquake records through spectral shape factor (SSF) and the total collapse uncertainty (β_{TOT}). Hence, shifted fragility curve is obtained by multiplying the basic fragility curve with SSF and uncertainty adjusted fragility curve is calculated using β_{TOT} as the standard deviation in lognormal cumulative distributive function. Total collapse uncertainty has the effect of flattening the basic fragility curve and therefore reduces the probability of collapse as shown in Figure 4-11.

a)

b)
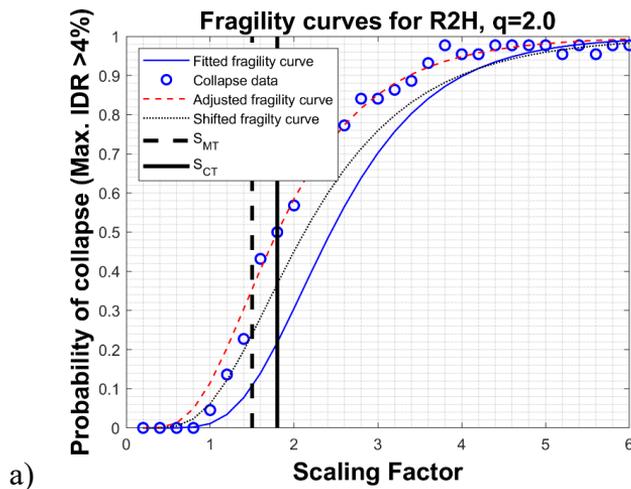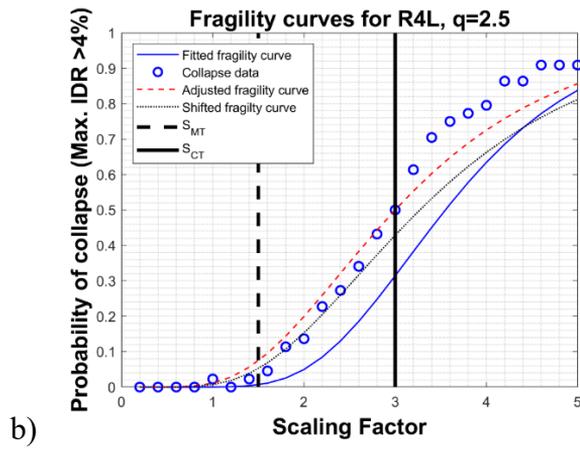
Figure 4-11 Fragility curves a: CFS gypsum sheathed shear walls archetypes; b: CFS wood sheathed shear walls archetypes

5. In plane quasi-static cyclic test on LWS façades

The recent seismic events have shown that the non-structural elements of a building can hamper the ability of building to have an immediate occupancy after the earthquake and can cause substantial economic losses. The collapse of non-structural elements can pose significant hazard to human life, causing a comparable damage to those caused by the collapse of structural elements. Despite the fact, that a correct seismic design ensures an adequate structural performance, buildings can still lose their functionality due to the damages in the non-structural elements. This is particularly due to the fact that the study of the seismic response of non-structural systems has received a lesser attention than the structural systems in past, which has led to a lack of specific requirements for individual non-structural systems. However, observations on their performance during the earthquakes in recent years is now promoting the interest to better understand their seismic response. The prediction of the seismic response of these systems is a complex problem that cannot be easily solved by traditional methods such as detailed FE simulations or analytical approaches. In this context, an experimental campaign to predict the in-plane response of non-structural infilled façades made of lightweight steel (LWS) drywall systems is conducted at University of Naples "Federico II" in collaboration with Knauf Gips KG. These experiments are also carried out to check their compliance with the Eurocode 8 EN 1998-1 [4] damage limitation requirements for non-structural building elements (see Section 2.2). This chapter shows the results of these experiments, which were conducted in

November/December 2018 at Department of Structures for Engineering and Architecture, University of Napoli Federico II, Italy.

5.1. Experimental program

Eight full-scale infilled façade specimens with varying geometrical details are tested under the in-plane quasi static cyclic loading protocol. The configurations are selected to study the effect of following parameters on the global behaviour of façade walls:

- The use of single or dual Cold Formed Steel (CFS) frame.
- Variation of the type of gypsums sheathing panels: standard gypsum boards (GKB) or Impact resistant gypsum boards (Diamant)
- Variation of the type of connection to the surrounding structural elements (fixed or sliding)
- Variation of CFS frame profile dimensions (web height and thickness)
- Presence of the exterior cladding

Based on these parameters, eight different wall configurations have been defined for testing. More information on the difference between tested configuration is shown in Table 5-1.

Table 5-1 Test program

Test No.	Wall frames properties					Connection to surroundings	Board properties			
	External Frame			Internal Frame			External Frame		Internal Frame	
	Stud thickness (mm)	Web height (mm)	Claddings	Stud thickness (mm)	Web height (mm)		Interior face	Exterior face	Interior face	Exterior face
1	0.6	75	NP*	0.6	50	Fixed	Diamant [1]	Aquapanel [2]	NP*	2 x Diamant [1]
2	0.6	75	NP*	NP*	NP*	Fixed	Diamant [1]	Aquapanel [2]	NP*	NP*
3	NP*	NP*	NP*	0.6	50	Fixed	NP*	NP*	NP*	2 x Diamant [1]
4	0.6	75	NP*	NP*	NP*	Sliding	GKB [3]	Aquapanel [2]	NP*	NP*
5	1	150	Yes	NP*	NP*	Fixed	GKB [3]	Aquapanel [2]	NP*	NP*
6	NP*	NP*	NP*	0.6	50	Fixed	NP*	NP*	NP*	2 x GKB [3]
7	1	150	NP*	NP*	NP*	Fixed	GKB [3]	Aquapanel [2]	NP*	NP*
8	0.6	75	NP*	NP*	NP*	Fixed	GKB [3]	Aquapanel [2]	NP*	NP*

*NP- Not Present; [1] Impact resistant gypsum board; [2] Outdoor cement board; [3] Standard gypsum board

5.2. Specimen description

All the configurations have the dimensions of 2400mm x 2700 mm (length x height). Figure 5-1 shows the generic configuration of the tested façades. Façades are infilled in a hot rolled steel testing frame. More information on the test setup is provided in next section. An infilled façade is the one which is surrounded by the building structural element on all sides. The façade could also be placed with an offset to the building structural elements (Figure 5-1) to accommodate wider inner space requirement in few cases. However, such special cases are not addressed explicitly in this study.
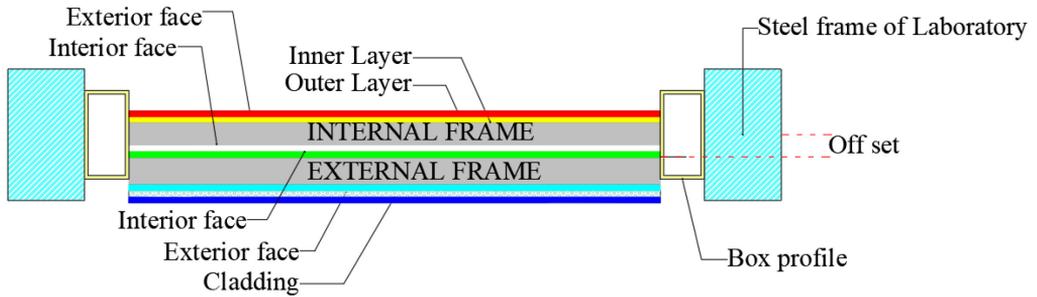
Figure 5-1 Generic configuration

Façades can be made of dual or single frame. In case of dual frame facades, the internal frame is sheathed with two 12.5 mm thick gypsum boards (GKB or Diamant) on its exterior face and it is not sheathed in its interior face, while the external frame is sheathed with 12.5 mm cement-based board (Aquapanel) on its exterior face and with a 12.5 mm thick gypsum board (GKB or Diamant) on its interior face. Except in the test 1 as shown in Table 5-1, rest of the facade walls are only made with either an external frame or an internal frame. The total wall thickness depends on the type of configuration as in some cases, there is only internal (test 3 and 6) or external frame (test 2, 4, 5, 7, and 8). The CFS frames of the façade are made by C-shaped profiles attached to the top and bottom with the U-shaped tracks spaced at 600 mm on the centre. All CFS members are fabricated with DX51D+Z steel grade. There exists also a construction practice to not use wall tracks for the higher thickness of CFS studs. In such cases (test 5 and 7), the studs are connected to the supporting structure by using L-profiles (Figure 5-2). A cladding layer is also applied in one wall specimen (test 5) to investigate its effect on wall performance. The cladding is made of slotted Ω vertical profiles spaced at about 600 mm on the centre, sheathed with 12.5 mm thick cement-based board (Aquapanel).

The use of cladding allows the walls to achieve higher hygrothermal performances through better ventilation.
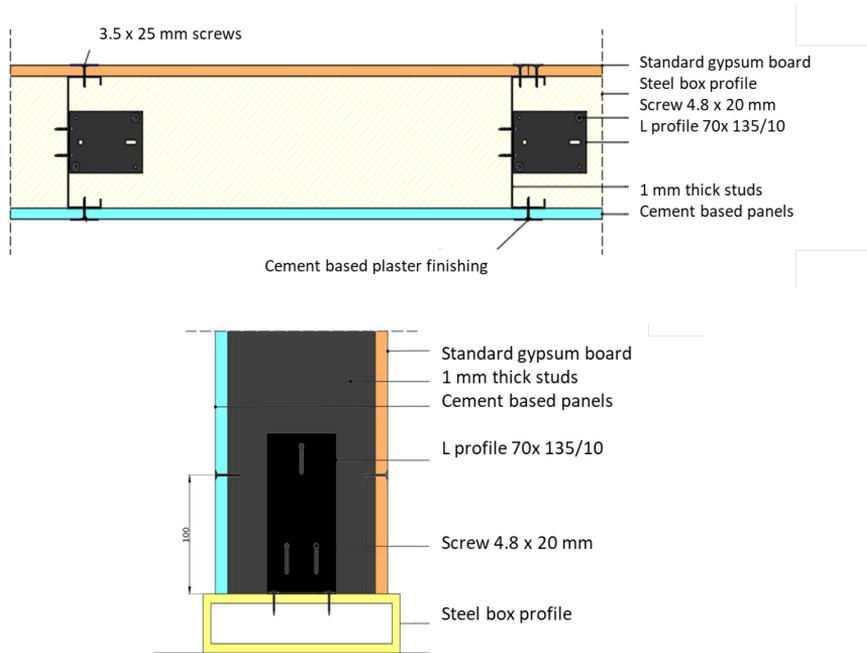
Figure 5-2 - Detail of the configuration with absence of tracks: plan view (top) and section (bottom)

The stud to track fixings are made by punching (Figure 5-3), while the panel to steel fixings are made by screws of different kinds, depending on the type of panels (cement based or gypsum based). The façade walls are connected to the surrounding structural elements through fixed connections made with self-drilling screws. In case of a "sliding" connections in a wall, (test 4), the studs and sheathing panels are not connected to the upper track and a gap between panels and surrounding structure is kept. This detail is commonly adopted to accommodate the building lateral deformations in case of the seismic events, by providing an in-plane sliding joint at the top connection, while the walls are fixed at the base. Figure 5-4 shows different type of connection details adopted in

the tested configurations while Table 5-2 shows a list of the materials used in the tested configurations.
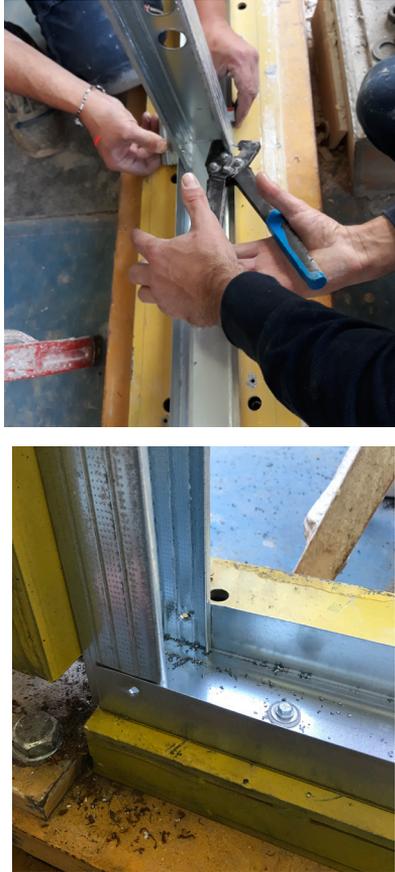
Figure 5-3 Realization of punching between tracks and studs
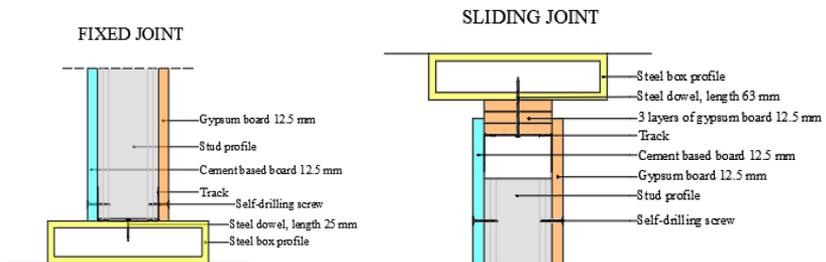
Figure 5-4 Different type of connection details

Table 5-2 Details of the materials used for the walls.

Materials		
Steel elements (shape flange width (mm)/ web width (mm)/ flange width (mm)	Track: U 40/50/40 Track: U 40/75/40 Studs: C 50/50/50 Studs: C 50/75/50 (*Figure on the right*) Studs: C 45/150/45	
Sheathing panels	12.5 mm thick gypsum board, Diamant or GKB 12.5 mm thick outdoor cement board, Aquapanel (*Figure on the right*)	
Frame fixings	Punching	
Panel-to-frame fixings	3.9 ×23 mm self-tapping screws spaced at 600 mm in case of the first layer of gypsum board TN 3.9×38 mm self-tapping screws spaced at 250 mm in case of the second layer of gypsum board Maxi SN25 self-tapping screws spaced at 200 mm in case of Aquapanel (*Figure on the right*) Punta TEKS screws to fix gypsum board to C 45/150/45 profiles spaced at 200 mm	
Wall track/stud-to-surrounding structure connections	Hilti S-MD 53 S5.5x25 dowel spaced at 500 mm on centre at the top and bottom wall tracks and at 800 mm on centre at the wall studs L KAW profiles and 4.8x20 mm screws for configurations without tracks (*Figure on the right*)	
Wall joint Finishes	Paper joint tape *(Figure on the right)* with gypsum-based plaster on the faces of wall made with gypsum boards. Glass mesh with an alkali-resistant coating and cement-based plaster the faces of wall made with Aquapanel	
Cladding	Omega profiles (*Figure on the right*) and 12.5 mm thick Aquapanel	

The general procedure for the specimen's construction is summarized in following steps:

1) The lower and upper tracks are connected to the supporting structure through steel dowels;

2) The studs are positioned at 600 mm spacing, while connecting the end ones to the surrounding structure and the intermediate ones to the tracks by punching in the case of fixed connections or leaving them unattached in case of sliding connections. In the configurations without tracks, the studs are positioned by connecting them directly to the surrounding structure using L-profiles;

3) The first layer of panel is connected: the outdoor cement board and the gypsum board are positioned respectively on the front and the rear sides of the walls;

4) The possible second layer of panel is attached with longer screws, which or more densely spaced; or, if provided, an internal frame is made;

5) Joint finishes are completed (Figure 5-5).

Figure 5-5 - Specimen at the end of the construction: a) Front side (Exterior face); b) Rear side (inner face)

Once the construction is finished, at least 2 days must pass before the tests are carried out, so that the finishes can dry completely. The weight of each tested walls is calculated considering the sheathing panels and the steel elements (studs and tracks) and neglecting the screws and dowels. Furthermore, an additional weight of 1 kg/m^2 was considered to take into account all the finishes.

5.3. Test set-up, instrumentation and loading protocol

5.3.1. Test setup

A specific 2D hinged steel frame is adopted for in-plane cyclic tests on infilled façades. The test set-up is a bidimensional frame made of S350JR [4] grade hot-rolled steel profiles and is designed for simulating the interface of a steel building surrounding structure. The walls are constrained to the laboratory floor using the bottom beam of the testing

frame. Lateral force is applied to the top beam of testing frame. Two hinged rectangular hollow vertical columns are placed at the two ends of the façades in order to simulate the columns behaviour of a building structure. The out-of-plane displacements are constrained by two steel portal frames equipped with roller wheels. Moreover, a sliding-hinge is placed between the loading actuator and the loading beam, in order to avoid any vertical load transfer. For each façade to be tested, new holes should be drilled in the beams and columns. To avoid excessive number of holes in beams and columns of the test set-up, steel box profiles are used. Steel box profiles are attached to façade facing ends of the beams and columns of the test set up and the studs and tracks of facades are attached to steel box profiles. The tests are performed by using a hydraulic load actuator having 500 mm stroke and 500 kN load capacity. The described test set up structure is shown in the following figures.
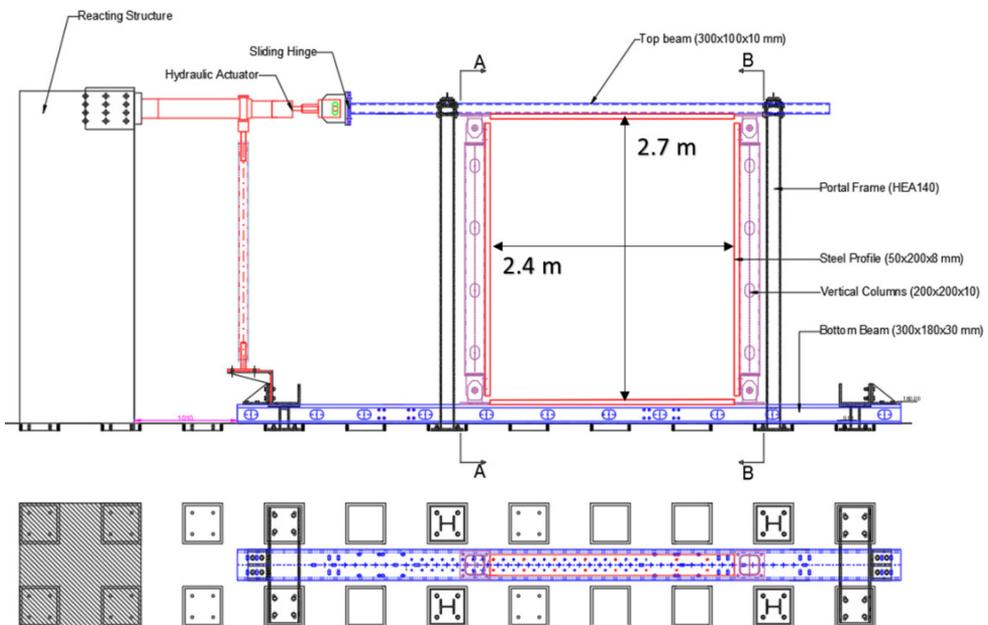
Figure 5-6 - Test set-up for in-plane tests (Elevation on top and plan on bottom)

Figure 5-7 Test set-up realized in laboratory

5.3.2. Instrumentation

The instrumentation for cyclic tests on façades include: one potentiometer (P_1) for measuring the wall top horizontal displacement (i.e. lateral drift), four linear variable differential transducers (named L_1, L_2, L_3 and L_4) for measuring the relative horizontal displacements between wall tracks and test set-up and four more (named L_5, L_6, L_7 and L_8) for measuring the relative vertical displacements between wall boundary studs and test set-up. A load cell is used to measure the applied loads. The

following figures provides further detail about the instrumentation, adopted for all tests.

Figure 5-8 Potentiometer P1

a)

b)

c)

d)
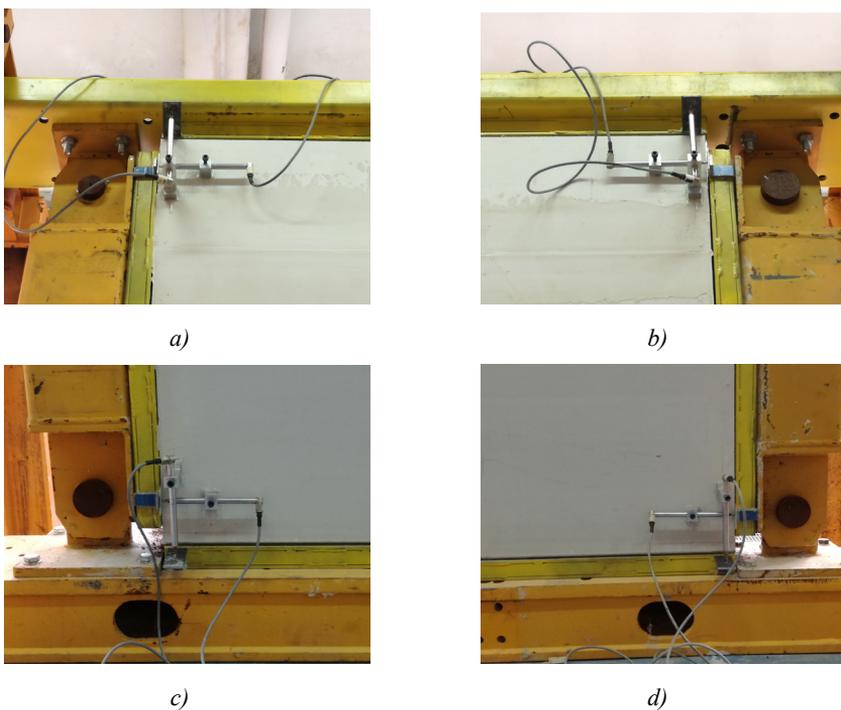
Figure 5-9 LVDT: a) L₁ and L₅; b) L₂ and L₆; c) L₃ and L₇; d) L₄ and L₈
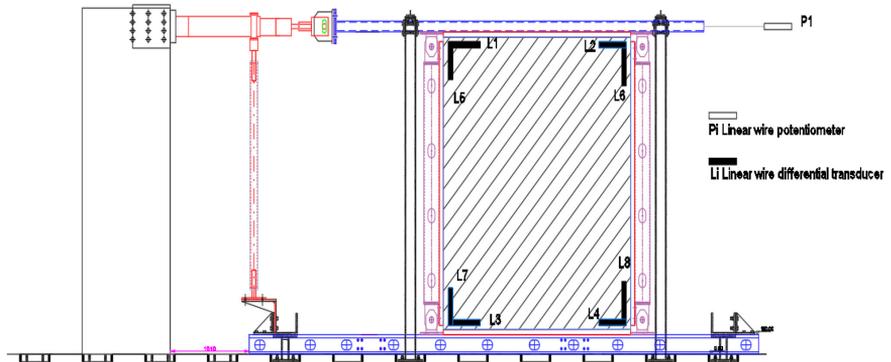
Figure 5-10 Schematization of used instrumentation

5.3.3. Loading protocol

The in-plane quasi static reversed cyclic tests are performed by subjecting the wall specimens to the loading protocol defined by FEMA 461 [2]. FEMA provides a loading history that consists of repeated cycles of step-wise increasing deformation amplitudes. In particular, two cycles for each amplitude (or step) and a specific relationship between consecutive step amplitudes is provided. The loading history, with a step number *n* generally greater than 10, is defined by several parameters:

- Δ_0, that is the targeted smallest deformation amplitude, and its recommended value in terms of inter-storey drift ratio ($\Delta = d/h$, in which d is the lateral displacement at the wall top and h is the wall height set equal to 2700 mm) is 0.0015;

- Δ_m, that is the targeted maximum deformation amplitude and its recommended value in terms of inter-storey drift ratio according to Eurocode EN 1998-1 [4] Section 4.4.3.2 is 0.03 (calculated based on $v = 0.5$ for Importance class I or II building with the storey height of 3.00 m);

- a_i, that is the inter-storey drift amplitude of the cycles in the step i^{th}

- a_{i+1} that is the inter-storey drift amplitude of the cycles in the step $i+1^{th}$, given by:

$$a_{i+1} = 1.4a_i$$

According to FEMA 461, the first amplitude a_1 should be equal to Δ_0 and the last one should be equal to Δ_m. The loading history should be continued by using increments of amplitude of $0.3\Delta_m$ until reaching the load capabilities of test setup. By imposing that a_n is exactly equal to Δ_m, the code provides the ratio a_i/a_n as shown in Table 5-3. In particular, the loading protocol used for performing the cyclic tests on the investigated walls is defined by imposing $a_1 = \Delta_0 = 0.15\%$ and $a_{10} = \Delta_m = 3\%$ for a total number of steps equal to 16. Figure 5-11 shows the adopted cyclic protocol. The displacement-controlled test procedure involved displacements at rates of 0.50 mm/s up to displacements of 10.74 mm, 1.00 mm/s for displacements from 10.74 mm to 29.48 mm, 1.50 mm/s for displacements from 29.48 mm to 80.89 mm, 3.00mm/s for displacements from 80.89 to 153.75 and 4.00 mm/s for displacements higher than 153.75 mm.
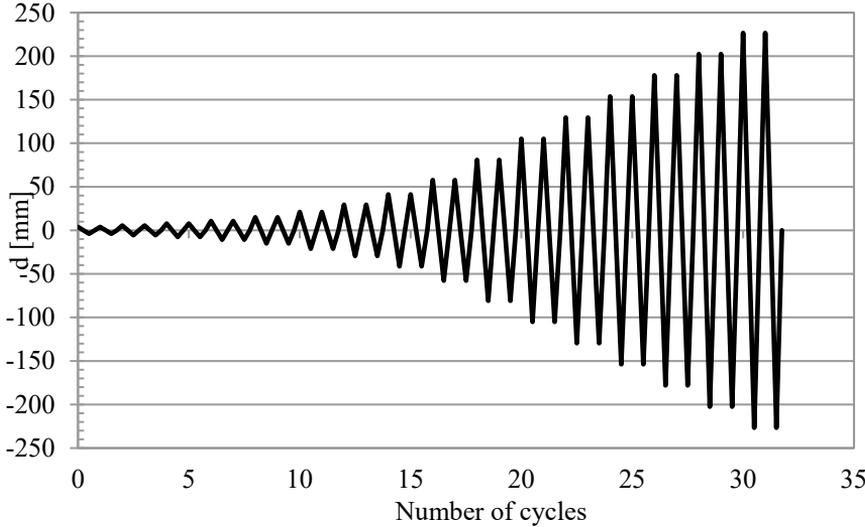
Figure 5-11 Cyclic loading protocol

Table 5-3 Adopted loading protocol

Step No.	No. of Cycles	drift Δ (%)	ai/an	d [mm]	v [mm/s]
1	2	0.15%	0.05	3.92	0.50
2	2	0.20%	0.07	5.48	
3	2	0.28%	0.09	7.67	
4	2	0.40%	0.13	10.74	
5	2	0.56%	0.19	15.04	1.00
6	2	0.78%	0.26	21.06	
7	2	1.09%	0.36	29.48	
8	2	1.53%	0.51	41.27	1.50
9	2	2.14%	0.71	57.78	
10	2	3.00%	1.00	80.89	
11	2	3.89%	1.01	105.15	3.00
12	2	4.79%	1.02	129.45	
13	2	5.69%	1.03	153.75	
14	2	6.59%	1.04	178.05	4.00
15	2	7.49%	1.04	202.35	
16	2	8.39%	1.05	226.65	

5.4. Test results

5.4.1. Force displacement hysteretic response

Data recorded by load cell and potentiometer are interpreted for analysing the global wall behaviour. Typical experimental response in terms of load vs. inter-storey drift curve obtained by quasi-static cyclic tests on façade configurations is shown in Figure 5-12. This response is pinched in nature and depicts degradation of strength and stiffness with increasing amplitudes of displacements. Detail test results along with the data recoded by different instruments are shown in Annex C.
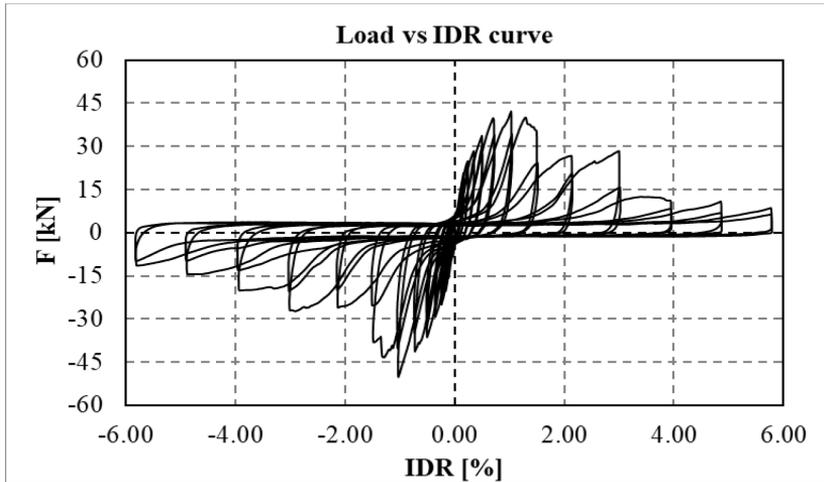
Figure 5-12 Typical experimental Load – IDR curve

The different behaviours exhibited by the walls are compared in terms of force drift backbone envelopes for all the configurations tested (Figure 5-13). For each specimen, the strength is evaluated considering maximum and minimum values of the load reached during the test (Figure 5-14), whereas the stiffness is obtained considering the secant stiffness evaluated at the 40% of the maximum or minimum load reached during the test (Figure 5-15).
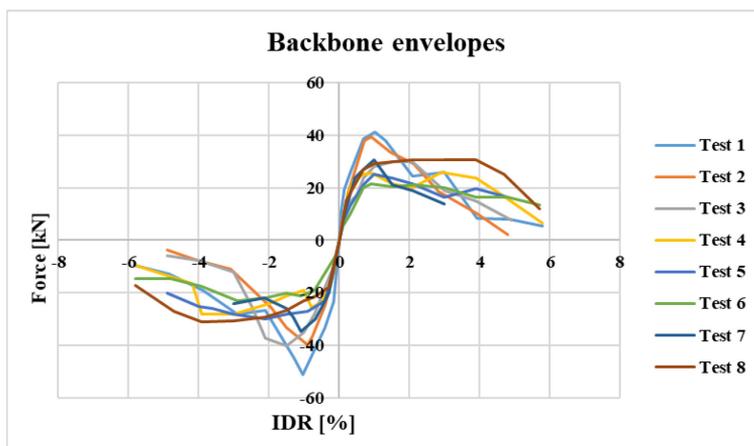

Figure 5-13 Backbone envelopes of the force drift curves for all tested configurations
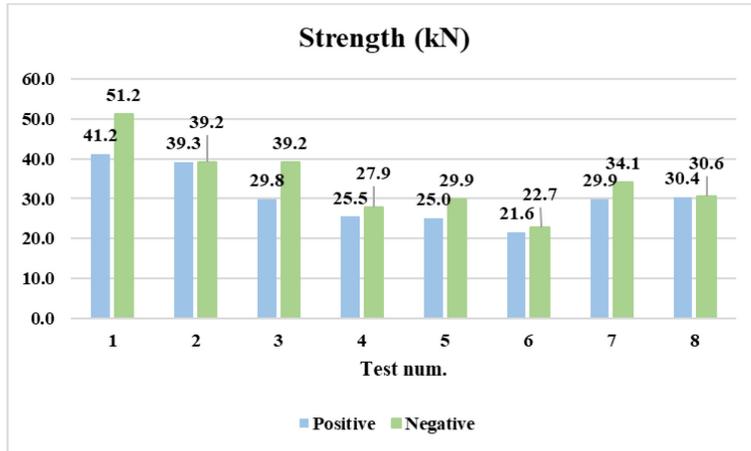
Figure 5-14 - Values of strength evaluated for both positive and negative loading directions
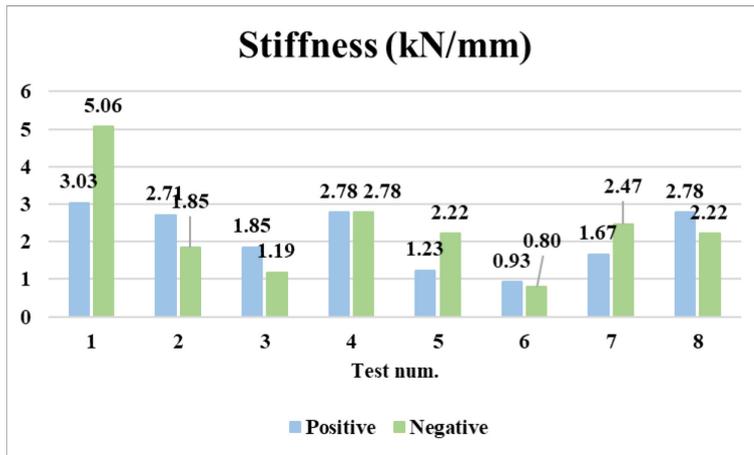
Figure 5-15 - Values of stiffness evaluated for both positive and negative loading directions

In order to study the effect of construction parameters, which are used to define the experimental program, comparison between different tested walls is made based on their strength and stiffness.

5.4.1.1. Effect of dual or single frame

The dual metal frame façades (Test 1) showed higher values of strength and stiffness compared to configurations with single metal frame.

The walls in test 2 and 3 individually represented the external and internal frame, respectively, that made up the wall of test 1. Despite the fact that the sum of strength and stiffness of wall in test 2 and 3 should be equal to the strength and stiffness of wall in test 1, this was not the case. In fact, wall in test 2 (external frame of wall in test 1) has rather comparable values of strength and stiffness to wall in test 1, while the addition of the second internal frame (test 3) slightly increases the values of resistance and stiffness, but overall does not provide a significant contribution.

5.4.1.2.   Effect of type of gypsum board

From the examination of the backbone envelopes and values of strength and stiffness for single frame walls, it can be noticed that the constructive parameter which mainly affected the wall response is the type of gypsum board. In fact, the specimens with the impact resistant gypsum board show greater strength values than those built with standard gypsum board (by comparing test 2 vs test 8).

5.4.1.3.   Effect wider and thicker profiles

Another important parameter worth observing is the different types of steel framing used for the walls. For example, wall in tests 5 and 7 are built, in fact, with different profiles having a web height of 150 mm, thickness of 1 mm and without the tracks in comparison with the other cases, which had profiles having a web height of 75 mm, thickness of 0.6 mm and with the tracks. Though, the stiffness of façades should increase with the increase in the thickness of frame but it is not true due to the fact that the façades with the thicker profiles are connected to surrounding structure using the L profiles and do not have any tracks. The absence of tracks in test 5 and 7 might have resulted in the reduction of the wall

stiffness. This reduction in stiffness of walls with thicker profiles but without the tracks can be observed by comparing walls in test 7 and Wall 8.

5.4.1.4.   Effect of claddings

Adding a cladding to the exterior faces does not does not affect the response much as it can be seen by comparing the strength and stiffness of walls in test 7 and 5. The reason behind this is the position of the second layer of outdoor cement board of cladding (see Figure 5-16), which has a bit out of plane position with respect to the columns and beams of the set-up due to it large overall thickness of the wall and, consequently, the external board is not constrained equally as the rest of the wall by the surrounding structural elements.
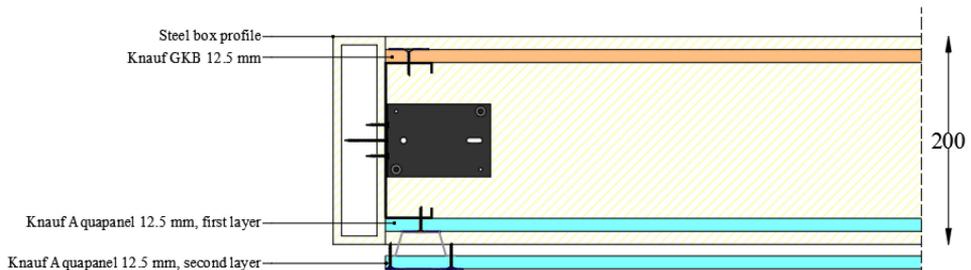
Figure 5-16 cross section of wall 5

5.4.1.5.   Effect of sliding connections

The effect of sliding connections on wall response can be examined by comparing results of test 4 and 8. If the comparison is made in terms of strength and stiffness, the two walls exhibited almost similar behaviour. However, the major role of the use of sliding connections is to improve

wall fragility to damages, which in fact they did by delaying the occurrence of damages to higher drifts.

5.4.2. Test results in fragility curves

The evaluation of the physical damages that the walls suffered during the tests is carried out through the observation of specimens, by making two pauses at each new amplitude achieved during the application of the loading protocol: the first pause corresponds to the achievement of the second positive peak of a particular amplitude and the second pause at the end of two cycles of a particular amplitude.

Under the action of lateral in plane loads, different type of damage mechanisms can appear in the drywalls, which range from superficial damages limited only to the face of panels or severe damages like the deformations in frame elements or complete detachment of panels from the steel frame. The main damage phenomena observed during the tests are summarized in the Table 5-4 and represented in Figure 5-17.

Table 5-4 Types of damage

Sheathing panels	1. Drop of gypsum dust
	2. Rupture of panel portions or spalling
	3. Crushing of panel
	4. Buckling of panel
	5. Crack in panel (cm^2)
	6. Slip between adjacent panels
	7. Out of plane collapse of panels
Finishes	8. Detachment of joint cover
Connections	9. Screw tilting (%)
	10. Screw breaking on panel edge (%)
	11. Screw pull out/trough (%)
Steel elements	12. Pull out of dowels (%)
	13. Local plastic deformation of studs/tracks
	14. Stud to track connection failure (%)
	15. Buckling failure of a stud/track and plastic hinges in studs
	16. Bending of boundary studs/detachment from panel/ detachment from top track
Global level	17. Detachment between façades wall and surrounding structural element (mm)
	18. Wall out of plane collapse
	19. Falling down of panels

a) Drop of gypsum dust

b) Rupture of panel portion or spalling

c) Crushing of panels

d) Buckling of panel

e) Crack in panel

f) Slip between adjacent panels

g) Out of plane collapse of panels

h) Detachment of the joint cover

i) Screw tilting

l) Screw breaking on panel edge

m) Screw pull out/trough

n) Local plastic deformation of stud

o) Stud to track connection of failure

p) Buckling failure of stud/track and plastic hinges

q) Detachment between wall and surrounding structural element

r) Falling down of panel

Figure 5-17 Main damage reported from the specimens during the test

In all types of tested walls, damage began with the drop of gypsum dust gathering at the bottom of wall, which is followed by the cracking in joints between panels and the detachment of joint cover tape. With the further increase in drift demands (0.8-1.5%), the corners of panel experienced crushing against the surrounding elements, which is usually followed or accompanied by the rupture of panel portion or spalling. Panels developed cracks and buckle depending on the type of panel being used. At higher drifts, complete detachment of panels from the frame has also been observed (4-6%). The panel to frame connection initially experienced tilting of screws (0.3-0.5%), which is followed by them

breaking at the panel edge or a complete pull out or pull through from the panel.

Similarly, frame elements have also shown various types of failure mechanisms. Initially, stud to track connections failed, which are usually made by a single clinching point. The failure is usually noticed by a sharp sound during the experiments as it is generally not to possible to see this mechanism at lower drift levels, when panels are intact on the frame. Only for the configuration made of solely internal frame, it has been possible to observe the frame elements on the rear side. Additionally, the frame elements experienced bending and buckling depending on different constraints from surrounding elements and applied actions (2-3%). A more severe damage is the wall detachment from the surrounding structural element and sometimes it resulted in wall collapsing in the out of plane direction. The occurrence of these phenomena during the application of the load history affects the response curve of the wall, resulting in a significant degradation of resistance and stiffness

The damage observations during the tests are associated to 3 DS-s defined according to the damage level and the required repair action. The DS-s are defined based on the available definitions in some relevant studies on partitions [99,148] as following:

- The first DS (DS1) is characterized by superficial damage to walls and it can be repaired with plaster, tape, and paint;
- The second DS (DS2) is characterized by local damage of sheathing panels and/or steel frame component and it requires the removal and replacement of sheathing panels and/or local repair of steel frame components;

- the third DS (DS3) is characterized by severe damage to walls and it requires the replacement of part or whole wall.

Table 5-5 correlates observed the damage phenomena (Figure 5-16) in the tested façades to the defined DS-s. For some type of damage phenomena, i.e. detachment between indoor facade walls and surrounding structural elements, crack in panel, screw pull out/trough, screw breaking on panel edge and pull out of dowel, the triggered DS depends on the level of produced damage; e.g, the detachment between wall and surrounding structural element can corresponds to DS1 or DS2 on the basis of the amount of detachment (DS1 if the detachment is ≤5 mm or DS2 if the detachment is >5 mm).

The tested façades are non-structural elements sensitive to the deformations; therefore, the in-plane behaviour is governed mainly by the IDR. For each test specimen, the drift value for which the single damage phenomenon occurred is noted and given in Table 5-6. The minimum value, for which a defined DS is triggered for each specimen, is also given in Table 5-6.

Table 5-5 Correlation between observed damage phenomena and DSs

	Observed damage phenomena	DS1	DS2	DS3
Sheathing panels	1. Drop of gypsum dust			
	2. Rupture of panel portions or spalling			
	3. Crushing of panel			
	4. Buckling of panel			
	5. Crack in panel (cm^2) [a]			
	6. Slip between adjacent panels			
	7. Out of plane collapse of panels			
Finishes	8. Detachment of joint cover			
Connections	9. Screw tilting (%)			
	10. Screw breaking on panel edge (%) [b]			
	11. Screw pull out/trough (%) [b]			
Steel elements	12. Pull out of dowels (%) [b]			
	13. Local plastic deformation of studs/tracks			
	14. Stud to track connection failure (%)			
	15. Buckling failure of a stud/track and plastic hinges in studs			
	16. Bending of boundary studs/detachment from panel/ detachment from top track			
Global level	17. Detachment between façades walls and surrounding structural element (mm) [c]			
	18. Wall out of plane collapse			
	19. Falling down of panels			

a$\leq$ 50 cm^2 for DS2; >50 cm^2 for DS3
b$\leq$ 5% for DS2; >5% for DS3
c$\leq$ 5 mm for DS1; >5 mm for DS3

Table 5-6 - IDR level recorded for each tested configuration and each damage phenomena

DS-s	Type of Damage	1	2	3	4	5	6	7	8
DS1	Detachment of joint cover paper	-	0.4	-	0.78	1.53	-	0.56	0.56
	Drop of gypsum dust	0.28	0.28	0.56	0.28	0.28	0.78	0.4	0.2
	Detachment between facade walls and surrounding structural element	0.56	0.4	0.4	0.56	0.4	0.28	0.28	0.2
	Screw tilting	0.4	0.4	-	0.28	0.4	0.28	0.4	0.28
	Min	**0.28**	**0.28**	**0.4**	**0.28**	**0.28**	**0.28**	**0.28**	**0.2**
DS2	Rupture of panel portions or spalling	0.78	1.09	1.53	1.53	0.78	1.09	0.78	0.78
	Crushing of wall corners	1.09	1.53	1.53	1.09	1.53	1.09	1.53	1.53
	Buckling of panel	-	1.53	2.14	-	-	3	1.53	4.79
	Crack in panel	1.09	1.53	1.53	1.09	-	1.09	1.53	-
	Slip between adjacent panels	1.53	-	-	3.89	-	3	-	-
	Detachment between façades wall and surrounding structural element	0.78	1.09	1.09	1.09	1.09	2.14	0.78	0.56
	Screw breaking on panel edge	1.09	-	1.53	0.56	0.78	1.53	1.53	1.09
	Screw pull out/through panels (%)	0.56	1.09	0.78	0.56	1.53	1.09	0.78	0.56

	Pull out of dowels (%)	-	-	-	-	-	-	-	-
	Local plastic deformation of studs/tracks	3	3	2.14	2.14	3.89	2.14	-	4.79
	Min	**0.56**	**1.09**	**0.78**	**0.56**	**0.78**	**1.09**	**0.78**	**0.56**
DS3	Crack in panel	-	3	3.89	-	-	4.79	2.14	-
	Out of plane collapse of panels	2.14	2.14	3	3	3	-	2.14	4.79
	Screw breaking on panel edge	1.53	2.14	3	1.53	-	3	3	1.53
	Screw pull out/through panels	1.53	2.14	1.09	1.53	-	1.53	1.53	0.78
	Pull out of dowels	-	-	-	-	-	-	-	-
	Stud to track connection failure	3.89	3	1.09	2.14	-	1.53	-	2.14
	Buckling failure of a stud/track, and plastic hinges in studs	3.89	3	2.14	4.79	1.53	3.89	-	5.69
	Bending of boundary studs/ detachment from panel/detachment from top track	-	-	-	-	-	-	-	-
	Falling down of panels	5.69	-	-	-	4.79	-	3.89	-
	Wall out of plane collapse	-	4.79	3.89	-	-	-	-	-
	Min	**1.53**	**2.14**	**1.09**	**1.53**	**1.53**	**1.53**	**1.53**	**0.78**

In order to do the fragility analysis, at least a group of 2 specimens are required to evaluate different statistical parameters. More the number of specimens in a group, better will be the quality of fragility data.

However, in the current study all of the specimens are distinct with each other in at least one construction parameter and it is not possible to have two or more exactly identical specimens in currently investigated experimental program. Therefore, in order to do the fragility analysis, the 8 tested specimens are divided into five groups based on one significant construction parameter that is common between the group of façades, i.e. type of construction (walls with dual metal frame, only external frame and only internal frame) or the type of connections with the structural support and the type of gypsum board used (GKB or Diamant). Based on these parameters, the tested façade specimens are divided in to following groups for the fragility analysis:

-   Group I: façades with only external frame with fixed upper connections (Walls in test 2, 5, 7 and 8);
-   Group II: façades with only internal frame with fixed upper connections (Walls in test 3 and 6);
-   Group III: façades with GKB (Walls in test 4, 5, 6, 7 and 8);
-   Group IV: façades with Diamant (Walls in test 1, 2 and 3);
-   Group V: façades with fixed connections (Walls in test 1, 2, 3, 5, 6, 7, 8).

   Finally, the fragility curves are developed following a procedure proposed by Porter at al. [149]. The fragility function $F_{dm}(edp)$ is represented by a log-normal distribution (Equation 5-1) and it is defined as the probability of the non-structural element to reach or exceed a certain limit state of damage (dm), given a particular demand value.

$$F_{dm}(edp) = \Phi\left(\frac{\ln\left(\frac{edp}{x_m}\right)}{\beta}\right)$$

(5-1)

Where Φ is the standard normal distribution function; edp (engineering parameter demand) is the considered demand parameter, x_m and β are the median and standard deviation of the log-normal distribution respectively. edp is the relative inter-floor displacement (IDR).

The study by Porter et al. [149] proposes different methods for the creation of fragility functions according to the type of experiments and the data that derived from it. Here, Method A is used.

The median and standard deviation values are calculated using following expressions:

$$x_m = \exp\left(\frac{1}{M}\sum_{i=1}^{M}\ln r_i\right)$$

(5-2)

$$\beta = \sqrt{\frac{1}{M-1}\sum_{i=1}^{M}(\ln (r_i/x_m))^2 + \beta_u^{\ 2}}$$

(5-3)

Where M is the number of tested specimens present in a group, r_i is the minimum IDR at which a particular DS is triggered in a specimen i of a group and is given in Table 5-6 and β_u is equal to 0.25, because all specimens are subjected to the same loading history [149].

The fragility curves are developed for the three limit states defined above (DS1, DS2, DS3) and for each group of specimens with similar characteristics. The fragility parameters are given in Table 5-7 and the

fragility curves are shown in the following figures, in which the IDR limits imposed by the Eurocode 8 (see Section 2.2.1) are also marked.
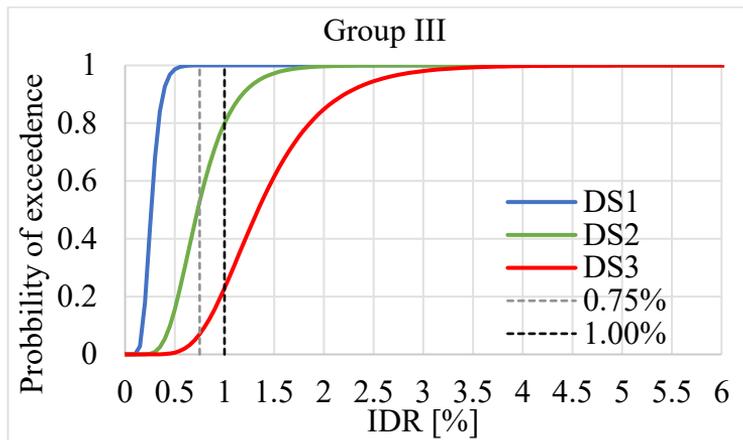
Table 5-7 Fragility parameters

Group	DS1		DS2		DS3	
	x_m	β	x_m	β	x_m	β
Group I	0.26	0.30	0.78	0.37	1.41	0.49
Group II	0.33	0.36	0.92	0.34	1.29	0.35
Group III	0.26	0.29	0.73	0.37	1.34	0.39
Group IV	0.32	0.32	0.78	0.42	1.53	0.42
Group V	0.28	0.32	0.78	0.37	1.39	0.41

a

)

b
)

c)

d
)

e)
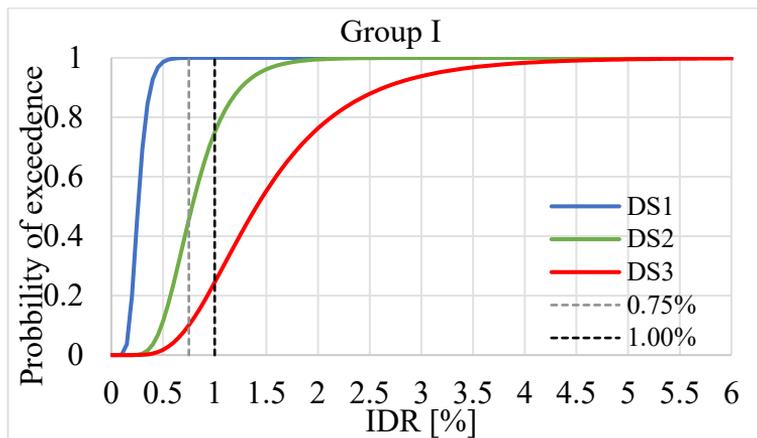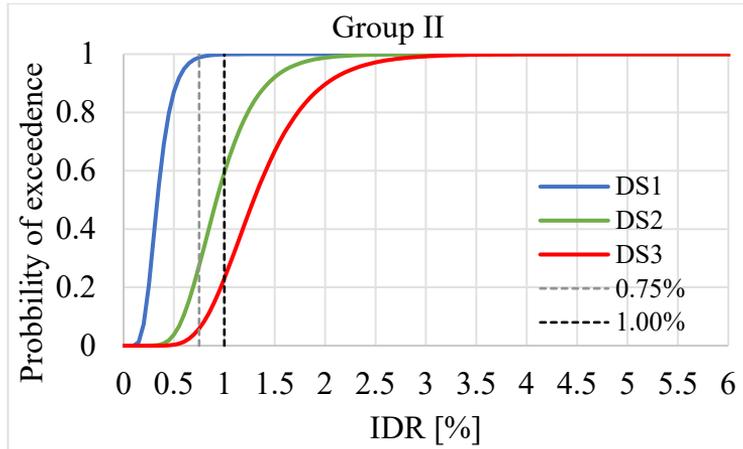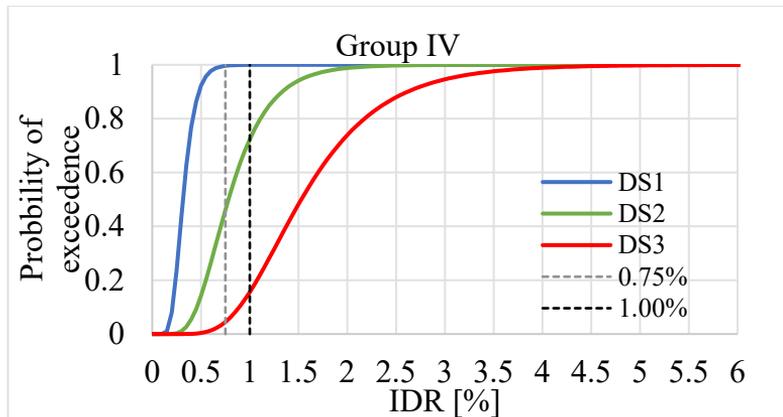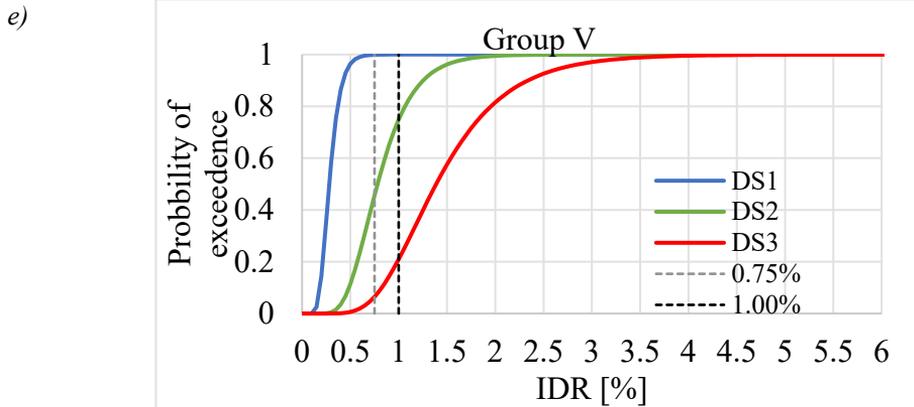
Figure 5-18 Fragility curves :a) Group I; b) Group II; c) Group III; d) Group IV; e) Group V

By observing the fragility curves, it is evident that the group II shows the best behaviour with the mean of the log-normal distribution highest for DS1 and DS2: 0.33% for DS1, 0.92% for DS2. Comparing the fragility curves of group III and IV, better fragility to DS-s is obtained for group IV. Instead, for DS3, the highest average value of 1.53 is shown by the group IV. Comparing the values obtained for groups III and IV, we note a slightly better behaviour for group IV: 0.26% for DS1, 0.73% for DS2, 1.34% for DS3 (Group III) and 0.32% for DS1, 0.78% for DS2, 1.53% for DS3 (Group IV). This shows that the use of high-performance Diamant board can improve the overall seismic behaviour of the wall slightly.

Considering the IDR limits for buildings imposed by Eurocode 8 for the relative displacement values of 0.75% and 1.00%, the probabilities of exceeding these limits is also evaluated for each defined group as shown in Table 5-8. Therefore, a 1% inter storey drift limit can be considered as an acceptable limit for façades based on the fact that for all groups of façades have around 0.2 probability of exceeding this limit

Table 5-8 - Probability of exceeding the limit provided by Eurocode 8

	Probability of exceeding the limit of 0.75%			Probability of exceeding the limit of 1.00%		
	DS1	DS2	DS3	DS1	DS2	DS3
Group I	1.00	0.46	0.10	1.00	0.75	0.24
Group II	0.99	0.27	0.06	1.00	0.59	0.23
Group III	1.00	0.53	0.07	1.00	0.80	0.23
Group IV	1.00	0.46	0.05	1.00	0.72	0.16
Group V	1.00	0.50	0.05	1.00	0.78	0.19

6. Numerical modelling of LWS indoor partition walls

Building codes around the globe are in a transition to update their design guidelines to meet the objectives of performance based seismic design (PBSD). The fulfilment of the objectives of PBSD requires number of collapse simulations of a building equipped with a certain type of lateral force resistant system and the non-structural elements. Numerical models with an ability to simulate post peak deteriorating behaviour are essential for these collapse simulations. Such type of models for the LFRS of a building are common among engineers and are also by-default built-in in most structural analysis software-s. Contrarily, it's quite rare to model the non-structural components for the advanced nonlinear analysis under the seismic actions, particularly due to absence of specific models for the individual components. Furthermore, as shown by Whittaker and Soong [150], the non-structural building components make up almost half of the investment cost in building construction, which makes their inclusion in a building model even more vital due to an increased economic risk associated to them.

Partition walls are one of the most common type of non-structural building component, used to divide the building's space to meet its functional requirements. There are different alternatives available for the construction of these partitions, among which LWS drywall partitions are one of the most commonly encountered partition types. Idealizing the hysteretic behaviour of partition walls, i.e. devising rules capable of describing the response under the cyclic actions, is an efficient strategy to

facilitate the development of a model that can be easily implemented in a building model, which takes into account of the effect of non-structural elements. This chapter expands on the notion of having simplified models for LWS partitions by first providing a description of the experimental database used to calibrate the model and then the explanation of different building blocks of the model. Subsequently, the ability of model to predict the wall response is gauged using different quantitative and qualitative parameters.

6.1. Description of modelled partition walls

A research project [99] was conducted at University of Naples "Federico II" over the last few years with an aim to overcome the lack of information on seismic behaviour of architectural non-structural lightweight steel (LWS) drywall components, i.e. indoor partition walls, outdoor façades and suspended continuous ceilings. The tested non-structural components were made of LWS frames sheathed with gypsum-based or cement-based boards. The research activity was organized in three levels: ancillary tests, component tests and assembly tests. Ancillary tests were carried out for evaluating the local behaviour of partitions, façades and ceilings. Component tests involved out of plane quasi-static monotonic and dynamic identification tests and in-plane quasi-static reversed cyclic tests on partitions. Finally, the dynamic behaviour was investigated through shake-table tests on different assemblages of partitions, façades and ceilings. The in-plane quasi-static cyclic tests conducted within this research project were used to calibrate the partition wall models presented here. In particular, cyclic tests were conducted on 12 configurations of internal partitions (Figure 6-1 a and b) infilled in a supporting structural frame, while, also considering the interaction with other non-structural

elements, such as external facades (Figure 6-1 c). The investigated construction parameters during the experimental campaign were the type of connection of wall to the surrounding structural elements (fixed or sliding), the distance between the steel studs of the wall, the type of panels and the type of finishes. In normal construction practices, the studs and tracks are fastened together (fixed connection) while in case of sliding connections the studs are not fastened to tracks and a gap is left between them allowing to accommodate wall lateral drifts. More information on the differences between the geometrical details of fixed and sliding connections can be found in [102]. Table 6-1 shows the geometrical and material characteristics of the tested specimens.

a)

b)

c)
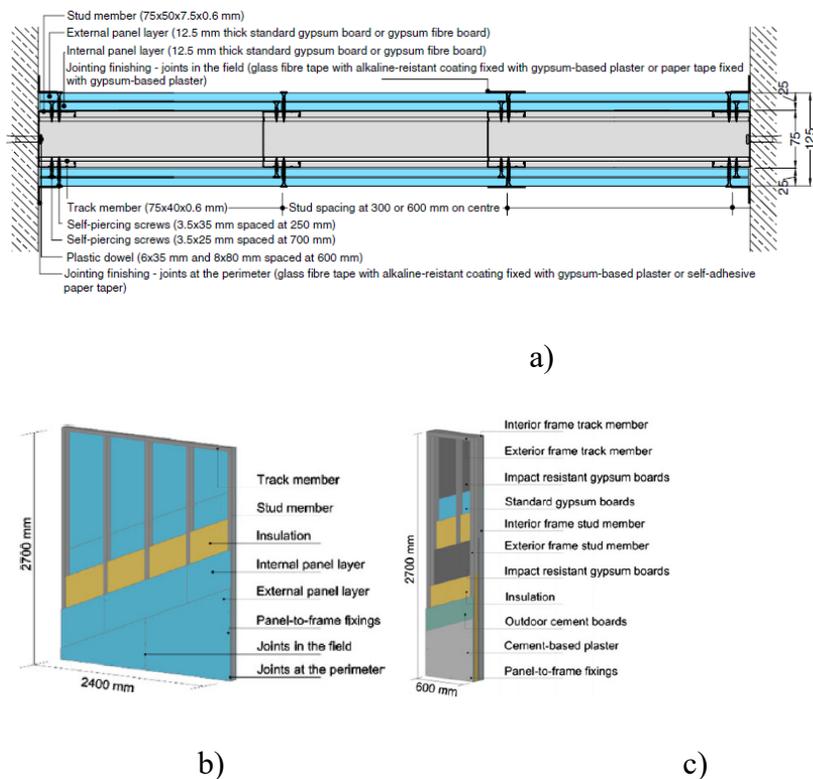
Figure 6-1 Configuration of partition wall type: a) plan view; b) 3D view; c) 3D view of the facades at the ends

Table 6-1 Dimensions and properties of the materials of the modelled partitions

Wall Dimensions	2400 mm Long, 2700 mm High, and 125 mm Thick	
Lightweight steel profiles	Steel grade	DX51D + Z
	Studs	75 × 50 × 7.5 × 0.6 mm (outside-to-outside web depth × outside-to-outside flange size × outside-to-outside lip size × thickness) lipped channel sections spaced at 300 or 600 mm on centre
Sheathing panels	Double layer of 12.5-mm-thick standard gypsum boards or gypsum-fibre boards for each wall face	
Frame fixings	Punching	
Panel-to-frame fixings	3.5 × 25 mm (nominal diameter × shank length) bugle head phosphated self-piercing screws spaced at 700 mm on centre for the installation of the internal panel layer 3.5 × 35-mm bugle head phosphated self-piercing screws spaced at 250 mm on centre for the installation of the external panel layer	
Jointing finishing	Joints in the field	Glass fibre tape with an alkaline-resistant coating fixed with gypsum-based plaster or paper tape fixed with gypsum-based plaster
	Joints at the perimeter (only for fixed connections)	Glass fibre tape with an alkaline-resistant coating fixed with gypsum-based plaster or self-adhesive paper tape
Wall-to-surrounding connections	6 × 35 mm (drilling hole diameter × minimum anchorage length) plastic dowels for fixed connections or 8 × 80-mm plastic dowels for sliding connections, spaced at 500 mm on centre at the wall top and bottom and 600 mm on centre at the wall ends	
Connections to outdoor façade wall	4.3 × 65-mm wafer head with partial thread phosphated self-piercing screws spaced at 500 mm on centre	

The 12 configurations can be subdivided as follows: 8 partition walls completely infilled in the structural elements (Prototype 1) and 4 partitions connected to structural elements at top and bottom, while at the ends connected to the facades (return walls) placed in a transverse direction (Prototype 2). Table 6-2 summarizes the main features of the tested configurations under in-plane quasi static cyclic loading protocol, whose

results were used to develop simplified numerical models. Based on the test results on the 12 tested configurations [102], the two most governing construction parameters, that significantly affect the response are the type of surrounding elements (Figure 6-2) and the type of connections to the surrounding (Figure 6-3). These two parameters are later used to group the partitions in subsequent sections of this chapter.
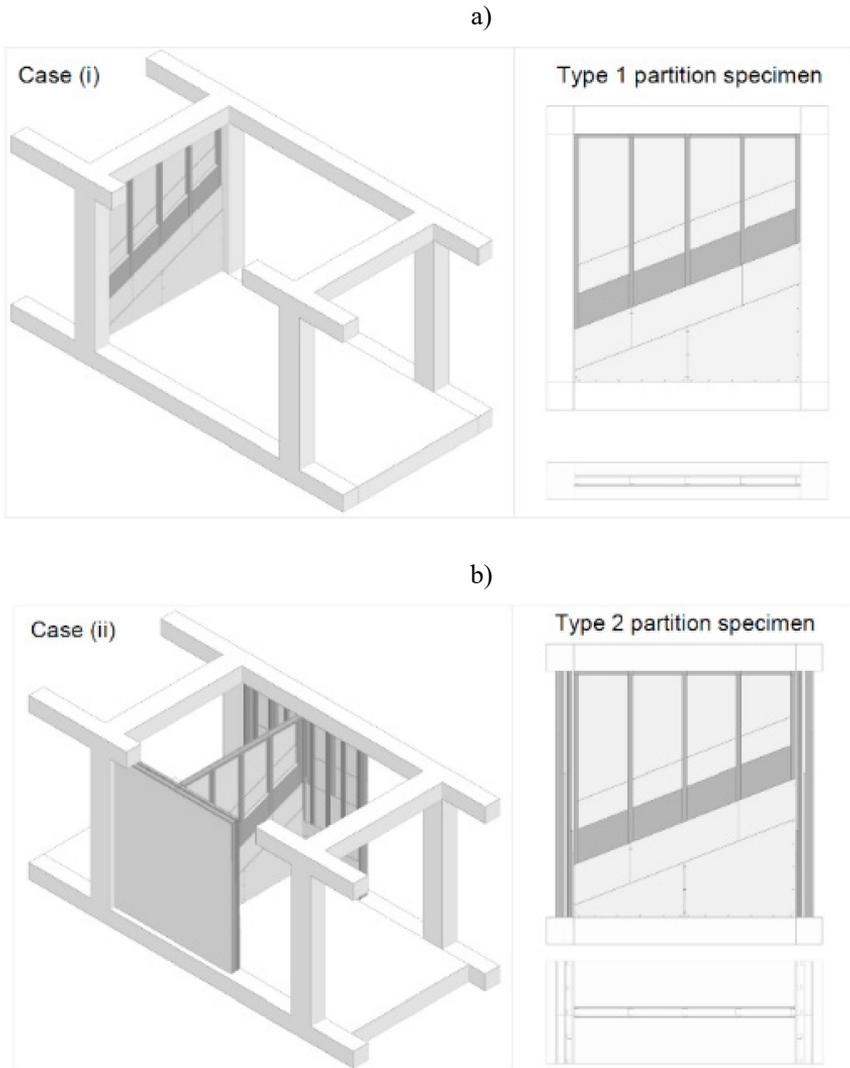
a)

b)

Figure 6-2 Cases of application of non-structural components: a) Prototype 1; b) Prototype 2
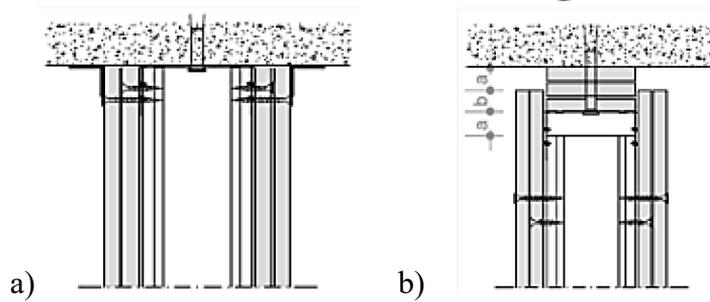
Figure 6-3 Fixed (a) and sliding (b) connections

Table 6-2 Main features of the tested configurations

ID	Prototype	Connection on top[1]	Connection to the sides[1]	Studs spacing (mm)	Type of panels
#1	1	F	F	600	GWB
#2, #3	1	F	F	600	GWB
#4	1	F	F	300	GWB
#5	1	F	F	600	GFB
#6	1	S	F	600	GWB
#7, #8	1	S	S	600	GWB
#9, #10	2	F	-	600	GWB
#11, #12	2	S	-	600	GWB

[1] F = fixed connections; S = sliding connections
[2] GWB = standard gypsum boards; GFB = gypsum-fibre boards

6.2. Model Description

A zerolength spring element lumped with the global hysteretic behaviour of the wall is developed in OpenSees [151] software for all of 12 tested partitions. A two-phase modelling approach is followed. In the first phase named "individual wall models", a model for each tested wall is developed with the material properties of the spring calibrated based on the respective wall test results. Subsequently, in the second phase named

"group models", models are created for 12 walls divided in 5 groups based on the key construction parameters common in them, which are defined in previous section. Pinching 4 material is used for the zerolength [92] element. Choice of Pinchinng4 material is motivated by the appreciable results obtained by other researchers, who also used it to simulate the response of LWS drywall partitions [120,124]. Pinching4 material is a uniaxial material that can represent pinched load deformation response with the ability to exhibit degradation under cyclic loading. In particular, the material rule can be defined through the set of 39 parameters. It includes 16 parameters for the definition of the backbone curve (ePf1, ePd1, ePf2, ePd2, ePf3, ePd3, ePf4, ePd4, eNf1, eNd1, eNf2, eNd2, eNf3, eNd3, eNf4, eNd4), 6 parameters for defining the cyclic behaviour (uForceP, uForceN, rDispP, rDispN, rForceP, rForceN), 5 parameters for governing the strength degradation (gF1, gF2, gF3, gF4, gFLim), 5 parameters for controlling the unloading stiffness degradation (gK1, gK2, gK3, gK4, gKLim), 5 parameters for controlling the reloading stiffness degradation (gD1, gD2, gD3, gD4, gDLim), and 2 parameters for limiting the maximum degradation in each cycle (gE, dmgType). The key parameters used in the study to define Pinching4 material are illustrated in Figure 6-4. More information on the calibration of the pinching4 material is provided in next sections.
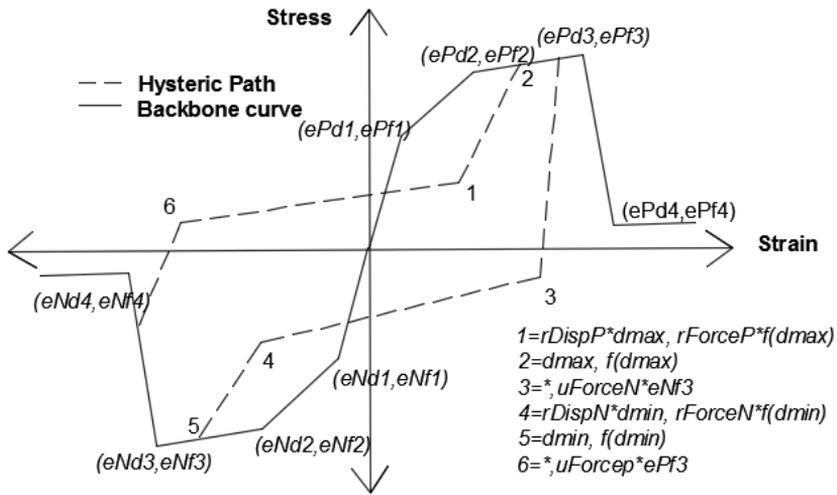
Figure 6-4 OpenSees definition of Pinching4 material

In order to transfer the load to the springs, it is connected via four truss elements to the surrounding structural frame elements as shown in Figure 6-5. The structural frame elements i.e. beam and columns are pin connected and hinged at the base as it was in the case of testing set up [102]. The complete model has 3 degrees of freedom: the horizontal and vertical translations and the rotation in the plane.
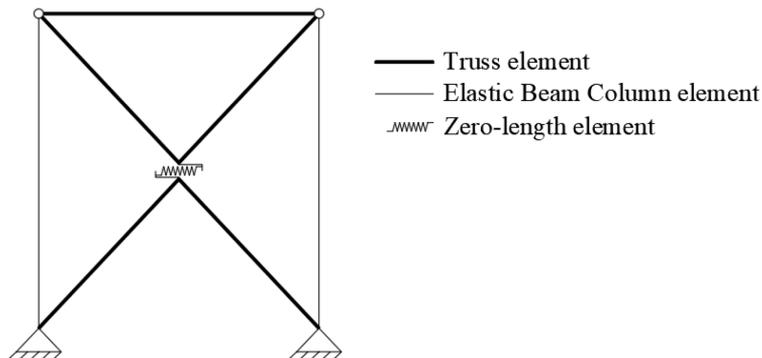

Figure 6-5 Model schematization

The columns and beams of the test set-up are modelled as elastic beam column and truss elements, respectively, using the same mechanical and geometrical characteristic as in the actual test set-up [102]. The use of truss elements for columns can cause the pin restraint to be imposed two times: once due to the external pin restraint and twice due to the pin restraint built-in within the truss elements. This is the main reason behind using different types of elements for beam and columns of the set-up. An alternate option is to use beam column elements for both beams and columns, but that would require to have two additional nodes at beam ends to release the bending moments between the nodes. However, this approach is not followed here to keep the integration of spring with building model simpler by not adding any new nodes. Nonetheless, the beam column elements of the columns also behave as the truss elements, because they are pinned at the base and connected to truss elements at top. The four diagonal truss elements connecting the spring to the frame have additional constraints at their ends to ensure the transfer of complete load applied from top beam to the spring. Subsequently, a deformed shape shown in Figure 6-6 is obtained, in which the total global lateral displacement of the wall is accommodated by the spring, only.
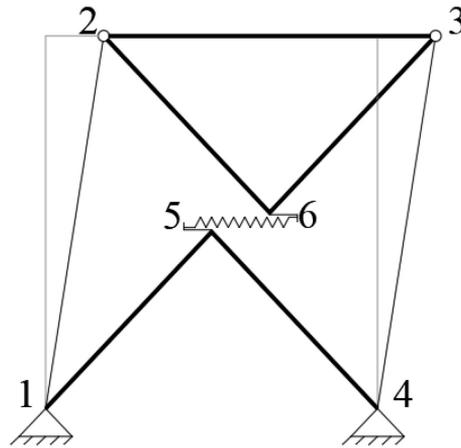
Figure 6-6 Deformed shape of the wall model under an in-plane load

6.3. Individual wall model

6.3.1. Hysteretic characterization

As mentioned earlier, the hysteretic response of LWS partition under in-plane loadings is characterized by severe pinching and the degradation of strength and stiffness in subsequent cycles. A four-point backbone curve (Figure 6-7) of pinching4 material is used to capture the envelope of experimental hysteretic response along with the strength degradation observed during the tests, after the wall had achieved its peak strength. The criteria used to select the four points of the backbone curve, which were equal and opposite for the positive and negative directions of hysteretic envelope, are as follows:

- Point 1 (ePd1, ePf1): the force is calculated considering 20% of the peak force recorded during the test (F_p) while the displacement is the corresponding displacement at that point;

- Point 2 (ePd2, ePf2): the force is calculated considering 80% of the peak force and the displacement is chosen through an energy balance

in such a way that the area below the experimental hysteretic envelope up to the peak point is equal to the area below the numerical backbone curve;

- Point 3 (ePd2, ePf2): the force is set equal to the peak force recorded during the test (F_P) while the displacement is the corresponding displacement at that point;

- Point 4: the force is calculated through an energy balance to have an area below the third and fourth points, of the experimental hysteretic envelope and the numerical backbone curve, equal. The displacement is fixed at a value 3.5% of IDR for the configurations having single partitions with fixed or partially sliding connections on top, 4.7% of IDR for the configurations having partitions connected to the return walls with fixed or sliding connections on top and 6.5% of IDR for the configurations having partitions sliding connections top and sides too. The differences in IDR-s for the configurations with and without sliding connections highlight the capability of sliding connections to accommodate higher drifts.
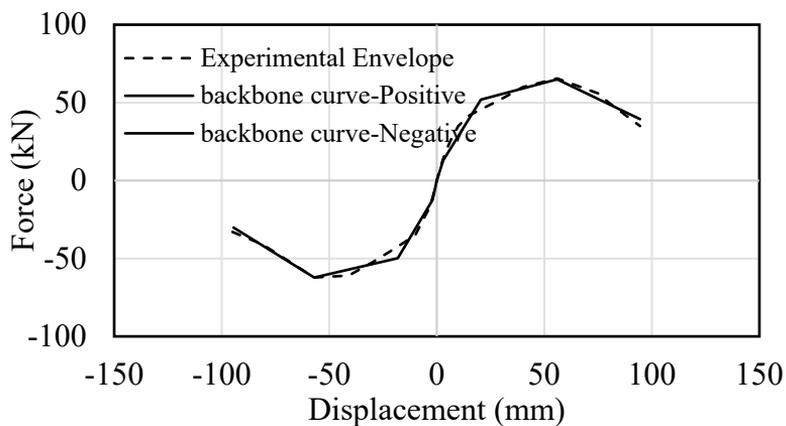

Figure 6-7 Backbone curve for Configuration 1

The unloading and reloading paths in hysteretic response curves are controlled by a series of parameters that govern the cyclic behaviour (rDispP, rForceP, uForceP, rDispN, rForceN, uForceN). As regards to the positive branches, *uForceP* defines the ratio between the strength developed upon unloading and maximum strength of the positive backbone curve. *rDispP* and *rForceP* mark the strength and displacement at which reloading occurs. In particular, *rForceP* is the ratio between the strength of reloading point and strength at maximum positive displacement of preceding cycles. *rDispP* is the ratio between the displacement of the reloading point and maximum positive displacement of preceding cycles. Obviously, same definitions apply for negative branches (*uForceN, rDispN, rForceN*). Symmetric values of these parameters are used for both positive and negative branches of hysteretic path. Therefore, only 3 independent parameters are defined (*uForceP=uForceN, rDispP=rDispN* and *rForceP=rForceN*). The experimental results showed that the points of unloading and reloading are characterized by very a low force values for all specimens of prototype 1, therefore the parameters uForceP and rForceP are taken equal to 0.01 and 0.1. This is not the case for prototype 2 configurations, that have less pronounced pinching. As far as rDispP in concerned, a best fit value is obtained by varying its value from 0.1 to 1.0 until a value is selected, with which minimum difference in the energy dissipated by the experimental and numerical results is obtained. Additionally, rest of the parameter were taken as zero except in some cases, where a value is used for them to achieve a best fit. Table 6-3 list the values of parameters of pinching4 material used for all tested configurations.

Table 6-3 Pinching 4 material properties

		#1	#2	#3	#4	#5	#6	#7	#8	#9	#10	#11	#12
	ePf1[kN]	12.3	13.0	11.8	13.8	17.6	8.9	9.6	11.2	4.3	3.3	1.5	1.8
	ePd1[mm]	3.0	3.0	5.0	4.0	5.0	7.0	31.0	29.0	3.0	3.0	1.5	3.0
	ePf2[kN]	49.1	52.0	47.3	55.3	70.4	35.4	38.3	45.0	17.2	13.4	6.1	7.2
	ePd2[mm]	12.0	21.0	34.0	41.0	37.0	66.0	94.2	111.0	16.0	10.0	6.7	10.0
Backbone curve parameters	ePf3[kN]	61.4	64.9	59.1	69.1	88.0	44.3	47.8	56.2	21.5	16.7	7.7	9.0
	ePd3[mm]	57.0	56.0	58.0	77.0	56.0	80.0	151.0	128.0	41.0	22.0	57.0	30.0
	ePf4[kN]	44.8	39.4	49.3	39.6	5.9	30.2	47.2	42.0	6.6	10.8	7.0	6.3
	ePd4[mm]	95.0	95.0	95.0	95.0	95.0	95.0	175.0	175.0	129.0	129.0	129.0	129.0
	eNf1[kN]	-11.5	-12.4	-11.5	-12.3	-16.9	-9.5	-9.8	-10.9	-3.8	-3.2	-1.7	-1.9
	eNd1[mm]	-3.0	-2.0	-5.0	-4.0	-5.0	-13.0	-35.0	-40.0	-3.0	-2.0	-2.0	-2.0
	eNf2[kN]	-46.1	-49.8	-46.0	-49.0	-67.6	-38.2	-39.0	-43.7	-15.4	-12.8	-6.8	-7.6
	eNd2[mm]	-11.0	-18.0	-22.0	-28.0	-32.0	-57.0	-90.0	-104.0	-14.0	-11.0	-12.0	-14.0
	eNf3[kN]	-57.6	-62.2	-57.5	-61.3	-84.5	-47.7	-48.8	-54.7	-19.2	-16.0	-8.5	-9.5
	eNd3[mm]	-40.0	-57.0	-57.0	-57.0	-57.0	-75.0	-130.0	-130.0	-30.0	-20.0	-30.0	-26.0
	eNf4[kN]	-42.2	-30.2	-39.6	-50.0	-35.0	-18.3	-36.5	-17.8	-5.2	-11.9	-8.9	-4.9
	eNd4[mm]	-95.0	-95.0	-95.0	-95.0	-95.0	-95.0	-175.0	-175.0	-129.0	-129.0	-129.0	-129.0
	rDispP	0.75	0.75	0.65	0.70	0.85	1.00	1.00	0.90	0.70	0.60	0.90	1.00
	rForceP	0.10	0.10	0.10	0.10	0.10	0.10	0.10	0.10	0.10	0.70	0.20	0.30
	uForceP	0.01	0.01	0.01	0.01	0.01	0.01	0.01	0.01	0.01	0.06	0.03	0.02
	gF$_i$ with i=1,2	0.0	0.0	0.0	0.0	0.0	0.0	0.0	0.0	0.0	0.0	0.0	0.0
	gF$_i$ with i=3,4	0.0	0.0	0.0	0.0	0.0	0.0	0.0	0.0	0.0	0.0	0.0	0.0
Cyclic parameters	gF$_{lim}$	0.0	0.0	0.0	0.0	0.0	0.0	0.0	0.0	0.0	0.0	0.0	0.0
	gD$_i$ with i=1,2	0.0	0.0	0.0	0.0	0.0	0.0	0.0	0.0	0.0	0.0	0.0	0.0
	gD$_i$ with i=3,4	0.0	0.0	0.0	0.0	0.0	0.0	0.0	0.0	0.0	0.0	0.0	0.0
	gD$_{lim}$	0.0	0.0	0.0	0.0	0.0	0.0	0.0	0.0	0.0	0.0	0.0	0.0
	gK$_i$ with i=1,2	0.0	0.0	0.0	0.0	0.0	-0.5	-1.1	-1.1	0.0	0.0	0.0	0.0
	gK$_i$ with i=3,4	0.0	0.0	0.0	0.0	0.0	-0.4	-1.2	-1.2	0.0	0.0	0.0	0.0
	gK$_{lim}$	0.0	0.0	0.0	0.0	0.0	-0.2	-0.8	-0.8	0.0	0.0	0.0	0.0
	gE	10.0	10.0	10.0	10.0	10.0	10.0	10.0	10.0	10.0	10.0	10.0	10.0
	dmgType						Energy						

6.3.2. Model validation

The developed model is used to simulate the results of in-plane quasi-static cyclic tests conducted on LWS partition walls. The model is analyzed under the same cyclic loading protocol as used in the tests [102]. The loading protocol (Figure 6-8) in the tests is defined by FEMA 461 [152] "Interim testing protocols for determining the seismic performance characteristic of structural and non-structural components". FEMA 461

provides a loading history that consists of repeated cycles of step-wise increasing deformation amplitudes.
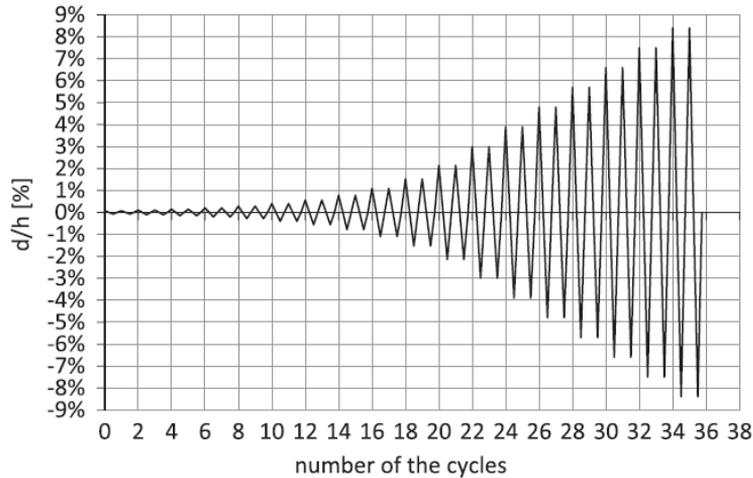

Figure 6-8 Loading protocol used for testing LWS partitions [148]

Figure 6-9 shows the comparison of hysteretic response curves of numerical models and the tested specimens for the two tested configurations: a partition wall with all fixed connections (Configuration 1): a partition walls with sliding connection on the top and side (Configuration 8). The results for rest of the wall models are shown in Annex D.
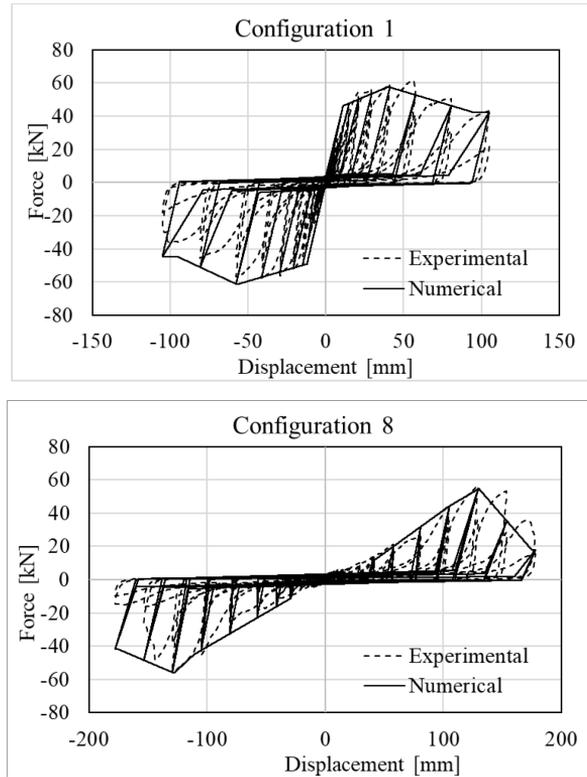
Figure 6-9 Comparison of numerical and experimental hysteretic response curves

As it can be seen from the preceding figures that the numerical model is effective in capturing the experimental response both in terms of the overall shape of the diagram and the position of the peaks for each cycle for two very distinct configurations of walls. To have a clear judgement on the accuracy of wall models in some quantitative manner, a comparison between the experimental and the numerical results is also made based on the dissipated energy using the following equations:

$$CE_{e,j} = \sum_{i=1}^{j} E_{e,i}, \; [i,j \leq n \tag{6-1}$$

$$CE_{n,j} = \sum_{i=1}^{j} E_{n,i}, \; [i,j \leq n] \tag{6-2}$$

$$\Delta_{E,i} = \frac{E_{n,i} - E_{e,i}}{E_{e,i}} \times 100, \ [i \leq n] \qquad\qquad (6\text{-}3)$$

$$\Delta_{CE,j} = \frac{CE_{n,j} - CE_{e,j}}{CE_{e,j}} \times 100, \ [j \leq n] \qquad\qquad (6\text{-}4)$$

where: $CE_{e,j}$ and $CE_{n,j}$ represent the cumulative energy dissipated for j^{th} cycle of the loading protocol obtained in experimental and numerical results, respectively; $E_{e,i}$ and $E_{n,i}$ represent the energy dissipated in i^{th} cycle of experimental and numerical results, respectively; $\Delta_{E,i}$ is the percentage difference of the energy dissipation for i^{th} cycle of loading protocol between numerical and experimental results; $\Delta_{CE,j}$ is the percentage difference of the cumulative energy for the jth cycle of loading protocol between numerical and experimental results; n is the last cycle of the loading protocol. Figure 6-10 shows the comparison of energy dissipated in each cycle of experimental and numerical hysteretic response curve along with value of $\Delta_{E,i}$ for last six cycles of higher amplitude of the loading protocol.
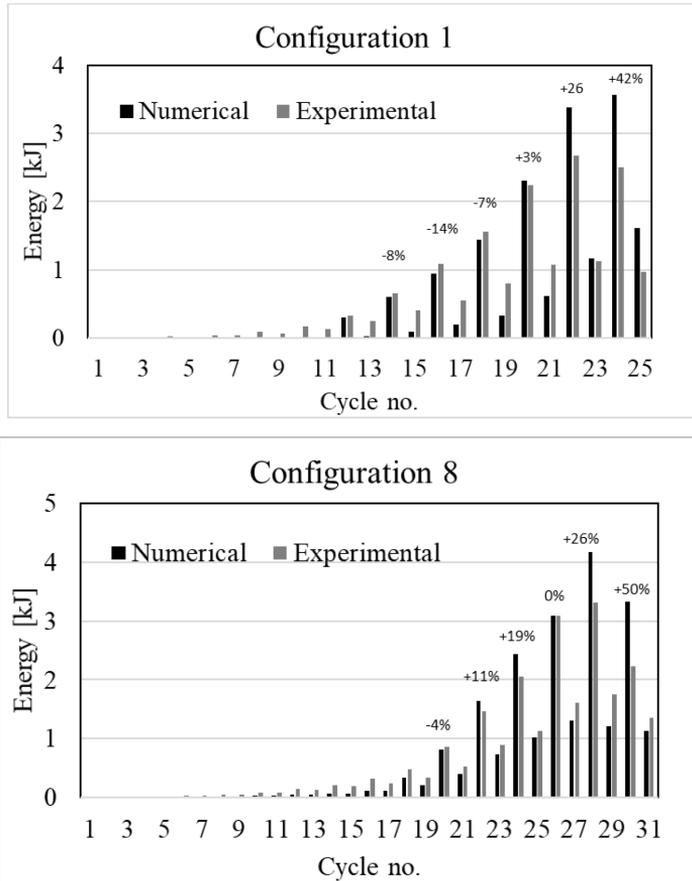
Figure 6-10 Comparison of numerical and experimental energy dissipated in each cycle of loading protocol

It can be seen from Figure 6-10 that the analytical model follows the trend of the experimental results in predicting the energy dissipated in different cycles of loading protocol. Though for some configurations (e.g. Configuration 1), it can be observed that the cycle of experimental hysteretic response for which there is the higher energy dissipation does not coincide with the cycle in numerical hysteretic response with the highest energy dissipation. This could be attributed to the points of backbone curve, which are selected through energy balances.

Using the equations (6-1) and (6-2), the cumulative energy dissipated is calculated for numerical and experimental hysteretic response curves and represented for some configurations in Figure 6-11.
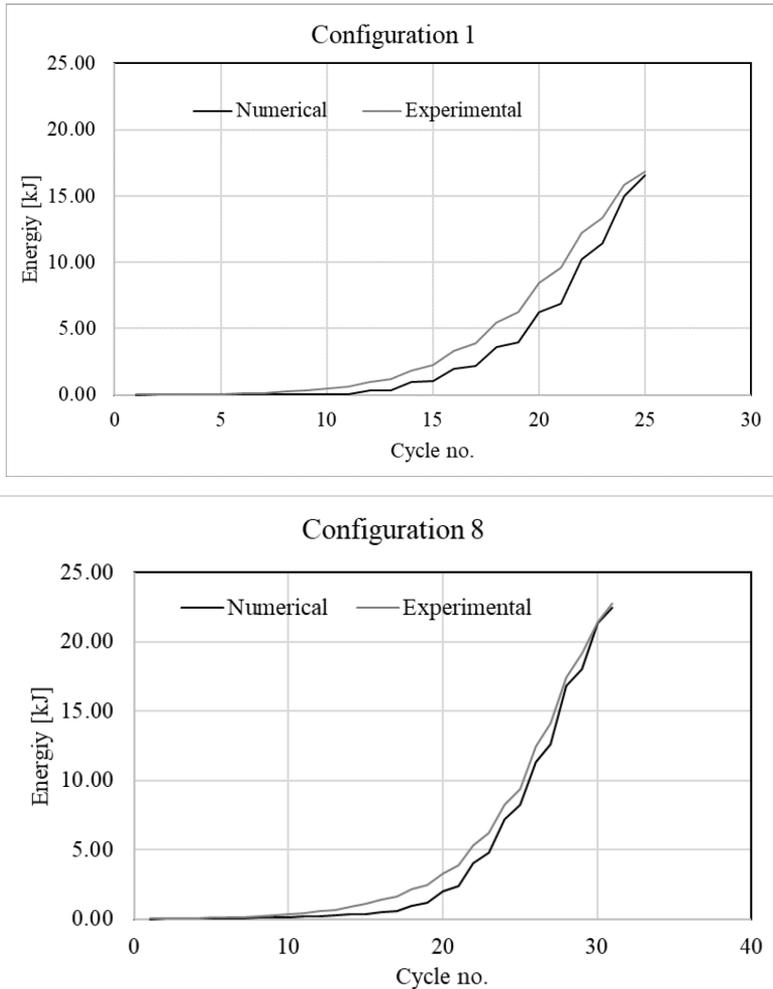
Figure 6-11 Comparison of numerical and experimental cumulative energy dissipated

The trend of the cumulated energy dissipated in numerical and experimental hysteretic responses is also consistent At the last loading cycles of the configuration 1 to 5 with fixed connection to the surrounding structural elements, the difference in cumulative energies of numerical and

experimental hysteretic responses is negligible, which confirms the validity of the developed model, while the difference ranges between -3% and 0%; for configuration 6 to 8 characterized by sliding connections and between -2% and -1% for the configuration 9 to 12.

6.4. Group models

6.4.1. Hysteretic characterization

The hysteretic characterization of the partition walls presented in Section 6.3 varied for each tested configuration and is entirely dependent on the test results. In order to limit the dependence of numerical models on the experimental data for partitions with particular construction parameters, certain groups of partitions are identified. These parameters include type of connections to the surrounding and the type of surrounding elements. The hysteretic characteristics of the model, that can simulate the response of group of partitions, are obtained by taking the mean of the parameters (pinching4 material) selected for individual partition walls (Section 6.3) in a group.

• Group I: partition walls with fixed connections to the surrounding structural elements (Configuration 1, 2, 3, 4 and 5)

• Group II: partition walls with sliding connections at top to the surrounding structural element (Configuration 6)

• Group III: partition walls with sliding connections at top and sides to the surrounding structural elements (Configuration 7 and 8)

• Group IV: partitions walls with transverse facades at their ends and connected at top with a fixed connection to surrounding structural element (Configuration 9 and 10)

• Group V: partitions walls with transverse facades at their ends and connected at top with a sliding connection to surrounding structural element (Configuration 11 and 12).

Figure 6-12 shows the backbone curve of the group model (average backbone curve) along with the curves of individual partitions in a group, while Table 6-4 shows the rest of parameters governing the cyclic behavior, which are also obtain by averaging the values of the partitions in a group.
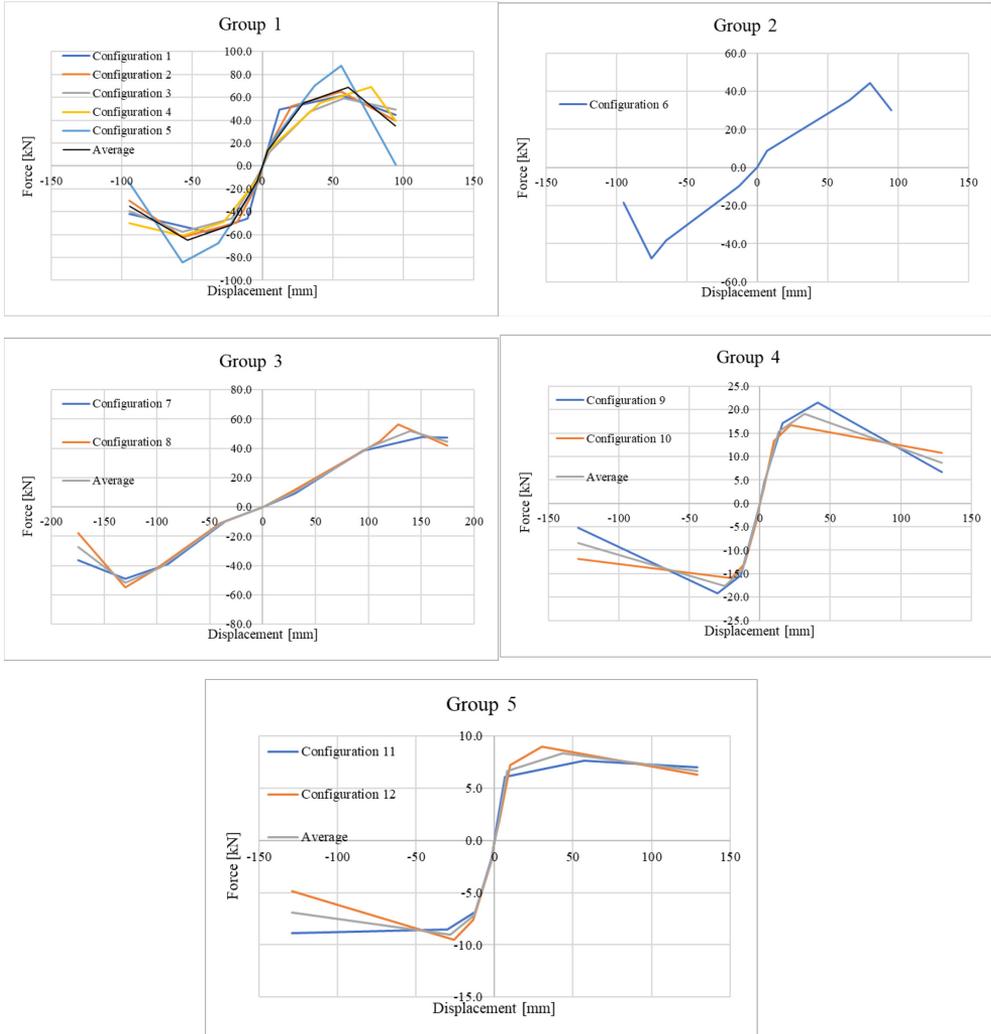
Figure 6-12 Backbone curves of group models

Table 6-4 Cyclic parameters for the group models

Average values for the cyclic parameters					
	Group 1	Group 2	Group 3	Group 4	Group 5
rDisp	0.74	1.00	0.95	0.65	0.95
rForce	0.10	0.10	0.10	0.09	0.25
uForce	0.01	0.01	0.01	0.01	0.03

6.4.2. **Model validation**

Once the parameters are defined, a comparison is made between the results of the group numerical model with the experimental data using the indicators introduced in previous section. Figure 6-13 evaluates the performance of group models in terms of cumulative energy dissipation. It can be seen that the difference between the group models and experimental results in terms of cumulative energy dissipation at the last cycle is never higher than 20%. Comparison is not made for the group 2 model since it has only one configuration within the group.
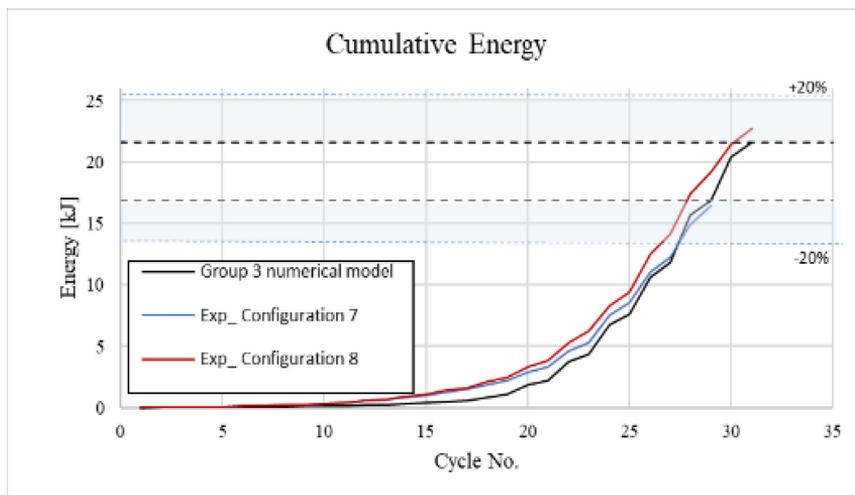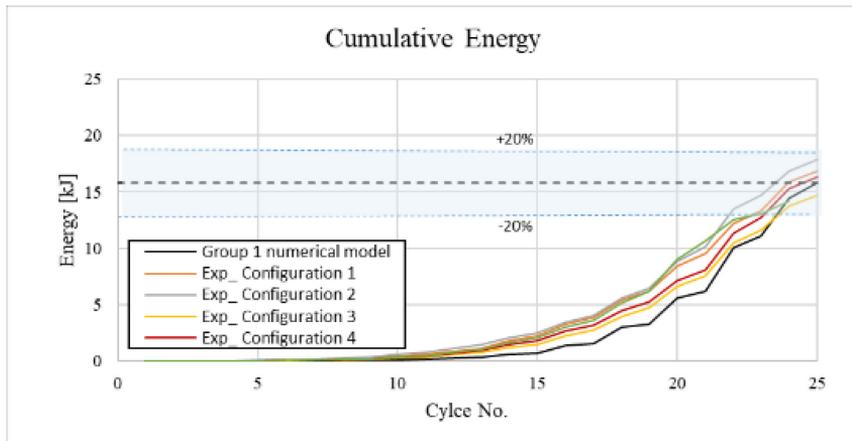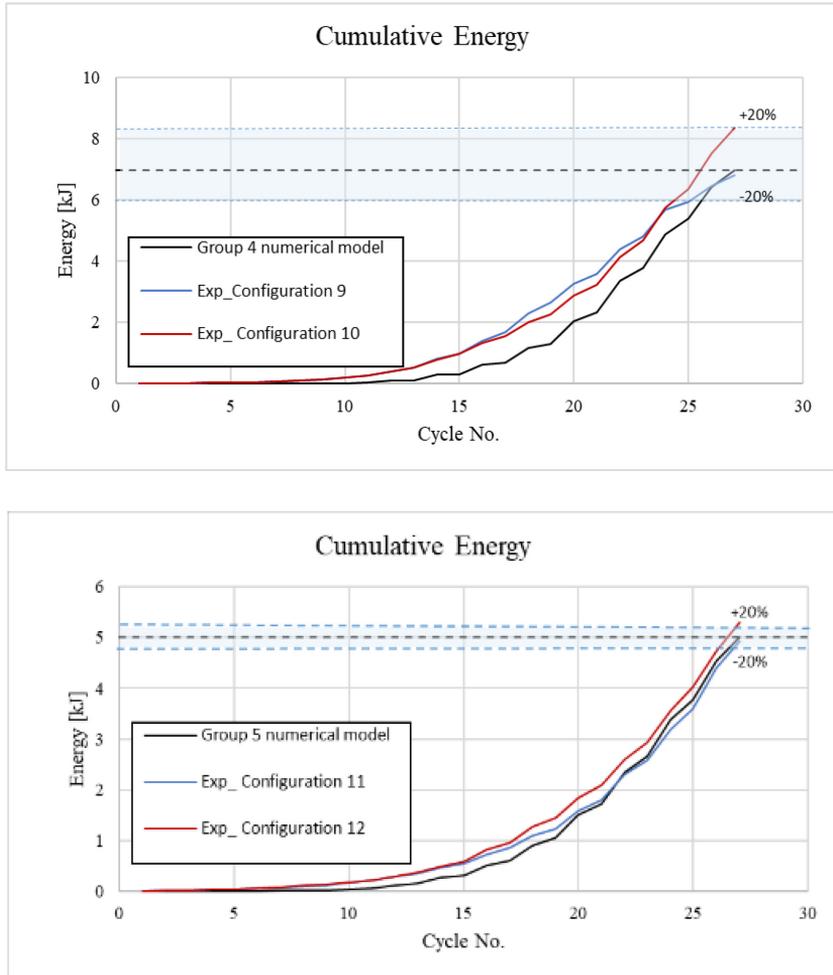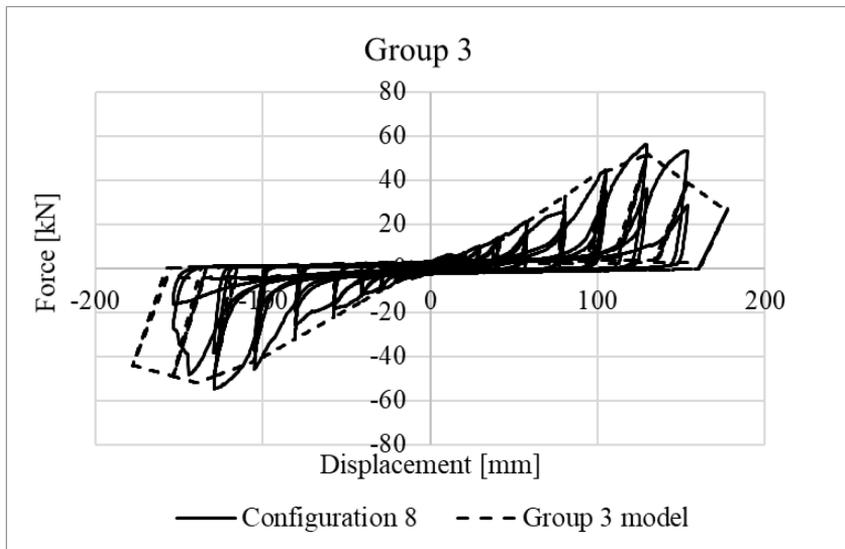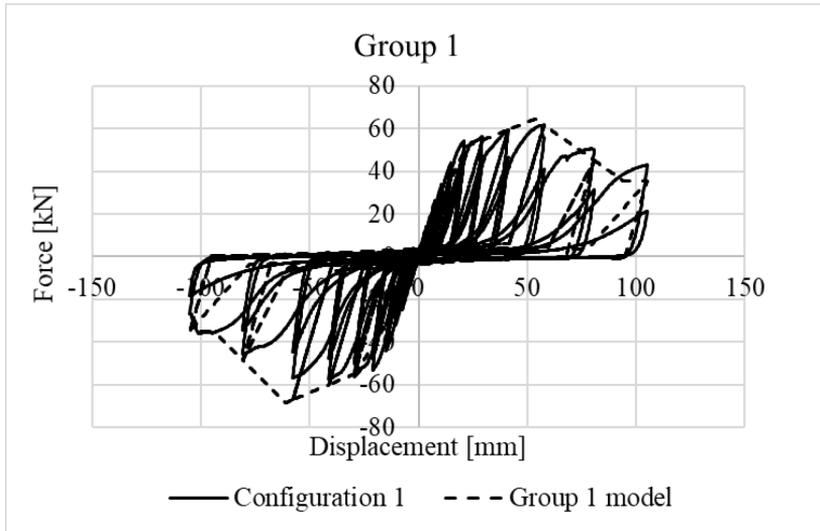
Figure 6-13 Cumulative energy dissipated by group models

Additionally, following figures also show the hysteretic response of all 5 group models while comparing them with one configuration with in the group.
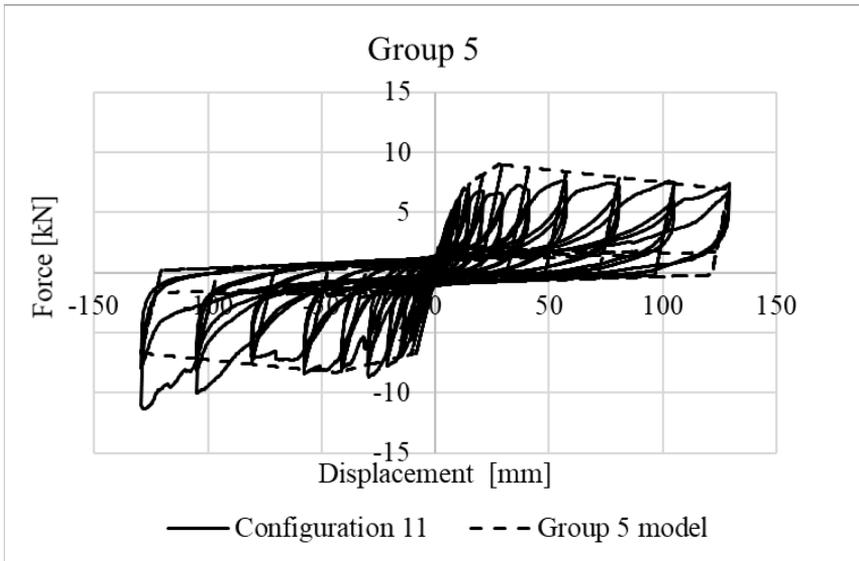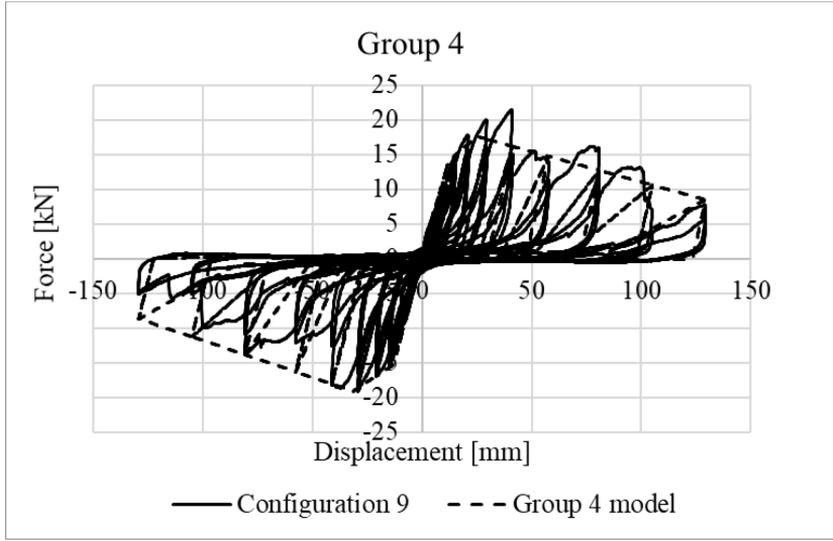
Figure 6-14 Hysteretic response curves of group models

7. Conclusions and Future work recommendations

Developing numerical and statistical tools for estimating the in plane seismic performance of LWS walls and a set of seismic design guidelines for LWS buildings that can be proposed for inclusion in next edition of Eurocodes was the main goal of this thesis. CFS framed structural walls which can used to provide resistance against the lateral loads in LWS building and CFS framed non-structural walls, which can used to fulfil different architectural demands in a building were studied.

The study on the structural walls involves checking of the collapse fragility of strap-braced and gypsum or wood sheathed shear walls using the iterative procedures of FEMA P695. Several residential and office archetypes, representing various heights are designed to withstand low, medium and high seismic loads. The design of archetypes follows the capacity design approach, which ensured that the plastic mechanism would only occur in the designated energy dissipative component. Numerical models of the archetypes are developed in two stages. Initially, a nonlinear FE model is developed for individual walls (LFRS) in OpenSees software. The model is a simplified truss model with diagonal truss elements representing the wall global force displacement hysteretic behaviour associated to the main ductile energy dissipating mechanism. The failure (local buckling/rupture of studs or rupture of hold down devices) of non-dissipative brittle elements of the wall is modelled implicitly by introducing limits on the strain in those elements. The limits on the strain correspond to relevant ultimate stress in the elements associated with

different modes of failure in non-dissipative elements. The reason behind not modelling the failure mechanism in non-dissipative elements in a more explicit manner is to keep the simplicity of model, so that it can be used with building model easily. In the next stage, wall models are merged with global building model developed in OpenSees software and analysed under the action of 44 earthquake records given in FEMA P695 [12] far-field record set. The analysis of models followed an incremental dynamic analysis approach until the collapse happens. Finally, by gauging the collapse performance of models against the FEMA P695 acceptance criteria for adjusted collapse margin ratios, the acceptability of a trial value of behaviour factor used in design of archetypes is established. A value of 2.5, 2.0 and 2.5 for behaviour factor of CFS strap-braced stud walls, CFS gypsum sheathed shear walls and CFS wood sheathed shear walls is found appropriate. Moreover, the proposed design method for the three investigate LFRS-s is able to predict their experimentally recorded peak strength with good accuracy. Design method is based on the capacity design philosophy, which allows the formation of designated energy dissipative mechanism in the walls through an overstrength in non-dissipative components. The method uses the formulations given in different part of Eurocodes or literature to evaluate the strengths of different wall components.

On the other hand, study on non-structural architectural components focuses on developing the numerical models for the most widely used LWS architectural components, i.e. partition walls and conducting in-plane quasi static cyclic test on façades. Simplified models using a single spring element lumped with the global hysteretic response of the wall are developed for LWS drywall partitions. The model is calibrated using

experimental data on the in-plane behavior of the partitions, which was obtained from the quasi-static cyclic tests conducted on them in past. The individual model for each partition is able to simulate its experimental hysteretic response. The model ability to simulate the experimental response is gauged through visual comparison of the experimental and the numerical hysteretic responses and quantitative comparisons in terms of the energy dissipation. In order to limit the dependence of numerical models on the experimental data, certain groups of partitions with particular construction parameters are identified and a model for each group is also developed. These parameters include type of connections to the surrounding and the type of surrounding elements. The hysteretic characteristics of group models are derived by taking the mean of the hysteretic parameters of the partitions within the group. Subsequently, accuracy of group models is also evaluated by comparing them against the individual partition wall tested specimens, which is found to be acceptable.

In-plane quasi static cyclic test tests are conducted to check the fragility of façades made with LWS frame elements to different damage states, to validate their compliance with the inter storey drift limits for non-structural components given in Eurocode 8 and to understand the effect of different construction parameters on their performance. Results reveal that adding an internal frame slightly increases the values of strength and stiffness, but overall does not provide a significant contribution to the wall. The façades with impact resistant gypsum boards showed much higher strength than the standard gypsum boards, while the behavior is not affected much by the type of frame (with or without tracks and thicker profiles). Moreover, the presence of cladding in one test did not change the response significantly due the fact that adding a cladding layer on the face

of façades increased the total thickness of the façade, resulting in a part of it not infilled within the testing frame. The use of sliding connections on top did not improve much the response in terms of strength and stiffness, while slight improvements are observed in terms of the fragility to different damage states. From the examination of the fragility data collected from the cyclic tests on façades, it should be noted that the minimum drift levels triggering DS1 in specimens with all fixed joints are in the range from 0.28% to 0.40%, minimum drift levels triggering DS2 in specimens with all fixed joints are in the range from 0.56% to 1.09% and minimum drift levels triggering DS3 in specimens with all fixed joints are in the range from 0.78% to 2.14%.

Future work recommendations

- The archetype design space used in this study is only comprised of the most probable building configurations that can adopt CFS walls as main seismic force resisting system. The design space is limited to archetypes that have regularity in plan and elevation. Nonetheless, earthquake standards around the world traditionally promotes the use regularity in plan and elevation of building but irregularities cannot be completely avoided in design due to the random nature of functional requirements of buildings. Such special cases should also be treated as part of behaviour factor evaluation process, which could be done in future studies.

- As shown by researchers based on their numerical studies [153] on CFS strap braced walls, that the few geometrical enhancements in walls can lead to an increase in behaviour factor. A topic of future

studies could also be to revaluate the behaviour factor for CFS strap braced walls considering these enhancements.

- In contrast with the value of 2.0 for behaviour factor of CFS gypsum sheathed shear walls, which is evaluated is this thesis, a value of 3.0 was used for the design of two storey CFS building prototype tested on the shake-table in a past research [140]. The tested prototype made with CFS gypsum sheathed shear walls showed a quite stiffer response even under an earthquake with 1.0g of PGA. In fact, the peak inter-storey drift of 0.80% for the 1st storey and 0.52% for the 2nd storey was observed. However, in case of shake-table tests, the specimens had all the finishes which could have resulted in the better seismic performance. This highlights the important contribution of non-structural finishes, which can enhance the performance of CFS gypsum sheathed shear walls as it was also shown by Macillo et al. [8], that a wall with finishes has a 50% more strength than the one without them. In this context, the studies involving seismic performance evaluation of LFRS-s in this thesis can be further expanded in future to consider also these finishes during the modelling process.

- Another important modelling consideration for LWS buildings is the floor response, which can show a semi rigid behaviour and could significantly alter the response of building. Moreover, sheathed floors similar to the light solution used in this study can assist in resisting a significant portion of seismic loads. This demands to adopt for a more detailed modelling approach for floor systems as the one used by Leng et al [9].

- Local buckling in chord studs of the walls is modelled using a much simpler approach of introducing limits on the strain in stud elements.

However, this approach requires to use truss elements for chord studs, which cannot resist any bending actions. In case of walls with larger aspect ratio (greater than 2.0), bending moment are acted upon the studs. In such case, beam column elements are the right choice. Yet, limit on strain cannot be enforced on beam column elements in OpenSees. Therefore, more research is also needed on explicit modelling of local buckling in studs.

- The presented models for LWS partitions can be used in future to conduct a case study to evaluate the effects of architectural non-structural components on the building seismic performance.

- Fragility curves for LWS façades are generated as a function of maximum inter storey drift ratios. A further expansion would be to associate these different inter storey drift levels to the building performance levels, which can assist in achieving a more rational performance based seismic design.

8. References

[1]   R. Bilham, R. Bendick, A FIVE YEAR FORECAST FOR INCREASED GLOBAL SEISMIC HAZARD, in: GSA Annu. Meet. Seattle, Washington, USA, 2017. doi:10.1130/abs/2017AM-300667.

[2]   P. Vitale, A. Spagnuolo, C. Lubritto, U. Arena, Environmental performances of residential buildings with a structure in cold formed steel or reinforced concrete, J. Clean. Prod. 189 (2018) 839–852. doi:10.1016/j.jclepro.2018.04.088.

[3]   Federal Emergency Management Agency, FEMA E-74 Reducing the Risks of Nonstructural Earthquake Damage, Washigton, D.C., 2011.

[4]   CEN, EN 1998-1 Eurocode 8: Design of Structures for earthquake resistance-Part 1: General rules, seismic actions and rules for buildings, European Committee for Standardization, Brussels, 2004.

[5]   A. Filiatrault, T. Sullivan, Performance-based seismic design of nonstructural building components: The next frontier of earthquake engineering, Earthq. Eng. Eng. Vib. 13 (2014) 17–46. doi:10.1007/s11803-014-0238-9.

[6]   Steel Studs & Joists, Canadian Sheet Steel Building Institute, (n.d.). cssbi.ca/products/steel-stud (accessed July 31, 2018).

[7]   O. Iuorio, V. Macillo, M.T. Terracciano, T. Pali, L. Fiorino, R. Landolfo, Seismic response of Cfs strap-braced stud walls:

Experimental investigation, Thin-Walled Struct. 85 (2014) 466–480. doi:10.1016/j.tws.2014.09.008.

[8]   V. Macillo, L. Fiorino, R. Landolfo, Seismic response of cold-formed steel shear walls sheathed with nailed gypsum panels: Experimental tests, Thin-Walled Struct. 120 (2017) 161–171. doi:http://dx.doi.org/10.1016/j.tws.2017.08.022.

[9]   J. Leng, K.D. Peterman, G. Bian, S.G. Buonopane, B.W. Schafer, Modeling seismic response of a full-scale cold-formed steel-framed building, Eng. Struct. 153 (2017) 146–165. doi:10.1016/j.engstruct.2017.10.008.

[10]   E. Rahmanishamsi, S. Soroushian, E.M. Maragakis, Analytical model for the in-plane seismic performance of cold-formed steel-framed gypsum partition walls, Earthq. Eng. Struct. Dyn. 45 (2016) 619–634. doi:10.1002/eqe.2676.

[11]   R. Landolfo, Lightweight steel framed systems in seismic areas: Current achievements and future challenges, Thin-Walled Struct. 140 (2019) 114–131. doi:10.1016/j.tws.2019.03.039.

[12]   FEMA, FEMA P695: Quantification of Building Seismic Performance Factors, Washigton, DC, USA, 2009.

[13]   SEI/ASCE, ASCE 7-16 Minimim Design Loads for Buildings and Other Structures, American Society of Civil Engineers, Reston, Virginia, 2016.

[14]   CEN, EN 1993-1-3 Eurocode 3: Design of steel structures-Part 1-3: General rules-Supplementary rules for cold-formed members and

sheeting, European Committee for Standardization, Brussels, 2006.

[15]   AISI, S100-16 North American Specification for the Design of Cold-Formed Steel Structural Members, American Iron and Steel Institute (AISI), 2016.

[16]   AUS/NZS 4600. Cold-formed steel structures, Australian/ New Zealand standard, Sydney (NSW, Australia), 2005.

[17]   National Building Code of Canada, National Research Council of Canada (NRCC), Ottawa, ON, Canada, 2015.

[18]   AISI, S400-15 North American Standard for Seismic Design of Cold formed Steel Structural Systems, American Iron and Steel Institute (AISI), 2015.

[19]   N. Yanagi, C. Yu, Effective Strip Method for the Design of Cold-Formed Steel Framed Shear Wall with Steel Sheet Sheathing, J. Struct. Eng. 140 (2014) 04013101. doi:10.1061/(ASCE)ST.1943-541X.0000870.

[20]   AS1170.4 Minimum Design Load on Structures, Part 4, Earthquake Load, Standards Association of Australia, Sydney (NSW, Australia), 1993.

[21]   Uniform Building Code, International Conference on Building Officials, Whittier, California, USA, 1967.

[22]   ASCE 41-13 Seismic Evaluation and Upgrade of Existing Buildings, American Society of Civil Engineers, Reston, VA, 2013.

[23]   L.. Fülöp, D. Dubina, Performance of wall-stud cold-formed shear panels under monotonic and cyclic loading Part I: Experimental

research,   Thin-Walled   Struct.   42   (2004)   321–338.
doi:10.1016/S0263-8231(03)00063-6.

[24]   M. Al-Kharat, C.A. a. Rogers, Inelastic performance of cold-formed
steel strap braced walls, J. Constr. Steel Res. 63 (2007) 460–474.
doi:10.1016/j.jcsr.2006.06.040.

[25]   M. Al-Kharat, C.A. Rogers, Inelastic performance of screw-
connected cold-formed steel strap-braced walls, Can. J. Civ. Eng.
35 (2008) 11–26. doi:10.1139/L07-081.

[26]   K. Velchev, G. Comeau, N. Balh, C.A. Rogers, Evaluation of the
AISI S213 seismic design procedures through testing of strap braced
cold-formed steel walls, Thin-Walled Struct. 48 (2010) 846–856.
doi:10.1016/j.tws.2010.01.003.

[27]   AISI-S213-07, North American Standard for Cold-Formed Steel
2007 Edition with Supplement No.1, American Iron and Steel
Institute (AISI), Washigton, DC, 2010.

[28]   A. Mirzaei, R.H. Sangree, K. Velchev, G. Comeau, N. Balh, C.A.
Rogers, B.W. Schafer, Seismic capacity-based design of narrow
strap-braced cold-formed steel walls, J. Constr. Steel Res. 115
(2015) 81–91. doi:10.1016/j.jcsr.2015.08.023.

[29]   H. Moghimi, H.R. Ronagh, Performance of light-gauge cold-
formed steel strap-braced stud walls subjected to cyclic loading,
Eng. Struct. 31 (2009) 69–83. doi:10.1016/j.engstruct.2008.07.016.

[30]   M. Zeynalian, H.R. Ronagh, A numerical study on seismic
performance of strap-braced cold-formed steel shear walls, Thin

Walled Struct. 60 (2012) 229–238. doi:10.1016/j.tws.2012.05.012.

[31]   M. Casafont, A. Arnedo, F. Roure, A. Rodríguez-Ferran, Experimental testing of joints for seismic design of lightweight structures. Part 3: Gussets, corner joints, x-braced frames, Thin-Walled Struct. 45 (2007) 637–659. doi:10.1016/j.tws.2007.05.008.

[32]   L. Fiorino, O. Iuorio, V. Macillo, M.T. Terracciano, T. Pali, R. Landolfo, Seismic Design Method for CFS Diagonal Strap-Braced Stud Walls: Experimental Validation, J. Struct. Eng. 142 (2016) 04015154. doi:10.1061/(ASCE)ST.1943-541X.0001408.

[33]   L. Fiorino, B. Bucciero, R. Landolfo, Shake table tests of three storey cold-formed steel structures with strap-braced walls, Bull. Earthq. Eng. (2019). doi:10.1007/s10518-019-00642-z.

[34]   T.-W. Kim, J. Wilcoski, D.A. Foutch, M.S. Lee, Shaketable tests of a cold-formed steel shear panel, Eng. Struct. 28 (2006) 1462–1470. doi:10.1016/j.engstruct.2006.01.014.

[35]   Federal Emergency Managment Agency (FEMA), FEMA 355F State of the art report on performance prediction and evaluation of steel moment frame buildings, Washigton, D.C., 2000.

[36]   M.T. Terracciano, B. Bucciero, T. Pali, V. Macillo, L. Fiorino, R. Landolfo, Design and numerical simulation of shake-table tests of CFS strap-braced stud structures, in: XXVI Congr. C.T.A. Coll. Dei Tec. Dell'Acciaio., Venezia, Italy, 2017: pp. 631–638.

[37]   N. Pastor, A. Rodríguez-Ferran, Hysteretic modelling of x-braced shear walls, Thin-Walled Struct. 43 (2005) 1567–1588.

doi:10.1016/j.tws.2005.06.010.

[38]   T.-W. Kim, J. Wilcoski, D.A. Foutch, Analysis of Measured and
        Calculated Response of a Cold-formed Steel Shear Panel Structure,
        J. Earthq. Eng. 11 (2007) 67–85. doi:10.1080/13632460601031862.

[39]   G.H.P. Rakesh Allahabadi, Drain-2DX, (1988).

[40]   G. Comeau, K. Velchev, C.A. Rogers, Development of seismic
        force modification factors for cold-formed steel strap braced walls,
        Can. J. Civ. Eng. (2010) 236–249. doi:10.1139/L09-153.

[41]   A.J. Carr, RUAUMOKO, (2000).

[42]   E.F. Gad, A.M. Chandler, C.F. Duffield, G. St, Lateral Behavior of
        Plasterboard -Clad Residential Steel Frames, J. Struct. Eng. 125
        (1999).

[43]   Swanson Analysis Systems Inc. (SASI), ANSYS, (1994).

[44]   A.D. Barton, Performance of steel framed domestic structures
        subjected to earthquake loads, PhD Thesis, Faculty of Engineering,
        Civil and Environmental Engineering, University of Melbourne,
        1997.

[45]   J. Ye, X. Wang, H. Jia, M. Zhao, Cyclic performance of cold-
        formed steel shear walls sheathed with double-layer wallboards on
        both   sides,   Thin-Walled   Struct.   92   (2015)   146–159.
        doi:10.1016/j.tws.2015.03.005.

[46]   N. Balh, J. DaBreo, C. Ong-Tone, K. El-Saloussy, C. Yu, C.A.
        Rogers, Design of steel sheathed cold-formed steel framed shear
        walls,   Thin-Walled   Struct.   75   (2014)   76–86.

doi:10.1016/j.tws.2013.10.023.

[47] Zhao, Cyclic performance of cold-formed steel stud shear walls, McGill University, Montreal, 2002.

[48] J.R. Tissell, Wood structural panel shear walls, Tacoma, Washignton, 1993.

[49] T.S. Tarpy, Shear resistance of steel-stud wall panels, in: Proc., 5th Int. Spec. Conf. Cold-Formed Steel Struct., St. Louis, MO, 1980: pp. 331–348.

[50] T.S. Tarpy, J.D. Girard, Shear resistance of steel-stud wall panels, in: Proc., 6th Int. Spec. Conf. Cold-Formed Steel Struct., St. Louis, MO, 1982: pp. 449–465.

[51] K.H. Klippstein, T.S. Tarpy Jr., Report CF 92-2 Shear Resistance of Walls with Steel Studs, 1992.

[52] A.J. Salenikovich, J.D. Dolan, W.S. Easterling, Racking performance of long steel-frame shear walls, in: Proc., 15th Int. Spec. Conf. Cold-Formed Steel Struct., 2000: pp. 471–480.

[53] A.E. Branston, F.A. Boudreault, C.Y. Chen, C.A. Rogers, Light-gauge steel-frame wood structural panel shear wall design method, Can. J. Civ. Eng. 33 (2006) 872–889. doi:10.1139/l06-036.

[54] R. Landolfo, G. Della Corte, L. Fiorino, Shear Behavior of Connections between Cold-Formed Steel Profiles and Wood or Gypsum-Based Panels: An Experimental Investigation, in: Struct. Congr. 2006, American Society of Civil Engineers, Reston, VA, 2006: pp. 1–10. doi:10.1061/40889(201)48.

[55]   R.L. Serrette, K. Ogunfunmi, Shear Resistance of Gypsum-Sheathed Light-Gauge Steel Stud Walls, J. Struct. Eng. 122 (1996) 383–389. doi:10.1061/(ASCE)0733-9445(1996)122:4(383).

[56]   R. Serrette, J. Encalada, B. Matchen, H. Nguyen, A. Williams, Rep. No. LGSRG-1-97 Additional shear wall values for light weight steel framing, Santa Clara, CA, 1997.

[57]   R. Serrette, G. Hall, H. Nguyen, Dynamic performance of light gauge steel framed shear walls, in: Proc., 13th Int. Spec. Conf. Cold-Formed Steel Struct., St. Louis, MO0, 1996: pp. 487–498.

[58]   R.L. Serrette, H. Nguyen, G. Hall, Rep. No. LGSRG-3-96 Shear wall values for light weight steel framing, Santa Clara, CA, 1996.

[59]   K.A. Morgan, M.A. Sorhouet, R.L. Serrette, Final Report: LGSRG-06-02 Performance of Cold-Formed Steel-Framed Shear Walls: Alternative Configurations, Santa Clara, CA, 2002.

[60]   R.L. Serrette, J. Encalada, M. Juadines, H. Nguyen, Static Racking Behavior of Plywood, OSB, Gypsum, and FiberBond Walls with Metal Framing, J. Struct. Eng. 123 (1997) 1079–1086. doi:10.1061/(ASCE)0733-9445(1997)123:8(1079).

[61]   R. Serrette, K. Chau, Estimating Drift in Cold-Formed Steel Frame Structures, in: Struct. Congr. 2006, American Society of Civil Engineers, Reston, VA, 2006: pp. 1–11. doi:10.1061/40889(201)53.

[62]   Q. Peck, N. Rogers, R. Serrette, Cold-Formed Steel Framed Gypsum Shear Walls: In-Plane Response, J. Struct. Eng. 138 (2012) 932–941. doi:10.1061/(ASCE)ST.1943-541X.0000521.

[63]   C.-L. Pan, M.-Y. Shan, Monotonic shear tests of cold-formed steel wall frames with sheathing, Thin-Walled Struct. 49 (2011) 363–370. doi:10.1016/j.tws.2010.10.004.

[64]   Z. Xuhong, S. Yu, Z. Tianhua, L. Yong, J. Jin, Study On Shear Resistance Of Cold-Formed Steel Stud Walls In Residential Structure, Adv. Eng. Struct. Mech. Constr. (2006) 423–435.

[65]   M. Accorti, N. Baldassino, R. Zandonini, F. Scavazza, C.A. Rogers, Response of CFS Sheathed Shear Walls, Structures. 7 (2016) 100–112. doi:10.1016/j.istruc.2016.06.009.

[66]   P. Liu, K.D. Peterman, B.W. Schafer, Impact of construction details on OSB-sheathed cold-formed steel framed shear walls, J. Constr. Steel Res. 101 (2014) 114–123. doi:10.1016/j.jcsr.2014.05.003.

[67]   COLA-UCI, Report of a testing program of light-framed walls with wood-sheathed shear panels, 2001.

[68]   B. Källsner, U.A. Girhammar, Plastic models for analysis of fully anchored light-frame timber shear walls, Eng. Struct. 31 (2009) 2171–2181. doi:10.1016/j.engstruct.2009.03.023.

[69]   W.J. McCutcheon, Racking Deformations in Wood Shear Walls, J. Struct. Eng. 111 (1985) 257–269. doi:10.1061/(ASCE)0733-9445(1985)111:2(257).

[70]   R.L. Tuomi, William J. McCutcheon, Racking Strength of Light-Frame Nailed Walls, J. Struct. Div. ASCE. 104 (1978) 1131–1140.

[71]   NAHB, RP 97-1 Monotonic Tests of Cold- Formed Steel Shear Walls With Openings, 1997.

[72]   H. Sugiyama, T. Matsumoto, Empirical Equations for the Estimation of Racking Strength of a Plywood-Sheathed Shear Wall with Openings, in: Summ. Tech. Pap. Annu. Meet. Trans A.I.J., 1994.

[73]   R. Serrette, D.P. Nolan, Reversed Cyclic Performance of Shear Walls with Wood Panels Attached to Cold-Formed Steel with Pins, J. Struct. Eng. 135 (2009) 959–967. doi:10.1061/(ASCE)ST.1943-541X.0000037.

[74]   X. Wang, J. Ye, Reversed cyclic performance of cold-formed steel shear walls with reinforced end studs, J. Constr. Steel Res. 113 (2015) 28–42. doi:10.1016/j.jcsr.2015.05.012.

[75]   S. Mohebbi, S.R. Mirghaderi, F. Farahbod, A. Bagheri Sabbagh, S. Torabian, Experiments on seismic behaviour of steel sheathed cold-formed steel shear walls cladded by gypsum and fiber cement boards, Thin-Walled Struct. 104 (2016) 238–247. doi:10.1016/j.tws.2016.03.015.

[76]   B.W. Schafer, D. Ayhan, J. Leng, P. Liu, D. Padilla-Llano, K.D. Peterman, M. Stehman, S.G. Buonopane, M. Eatherton, R. Madsen, B. Manley, C.D. Moen, N. Nakata, C. Rogers, C. Yu, Seismic Response and Engineering of Cold-formed Steel Framed Buildings, Structures. 8 (2016) 197–212. doi:10.1016/j.istruc.2016.05.009.

[77]   L. Fiorino, V. Macillo, R. Landolfo, Shake table tests of a full-scale two-story sheathing-braced cold-formed steel building, Eng. Struct. 151 (2017) 633–647. doi:10.1016/j.engstruct.2017.08.056.

[78]   R. Landolfo, O. Iuorio, L. Fiorino, Experimental seismic

performance evaluation of modular lightweight steel buildings within the ELISSA project, Earthq. Eng. Struct. Dyn. (2018). doi:10.1002/eqe.3114.

[79]   L.. Fülöp, D. Dubina, Performance of wall-stud cold-formed shear panels under monotonic and cyclic loading: Part II: Numerical modelling and performance analysis, Thin-Walled Struct. 42 (2004) 339–349. doi:10.1016/S0263-8231(03)00064-8.

[80]   I. Shamim, C. a. Rogers, Steel sheathed/CFS framed shear walls under dynamic loading: Numerical modelling and calibration, Thin-Walled Struct. 71 (2013) 57–71. doi:10.1016/j.tws.2013.05.007.

[81]   J. Leng, B.W. Schafer, S.G. Buonopane, Seismic Computational Analysis of CFS-NEES Building, in: Int. Spec. Conf. Cold-Formed Steel Struct., 2012: p. 4.

[82]   S. Kechidi, N. Bourahla, Deteriorating hysteresis model for cold-formed steel shear wall panel based on its physical and mechanical characteristics, Thin-Walled Struct. 98 (2016) 421–430. doi:10.1016/j.tws.2015.09.022.

[83]   N. Bourahla, T. Boukhemacha, N. Allal, A. Attar, EQUIVALENT SHEAR LINK MODELING AND PERFORMANCE ANALYSIS OF COLD FORMED STEEL STRUCTURES UNDER EARTHQUAKE LOADING, Proc. 9th U.S. Natl. 10th Can. Conf. Earthq. Eng. (2010).

[84]   M. Nithyadharan, V. Kalyanaraman, Modelling hysteretic behaviour of cold-formed steel wall panels, Eng. Struct. 46 (2013) 643–652. doi:10.1016/j.engstruct.2012.08.022.

[85]   J. Martínez-Martínez, L. Xu, Simplified nonlinear finite element analysis of buildings with CFS shear wall panels, J. Constr. Steel Res. 67 (2011) 565–575. doi:10.1016/j.jcsr.2010.12.005.

[86]   S.G. Buonopane, G. Bian, T.H. Tun, B.W. Schafer, Computationally efficient fastener-based models of cold-formed steel shear walls with wood sheathing, J. Constr. Steel Res. 110 (2015) 137–148. doi:10.1016/j.jcsr.2015.03.008.

[87]   S. Esmaeili Niari, B. Rafezy, K. Abedi, Seismic behavior of steel sheathed cold-formed steel shear wall: Experimental investigation and numerical modeling, Thin-Walled Struct. 96 (2015) 337–347. doi:10.1016/j.tws.2015.08.024.

[88]   X. Zhou, Y. He, Y. Shi, T. Zhou, Y. Liu, Experiment and FE analysis on shear resistance of cold-formed steel stud assembled wall in residential structure, 2010. doi:10.18057/IJASC.2010.6.3.7.

[89]   Y. Telue, M. Mahendran, Behaviour and design of cold-formed steel wall frames lined with plasterboard on both sides, Eng. Struct. 26 (2004) 567–579. doi:10.1016/j.engstruct.2003.12.003.

[90]   C. Ding, Monotonic and Cyclic Simulation of Screw-Fastened Connections for Cold-Formed Steel Framing, Virginia Polytechnic Institute and State University, 2015. https://vtechworks.lib.vt.edu/handle/10919/55270.

[91]   V. Parkash, G.H. Powell, S. Campbell, Drain-3DX Base program description and user guide, (1994).

[92]   L.N. Lowes, N. Mitra, A. Altoontash, A beam-column joint model

for simulating the earthquake response of reinforced concrete frames a beam-column joint model for simulating the earthquake response of reinforced concrete frames, Berkeley, 2004.

[93] S. Mazzoni, F. McKenna, M.H. Scott, G.L. Fenves, Open System for Earthquake Engineering (OpenSees), (2009).

[94] CSI, Structural Analysis Program SAP2000, (2016). https://www.csiamerica.com/products/sap2000.

[95] G.C. Foliente, Hysteresis Modeling of Wood Joints and Structural Systems, J. Struct. Eng. 121 (1995) 1013–1022. doi:10.1061/(ASCE)0733-9445(1995)121:6(1013).

[96] HKS, ABAQUS/standard users manual, (1996). https://www.3ds.com/products-services/simulia/products/abaqus/.

[97] S. Kechidi, N. Bourahla, J.M. Castro, Seismic design procedure for cold-formed steel sheathed shear wall frames: Proposal and evaluation, J. Constr. Steel Res. 128 (2017) 219–232. doi:10.1016/j.jcsr.2016.08.018.

[98] I. Shamim, C.A. Rogers, Numerical evaluation: AISI S400 steel-sheathed CFS framed shear wall seismic design method, Thin-Walled Struct. 95 (2015) 48–59. doi:10.1016/j.tws.2015.06.011.

[99] L. Fiorino, B. Bucciero, R. Landolfo, Evaluation of seismic dynamic behaviour of drywall partitions, façades and ceilings through shake table testing, Eng. Struct. 180 (2019) 103–123. doi:10.1016/j.engstruct.2018.11.028.

[100] L. Fiorino, V. Macillo, R. Landolfo, Experimental characterization

of quick mechanical connecting systems for cold-formed steel structures, Adv. Struct. Eng. (2016) 136943321667131. doi:10.1177/1369433216671318.

[101] L. Fiorino, T. Pali, B. Bucciero, V. Macillo, M. Teresa Terracciano, R. Landolfo, Experimental study on screwed connections for sheathed CFS structures with gypsum or cement based panels, Thin-Walled Struct. 116 (2017) 234–249. doi:10.1016/j.tws.2017.03.031.

[102] T. Pali, V. Macillo, M. Teresa, T. Bianca, R. Landolfo, In - plane quasi - static cyclic tests of nonstructural lightweight steel drywall partitions for seismic performance evaluation, (2018) 1566–1588. doi:10.1002/eqe.3031.

[103] L. Fiorino, T. Pali, R. Landolfo, Out-of-plane seismic design by testing of non-structural lightweight steel drywall partition walls, Thin-Walled Struct. 130 (2018) 213–230. doi:10.1016/j.tws.2018.03.032.

[104] J. McCormick, Y. Matsuoka, P. Pan, M. Nakashima, Evaluation of Non-Structural Partition Walls and Suspended Ceiling Systems through a Shake Table Study, in: Struct. Congr. 2008, American Society of Civil Engineers, Reston, VA, 2008: pp. 1–10. doi:10.1061/41016(314)223.

[105] Y. Matsuoka, K. Suita, S. Yamada, Y. Shimada, M. Akazawa, Non-Structural Component Performance In 4-Story Frame Tested To Collapse, 14th World Conf. Earthq. Eng. (2008).

[106] R. Retamales, G. Mosqueda, A. Filiatrault, A. Reinhorn, Technical Report MCEER-08-0026 New Experimental Capabilities and

Loading Protocols for Seismic Qualification and Fragility Assessment of Nonstructural Systems, 2008.

[107] G. Magliulo, C. Petrone, V. Capozzi, G. Maddaloni, P. Lopez, G. Manfredi, Seismic performance evaluation of plasterboard partitions via shake table tests, Bull. Earthq. Eng. 12 (2014) 1657–1677. doi:10.1007/s10518-013-9567-8.

[108] R. Retamales, R. Davies, G. Mosqueda, A. Filiatrault, Experimental seismic fragility of cold-formed steel framed gypsum partition walls, J. Struct. Eng. 139 (2013) 1285–1293.

[109] X. Wang, E. Pantoli, T.C. Hutchinson, J.I. Restrepo, R.L. Wood, M.S. Hoehler, P. Grzesik, F.H. Sesma, Seismic Performance of Cold-Formed Steel Wall Systems in a Full-Scale Building, J. Struct. Eng. 141 (2015) 04015014. doi:10.1061/(ASCE)ST.1943-541X.0001245.

[110] C. Jenkins, S. Soroushian, E. Rahmanishamsi, E.M. Maragakis, Experimental fragility analysis of cold-formed steel-framed partition wall systems, Thin-Walled Struct. 103 (2016) 115–127. doi:10.1016/j.tws.2016.02.015.

[111] S.A. Freeman, Racking tests of high-rise building partitions, J. Struct. Div. Proc. Am. Soc. Civ. Eng. (1977) 1673–1685.

[112] T.-H. Lee, M. Kato, T. Matsumiya, K. Suita, M. Nakashima, Seismic performance evaluation of non-structural components: drywall partitions, Earthq. Eng. Struct. Dyn. 36 (2007) 367–382. doi:10.1002/eqe.638.

[113] J.I. Restrepo, A.M. Bersofsky, Performance characteristics of light gage steel stud partition walls, Thin-Walled Struct. 49 (2011) 317–324.

[114] G. Araya-Letelier, E. Miranda, Novel sliding/frictional connections for improved seismic performance of gypsum wallboard partitions, in: 15th World Conf. Earthq. Eng., Lisbon, 2012.

[115] A.S. Tasligedik, Damage mitigation strategies for non-structural infill walls., University of Canterbury, 2014.

[116] C. Petrone, G. Magliulo, P. Lopez, G. Manfredi, Seismic fragility of plasterboard partitions via in-plane quasi-static tests, Earthq. Eng. Struct. Dyn. 44 (2015) 2589–2606. doi:10.1002/eqe.2600.

[117] X. Wang, T.C. Hutchinson, G. Hegemier, S. Gunisetty, P. Kamath, B. Meacham, Earthquake and fire performance of a mid-rise cold-formed steel framed building – test program and test results: rapid release (preliminary) report, San Diego, CA, 2016.

[118] C. Petrone, G. Magliulo, P. Lopez, G. Manfredi, Seismic fragility of plasterboard partitions via in-plane quasi-static tests, Earthq. Eng. Struct. Dyn. 44 (2015) 2589–2606. doi:10.1002/eqe.2600.

[119] A.S. Tasligedik, S. Pampanin, A. Palermo, Low damage seismic solutions for non-structural drywall partitions, Bull. Earthq. Eng. 13 (2015) 1029–1050. doi:10.1007/s10518-014-9654-5.

[120] R.L. Wood, T.C. Hutchinson, Design-Oriented Model for Capturing the In-Plane Seismic Response of Partition Walls, J. Struct. Eng. 140   (2014)   04014023.   doi:10.1061/(ASCE)ST.1943-

541X.0000899.

[121] R.D. Davies, R. Retamales, G. Mosqueda, A. Filiatrault, Technical Report MCEER-11-0005 Experimental Seismic Evaluation, Model Parameterization, and Effects of Cold-Formed Steel-Framed Gypsum Partition Walls on the Seismic Performance of an Essential Facility, 2011.

[122] G. Magliulo, C. Petrone, V. Capozzi, G. Maddaloni, P. Lopez, G. Manfredi, Seismic performance evaluation of plasterboard partitions via shake table tests, Bull. Earthq. Eng. 12 (2014) 1657–1677. doi:10.1007/s10518-013-9567-8.

[123] R. Retamales, R. Davies, G. Mosqueda, A. Filiatrault, Experimental Seismic Fragility of Cold-Formed Steel Framed Gypsum Partition Walls, J. Struct. Eng. 139 (2013) 1285–1293. doi:10.1061/(ASCE)ST.1943-541X.0000657.

[124] E. Rahmanishamsi, S. Soroushian, E.M. Maragakis, Analytical model for the in-plane seismic performance of cold-formed steel-framed gypsum partition walls, Earthq. Eng. Struct. Dyn. 45 (2016) 619–634. doi:10.1002/eqe.2676.

[125] C. Petrone, G. Magliulo, G. Manfredi, Shake table tests on standard and innovative temporary partition walls, Earthq. Eng. Struct. Dyn. 46 (2017) 1599–1624. doi:10.1002/eqe.2872.

[126] A. Sato, C.M. Uang, A FEMA P695 study for the proposed seismic performance factors for cold-formed steel special bolted moment frames, Earthq. Spectra. 29 (2013) 259–282. doi:10.1193/1.4000099.

[127] CEN, EN 1991-1-1 Eurocode 1: Actions on structures-Part 1-1: General actions-Densities, self-weight, imposed loads for buildings, European Committee for Standardization, Brussels, 2004.

[128] E. V. Leyendecker, R.J. Hunt, A.D. Frankel, K.S. Rukstales, Development of Maximum Considered Earthquake Ground Motion Maps, Earthq. Spectra. 16 (2000) 21–40. doi:10.1193/1.1586081.

[129] CEN, EN 1990 Eurocode - Basis of structural design, European Committee for Standardization, Brussels, 2002.

[130] CEN, EN 1993-1-1 Eurocode 3: Design of steel structures-Part 1-1: General rules and rules for buildings, European Committee for Standardization, Brussels, 2005.

[131] V. Macillo, O. Iuorio, M.T. Terracciano, L. Fiorino, R. Landolfo, Seismic response of Cfs strap-braced stud walls: Theoretical study, Thin-Walled Struct. 85 (2014) 301–312. doi:10.1016/j.tws.2014.09.006.

[132] D. Vamvatsikos, C.A. Cornell, Applied incremental dynamic analysis, Earthq. Spectra. 20 (2004) 523–553. doi:10.1193/1.1737737.

[133] V. Macillo, S. Shakeel, L. Fiorino, R. Landolfo, Development and Calibration of a Hysteretic Model for CFS Strap braced stud walls, Adv. Steel Constr. 14 (2018) 336–359. doi:10.18057/IJASC.2018.14.3.2.

[134] D. Dubina, Behavior and performance of cold-formed steel-framed houses under seismic action, 64 (2008) 896–913.

doi:10.1016/j.jcsr.2008.01.029.

[135] J. Woessner, D. Laurentiu, D. Giardini, H. Crowley, F. Cotton, G. Grünthal, G. Valensise, R. Arvidsson, R. Basili, M.B. Demircioglu, S. Hiemer, C. Meletti, R.W. Musson, A.N. Rovida, K. Sesetyan, M. Stucchi, The 2013 European Seismic Hazard Model: key components and results, Bull. Earthq. Eng. 13 (2015) 3553–3596. doi:10.1007/s10518-015-9795-1.

[136] J.W. Baker, Efficient Analytical Fragility Function Fitting Using Dynamic Structural Analysis, Earthq. Spectra. 31 (2015) 579–599. doi:10.1193/021113EQS025M.

[137] CEN, EN 1993-1-1 Eurocode 3 : Design of steel structures -Part 1-1: General rules and rules for buildings, European Committee for Standardization, Brussels, 2005.

[138] CEN, EN 1990 Eurocode 0: Basis of structural design, European Committee for Standardization, Brussels, 2002.

[139] Report of a testing program of light-framed walls with wood-sheathed shear panels, 2001.

[140] L. Fiorino, V. Macillo, R. Landolfo, Shake table tests of a full-scale two-story sheathing-braced cold-formed steel building, Eng. Struct. 151 (2017) 633–647. doi:10.1016/j.engstruct.2017.08.056.

[141] CEN, EN 1995-1-1 Eurocode 5: Design of timber structures Part 1-1: general - Common rules and rules for buildings, European Committee for Standardization, Brussels, 2005.

[142] K.D. Peterman, N. Nakata, B.W. Schafer, Hysteretic

characterization of cold-formed steel stud-to-sheathing connections, J. Constr. Steel Res. 101 (2014) 254–264. doi:10.1016/j.jcsr.2014.05.019.

[143] L. Fiorino, S. Shakeel, V. Macillo, R. Landolfo, Behaviour factor (q) evaluation the CFS braced structures according to FEMA P695, J. Constr. Steel Res. 138 (2017) 324–339. doi:10.1016/j.jcsr.2017.07.014.

[144] P. Liu, K.D. Peterman, B.W. Schafer, Impact of construction details on OSB-sheathed cold-formed steel framed shear walls, J. Constr. Steel Res. 101 (2014) 114–123. doi:10.1016/j.jcsr.2014.05.003.

[145] K.D. Peterman, A.M. Asce, M.J.J. Stehman, R.L. Madsen, M. Asce, S.G. Buonopane, M. Asce, N. Nakata, M. Asce, B.W. Schafer, Experimental Seismic Response of a Full-Scale Cold-Formed Steel-Framed Building . I : System-Level Response, 142 (2016) 1–12. doi:10.1061/(ASCE)ST.1943-541X.0001578.

[146] M. Zeynalian, A.Z. Shahrasbi, H.T. Riahi, Seismic Response of Cold Formed Steel Frames Sheathed by Fiber Cement Boards, Int. J. Civ. Eng. 16 (2018) 1643–1653. doi:10.1007/s40999-018-0307-y.

[147] K.D. Peterman, M.J.J. Stehman, R.L. Madsen, S.G. Buonopane, N. Nakata, B.W. Schafer, Experimental Seismic Response of a Full-Scale Cold-Formed Steel-Framed Building. I: System-Level Response, J. Struct. Eng. 142 (2016) 04016127. doi:10.1061/(ASCE)ST.1943-541X.0001577.

[148] T. Pali, V. Macillo, M.T. Terracciano, B. Bucciero, L. Fiorino, R.

Landolfo, In-plane quasi-static cyclic tests of nonstructural lightweight steel drywall partitions for seismic performance evaluation, Earthq. Eng. Struct. Dyn. 47 (2018) 1566–1588. doi:10.1002/eqe.3031.

[149] K. Porter, R. Kennedy, R. Bachman, Creating Fragility Functions for Performance-Based Earthquake Engineering, Earthq. Spectra. 23 (2007) 471–489. doi:10.1193/1.2720892.

[150] A.S. Whittaker, T.T. Soong, An overview of nonstructural components research at three U.S. Earthquake Engineering Research Center, in: Proc. Semin. Seism. Des. Performance, Retrofit Nonstructural Components Crit. Facil. ATC 29-2, 2003.

[151] S. Mazzoni, F. McKenna, M.H. Scott, G.L. Fenves, OpenSees, (2009).

[152] FEMA, FEMA 461 : Interim testing protocols for determining the seismic performance characteristic of structural and non-structural components, Federal Emergency Managment Agency, Washigton, D.C., 2007.

[153] M. Zeynalian, H.R. Ronagh, A numerical study on seismic performance of strap-braced cold-formed steel shear walls, Thin-Walled Struct. 60 (2012) 229–238. doi:10.1016/j.tws.2012.05.012.

9. Publication record

In Scopus indexed Journals (* indicates co-first authors)

1. **S. Shakeel**, R. Landolfo, L. Fiorino, Behavior factor evaluation of CFS shear walls with gypsum board sheathing according to FEMA P695 for Eurocodes. *Thin-Walled Structures*, 141 (2019) 194–207.
2. V. Macillo, **S. Shakeel***, L. Fiorino, R. Landolfo, Development and calibration of a hysteretic model for CFS strap braced stud walls, *Advanced Steel Construction*, 14 (2018), 336–359.
3. L. Fiorino, **S. Shakeel***, V. Macillo, R. Landolfo, Seismic response of CFS shear walls sheathed with nailed gypsum panels: Numerical modelling, *Thin-Walled Structures*. 122 (2018) 359–370.
4. L. Fiorino, **S. Shakeel***, V. Macillo, R. Landolfo, Behaviour factor (q) evaluation the CFS braced structures according to FEMA P695, *Journal of Constructional Steel Research*. 138 (2017) 324–339.

In Conference Proceedings (* indicates co-first authors)

1. **S. Shakeel**, et al., Seismic behavior of Lightweight Steel Drywall Partitions: Preliminarily Fragility Analysis Based on Available Data. *4th International Workshop on the Seismic Performance of Non-Structural Elements SPONSE Pavia, Italy.* (2019) 169-177.
2. **S. Shakeel**, L. Fiorino, R. Landolfo, Numerical evaluation of the behaviour factor of lightweight steel lateral force resisting systems according to FEMA P695. *COMPDYN 2019 7th ECCOMAS Thematic Conference on Computational Methods in Structural Dynamics and Earthquake Engineering, Crete, Greece.* (2019).
3. **S. Shakeel,** A. Campiche, R. Landolfo, Behaviour factor evaluation of CFS shear walls with gypsum board sheathing according to FEMA P695. *Seventh International Conference on Structural Engineering, Mechanics and Computation (SEMC 2019), Cape Town, South Africa.* (2019) 1101-1106.
4. **S. Shakeel**, Quantifying the seismic ductility of lightweight steel lateral force resisting systems through procedures of FEMA P695. *International Colloquia on Stability and Ductility of Steel (SDSS), Prague, Czech Republic.* (2019).

5. R. Landolfo, **S. Shakeel***, L. Fiorino, Cold-Formed Steel lateral force resisting systems: proposal of seismic design criteria for 2nd generation of Eurocode 8. *VIII ANIDIS Conference - Seismic Engineering in Italy, Ascoli Piceno, Italy.* (2019) SG07-2.
6. **S. Shakeel**, L. Fiorino, R. Landolfo, Numerical Modelling of Lightweight Steel Drywall Partitions for in-Plane Seismic Performance Evaluations. *XXVII Congresso del Collegio dei Tecnici dell'Acciaio, Bologna, Italy.* (2019) 417-424.
7. **S. Shakeel**, L. Fiorino*, R. Landolfo, In-Plane Quasi-Static Cyclic Tests on Infilled Façades Made of Lightweight Steel Drywall Systems: Preliminary Results. *XXVII Congresso del Collegio dei Tecnici dell'Acciaio, Bologna, Italy.* (2019) 425-432.
8. **S. Shakeel** et al., CFS strap braced stud walls: behaviour factor evaluation according to FEMA P695 methodology, XXVI *Congr. C.T.A. Le Giornate Ital. Della Costr. Acciaio, Venezia, Italy* (2017) 83–90.